TO STUDY THE EFFECTS OF DOPING ON NANO-STRUCTURAL ZnO THIN FILM

THESIS

submitted in fulfillment of the requirement of the degree of

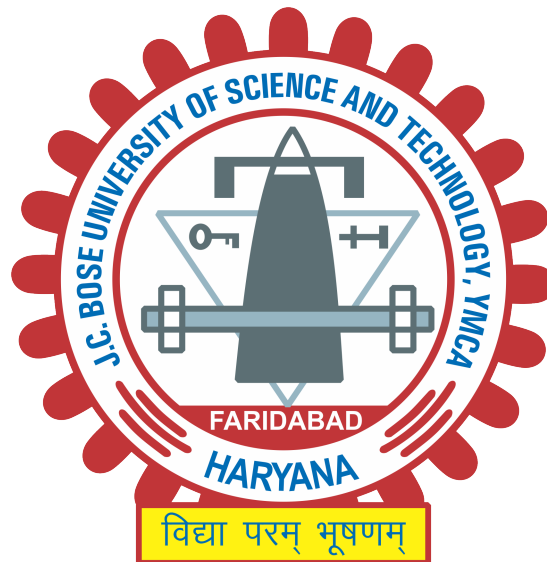## DOCTOR OF PHILOSOPHY

to

Faculty of Sciences

by

Shital Prasad

(Regn. No.: YMCAUST/Ph21/2012)

Under the Supervision of

Dr. Sonia

Department of Physics

J.C. Bose University of Science and Technology, YMCA,

Faridabad-121006, (Haryana), INDIA

January 2023

DEDICATED

to

My family

Seema Saini, Yukti Saini, Himank Saini and Himakshi Saini

DECLARATION

I hereby declare that this thesis entitled **"TO STUDY THE EFFECTS OF DOPING ON NANO-STRUCTURAL ZnO THIN FILM"** by **SHITAL PRASAD**, being submitted in fulfillment of the requirements for the Degree of Doctor of Philosophy in DEPARTMENT OF PHYSICS under Faculty of Sciences, JC Bose University of Science and Technology, YMCA, Faridabad, during the academic year 2021-22, is a bonafide record of my original work carried out under guidance and supervision of **Dr. SONIA, ASSOCIATE PROFESSOR, DEPARTMENT OF PHYSICS** and has not been presented elsewhere.

I further declare that the thesis does not contain any part of any work which has been submitted for the award of any degree either in this university or in any other university.

<div align="right">

Shital Prasad
YMCAUST/Ph21/2012

</div>

CERTIFICATE

This is to certify that this thesis entitled **"TO STUDY THE EFFECTS OF DOPING ON NANO-STRUCTURAL ZnO THIN FILM"** by **SHITAL PRASAD**, submitted in fulfillment of the requirement for the Degree of Doctor of Philosophy in **DEPARTMENT OF PHYSICS** under Faculty of Sciences of JC Bose University of Science and Technology, YMCA, Faridabad, during the academic year 2021-22, is a bonafide record of work carried out under my guidance and supervision.

I further declare that to the best of my knowledge, the thesis does not contain any part of any work which has been submitted for the award of any degree either in this university or in any other university.

Dr. Sonia
ASSOCIATE PROFESSOR
Department of Physics
Faculty of Sciences
JC Bose University of Science and Technology,
YMCA, Faridabad

Dated:

ACKNOWLEDGEMENTS

ABSTRACT

In this work undoped, doped and co-doped ZnO thin films are successfully synthesized on glass substrate by solution based sol-gel process using spin deposition technique at various substrate rotating speeds. The effect of spin deposition speed on undoped ZnO thin films absorbance, transmittance, fluorescence, and vibrational properties were investigated. The doping of elements Ni, Al, Co and Mn were used for the preparation of ZnO thin films and deposited doped films were characterized. The influence of spin deposition speed on doped ZnO thin films was studied using UV-visible, optical, fluorescent and Raman spectroscopy. Co-doped ZOTFs for the doping elements Al-Ni and Mn-Ni were also successfully fabricated. The effect of spin deposition speed on Al-Ni co-doped films was investigated, whereas the effect of annealing temperature on Mn-Ni co-doped ZnO thin films was investigated. The structural, surface morphology, UV-visible, optical, fluorescent and vibrational characteristics of co-doped ZnO thin films were investigated. According to U-V visible spectra, the optical transmittance of doped thin films is roughly 80 % in the visible spectrum. The optical transparency in the visible region is further enhanced by the doping of Al and Ni. It has also been observed that when the spin coating speed rises thin film transparency increases. Using the Vander Pauw four probe technique, the resistivity of Ni doped, Ni-Al co-doped and Mn-Ni co-doped ZnO thin films were measured. The transparency and resistivity of doped ZnO thin films make them suitable for use as a transparent conducting oxide (TCO) or transparent electrode in solar cells. The direct optical band gap of thin films was determined to be around 3.27 eV.

The refractive index (n), extinction coefficient (k), real part (ε_r) and imaginary (ε_i) parts of dielectric constant were calculated for Ni doped, Ni-Al co-doped and Mn-Ni co-doped ZnO thin films. The value of the refractive index varies in the range 1.2 to 3 while the value of the extinction coefficient was found to be less than 0.35. The values of the real and imaginary part of the dielectric constant were calculated in the energy range from 1.12 eV to 4 eV. The photoluminescence spectra of all thin films show an emission peak at about 385nm, originating from the exciton recombination associated to the near band edge (NBE) transition of ZnO. Besides the NBE emission thin films also show green emission band which may be due to the oxygen vacancies and antisite oxygen. The thin films features hexagonal wurtzite structure with (002) preferred orientation along the c-axis, as revealed by XRD patterns. The crystallinity and grain size of thin films improve as the annealing temperature increases.

Contents

List of Tables

List of Figures

List of Abbreviations

2ME	2-Methoxyethanol
ANDZO	Al-Ni co-doped Zinc Oxide
ACH	Aluminium Chloride Hexahydrate
ADZO	Aluminum Doped Zinc Oxide
CDZO	Cobalt Doped Zinc Oxide
CB	Conduction Band
CVD	Chemical Vapour Deposition
DMS	Dilute Magnetic Semiconductor
DW	Deionized Water
DC	Dielectric Constant
EDX	Energy Dispersive X-Ray Spectroscopy
FWHM	Full Width at Half Maxima
hcp	Hexagonal Closed Packed
ITO	Indium Tin Oxide
MDZO	Manganese Doped Zinc Oxide
MOSFET	Metal Oxide Semiconductor Field Effect Transistors
MNDZO	Mn-Ni co-doped Zinc Oxide
ME	Monoethenolamine
NBE	Near Band Edge
NIR	Near Infra Red
NDZO	Nickel doped Zinc Oxide
PL	Photoluminescence

RI	Refractive Index
RPM	Rotation per Minute
SEM	Scanning Electron Microscope
TFT	Thin Film Transistor
TCO	Transparent Conducting Oxide
UZOTF	Undoped ZnO Thin Films
VB	Valance Band
XRD	X-Ray Diffraction
ZAD	Zinc Acetate Dehydrate
ZnO	Zinc Oxide
ZOTF	ZnO Thin Film

CHAPTER 1

INTRODUCTION

1.1   INTRODUCTION

Among the most studied materials, Zinc Oxide (ZnO) is the second most researched material after silicon. It is a material that we come into contact with every day. Paint manufacturers and paper makers use zinc white as a pigment. It is used in a variety of products in the semiconductor, solar cell and photovoltaic industries. Numerous researchers are interested in it because of its exceptional electrical characteristics, which allow it to be employed in electronic and optoelectronic devices that work in the blue and UV bands. Zinc oxide (ZnO) is a semiconductor that belongs to the II-VI group and has a melting temperature of 1975 degrees Celsius. Hexagonal wurtzite and cubic zincblende are the two major types of zinc oxide crystallization. At ambient temperatures, the wurtzite structure is the most stable and consequently the most prevalent. The zincblende structure is stable when grown on cubic lattice substrates. Each zinc atom and each oxide atom have a tetrahedral centre. Along with the wurtzite and zincblende structures, a rocksalt structure can also be grown only under pressures of about 10 GPa [1]. Non-inversion symmetry along with other lattice symmetries induces piezoelectric properties in the hexagonal and zincblende structures while pyroelectric properties in hexagonal ZnO. The lattice parameters of the wurtzite structure are a = 3.2500 Å and c = 5.2060 Å and ratio c/a $\sim$ 1.60 is very close to the ideal value 1.633 of hexagonal closed packed (hcp) structure [2].

The use of ZnO materials for short-wavelength optoelectronic devices has been extensively studied in recent years and is thought to be one of the best semiconductor material. At ambient temperature, it possesses a rather huge direct band gap of 3.37 eV, which may be further modified by extrinsic doping with other elements. Higher

breakdown voltages, the capacity to endure huge electric fields, lower electronic distortion and high temperature and high-power operation are all advantages of a wide band gap. ZnO offers several benefits including a large supply of raw materials, non-toxicity, great thermal and chemical stability, environmental friendliness and biocompatibility. The exciton binding energy of ZnO is 60 meV, which is rather high. ZnO excitons are relatively stable at room temperature and even at higher temperatures because of its substantial binding energy. ZnO materials are particularly well suited for the manufacturing of laser diodes and ultraviolet light-emitting diodes due to large exciton binding energy and wide band gap [3, 4]. ZnO is a promising resource for semiconductor device applications because of its diverse physical, mechanical and electrical characteristics. Heat-resistant windows are made with a ZnO/Al coating. It is suitable for use on polycarbonate (PC) in outdoor applications providing protection from UV rays, reducing oxidation and photo-yellowing. A ZnO thin film or nanowire can be applied to dye-sensitive solar cells and field emission devices [5–8]. ZnO has several optoelectronic uses that are comparable to that of GaN which has a similar band gap of 3.4 eV. However, ZnO has a higher exciton binding energy than GaN resulting in strong room temperature emission. ZnO nanorods can be used as conducting channels in field effect transistors [9–11]. ZnO has also emerged as a high-temperature ferromagnetic material that can be used as a dilute magnetic semiconductor in spintronics applications. Standard semiconductors with transition metal doping are used in dilute magnetic semiconductors. They have one-of-a-kind spintronics characteristics with potential technological uses. Due to its multi-functionality in opticomagnetic applications doped zinc oxides are among the finest options for DMS. ZnO-based DMS due to features like transparency in the visual area and piezoelectricity have piqued the scientific community's interest as a promising choice for the manufacturing of spin transistors and spin-polarized light-emitting diodes [12–14].

Transparent conducting oxides are a type of metal oxide that has two diametrically opposed properties: high visible optical transparency and high electrical conductivity. TCOs have been used in a variety of optoelectronic devices, including light emitting diodes (LEDs), solar cells, flat panels and flexible displays. Because of its high transmittance in the visible region and low resistivity, indium tin oxide (ITO) is the most commonly used TCO for optoelectronic applications. However, Indium's high cost and scarcity limit its use in optoelectronic devices. As a result, researchers are looking for other materials for TCO applications. ZnO thin films have high transmittance and low resistance which can be further improved by metal doping. Because of its benign na-

ture, low cost, good stability and lack of toxicity, ZnO is the most preferred material. As a result, there is a lot of interest in studying more about the electrical and transport properties of doped ZnO films, which is important for future TCO enhancement [15–18].

Even in the absence of purposeful doping, most ZnO has an n-type nature. Its origin is attributed to native defects such as oxygen vacancies or zinc interstitials. Controllable n-type doping can be accomplished by replacing Zn with group-III (such as Al, Ga, In) elements or oxygen with group-VII (such as chlorine and iodine) elements. It's still challenging to get consistent p-type doping in ZnO. This issue arises from the poor solubility of p-type dopants and their compensation by copious n-type impurities. It affects not just ZnO but also GaN and ZnSe, which are analogous compounds. The lack of p-type ZnO limits its electrical and optoelectronic use, which typically needs n-type and p-type semiconductor junctions [19, 20]. The sol-gel, CVD, PLD, RF sputtering, SILAR and spray pyrolysis are some of the synthesis processes that may be used to make ZnO thin films. Sol-gel technique is the simplest one of these. Further, the thin films produced by this method show excellent reproducibility and thermal stability. In addition to being a simple procedure, this deposition method offers several other benefits over other deposition processes including room temperature processing, cost-friendliness, reliability and ease of doping options. Thin films, powders, thick ceramics and fibres may all be made using the sol-gel process. Dip coating and spin coating are two methods to deposit thin films using the sol-gel process. In the dip coating method, the substrate is slowly dipped in the sol and then removed at a consistent pace. The substrate is uniformly coated on both sides of the dipped area. In the spin coating approach, the substrate is rotated at a constant speed and the sol is dropped on it by some means. Due to the effect of centrifugal force, the substrate is thoroughly and uniformly coated by the solution. The thin films for this study have been deposited using a spin coating technique.

1.2   CRYSTAL STRUCTURE AND LATTICE PARAMETERS

Zinc oxide can be formed into three different structures: hexagonal wurtzite, zinc blende and rock salt. Hexagonal wurtzite is the most thermodynamically stable structure at standard temperature and pressure. Under certain conditions, the other two structures, zinc blende and rock salt are also reported to emerge. The zinc blende state is stable only when grown on cubic substrates and the rock salt structure can only be

produced at extremely high pressures. ZnO's wurtzite crystal structure is illustrated in Figure 1.1. The ZnO hexagonal wurtzite structure belongs to the space group known as P6$_3$mc. This structure is made up of two interpenetrating HCP sub-lattices of Zn
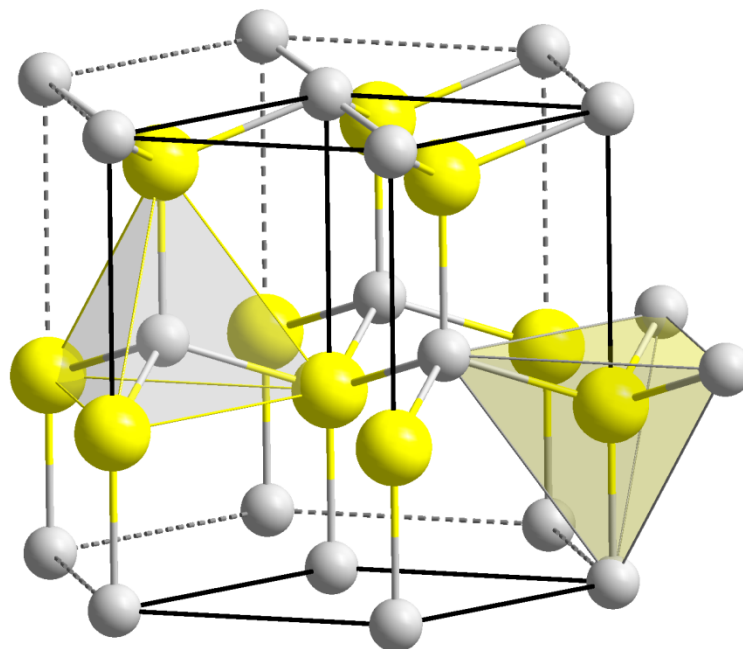
Figure 1.1: The hexagonal wurtzite structure of ZnO. Zn atoms are shown as small white spheres and O atoms as large yellow spheres.

and O atoms. Out of two sub-lattices of Zn and O, one sub-lattice displaces the other sub-lattice along the c-axis by 0.375 c. This structure surrounds each zinc ion with tetrahedra of O ions and vice versa.

It is the hexagonal axis of the tetrahedral structure that produces polar symmetry, which accounts for ZnO's piezoelectric and spontaneous polarization properties. ZnO hexagonal unit cell has lattice parameters as a=3.2499 Å and c=5.2066 Å with c/a value around 1.602. The ratio c/a deviates significantly from the standard value of c/a=1.633 for hcp structure. The four face terminations of wurtzite ZnO are the polar Zn terminated (0001) and O terminated (000$\bar{1}$) faces (c-axis oriented), as well as the non-polar (112$\bar{0}$) (a-axis) and (101$\bar{0}$) faces, which each contain an equal number of Zn and O atoms. The polar faces have varied chemical and physical properties and the O-terminated face's electronic structure is somewhat different from the other three faces. The polar and (1010) surfaces are more stable in comparison with the (112$\bar{0}$) face. Table 1.1 outlines the key physical attributes of ZnO.

Table 1.1: Key physical attributes of ZnO

Sr. No.	Property	Value
1	Stable Crystal Structure	Hexagonal Wurtzite
2	Exciton Binding Energy	60 meV
3	Energy Band Gap (E_g)	3.37 eV
4	Atomic Mass (M)	81.4 g/mol
5	Debye Temperature (TD)	837 K
6	Density (ρ)	$5.6 \times 10^3 Kg/m^3$
7	Effective Mass Electron (m_e^*)	$0.24 m_e \, Kg (m_e = 9.1 \times 10^{-31} Kg)$
8	Effective Mass Hole (m_h^*)	$0.59 \times m_e \, Kg$
9	Lattice Constants	a=b=0.324982 nm c=0.520661 nm
10	Static Dielectric Constant (ε_s)	8.75
11	Optical Dielectric Constant	3.7
12	Thermal Expansion Coefficient (α)	$6.5 \times 10^{-6} K^{-1}$
13	Electron mobility (μ_e)	200 cm^2 V^{-1} s^{-1}

1.3 ELECTRONIC PROPERTIES

ZnO has a 60 meV excitonic binding energy at ambient temperature [21], good electron mobility (205 cm^{2}V^{-1}s^{-1} [22] and a luminescence around 380 nm [23]. Interesting electronic properties of doped and undoped ZnO make it a contender for a wide range of technologically relevant applications such as photovoltaics [24], photonics [25], piezoelectrics [26], sensors [27], varistors [28], spintronics [29], LEDs [30], transparent transistors [31] and conducting electrodes [32, 33]. No matter how it is doped, ZnO is n-type, regardless of intentional doping.

1.3.1 Energy Band Gap

Several groups have estimated the band structure of ZnO. The band structure of bulk wurtzite ZnO is shown in Figure 1.2. The top of the valance band and the bottom of the conduction band both appear at k=0 indicating that ZnO is a semiconductor with a direct band gap. Zn 3d levels are represented by the bottom ten bands (which occur around~9 eV). O 2p states represent the next six bands which occur from -5 eV to 0 eV.

ZnO is characterized by a large direct band gap of 3.37 eV at ambient temperature. A large band gap has several advantages including higher breakdown voltages, the ability to endure large electric fields, lower noise and the potential to operate at high temperatures and high power. ZnO can be intrinsically doped to control its band gap between 3
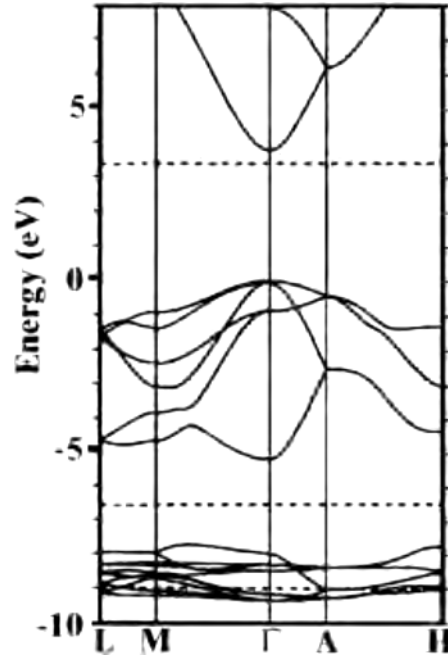
Figure 1.2: Band structure of bulk wurtzite ZnO

and 4 eV by external doping [34].

1.3.2   Intrinsic Defects in ZnO

ZnO is an intrinsically n-type material due to the presence of intrinsic defects such as oxygen vacancies (V_O) and zinc interstitials (Zn_i). In ZnO, there are various inherent point defects [35, 36]. Zinc and oxygen vacancies (V_{Zn} and V_O) and interstitials of Zinc and Oxygen (Zn_i and O_i) seem to be the most prevalent defects. These defects can be ionized by small amounts of energy, which in turn create holes and electrons. (V_{Zn} and O_i) act as acceptors and (V_O and Zn_i) as donors. Zinc vacancies cause states to form within the band gap near the valence band maximum [37]. Shallow acceptors are also formed by oxygen interstitials [38]. In n-type ZnO, the major compensating defects have been identified as V_{Zn} and O_i [36, 37]. The formation energy of oxygen vacancies is lowest among the donor defects [37]. Zinc interstitials function as a shallow donor by occupying the octahedral location in the wurtzite structure. However, since the energy required to create them in n-type ZnO is so high that they can only be formed in out-of-equilibrium conditions [37]. In a schematic band structure, Figure 1.3 displays the energy levels of such defects. The native n-type conductivity of ZnO might be explained by donor defects. [37]. However, other researchers claim that native defects are insufficient to explain ZnO's n-type character and suggest extrinsic doping by hydrogen (H) residual impurity [39].
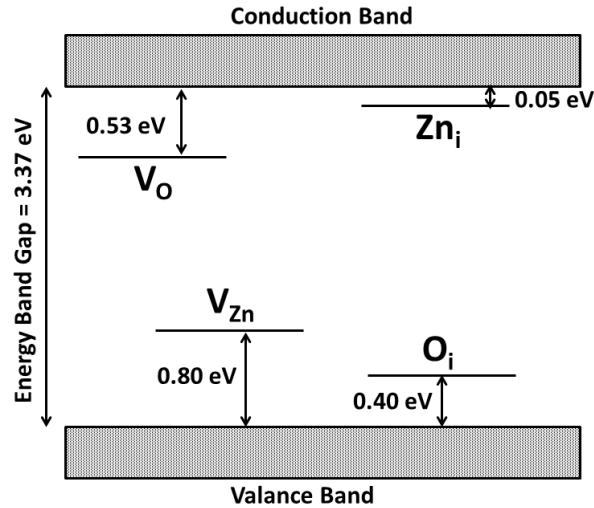
Figure 1.3: Schematic band structure of defect energy levels

1.3.3   Doping in ZnO

Extrinsic doping is required to improve the conductivity of ZnO. Dopants from group III are the most frequent dopants, whereas doping using group IV atoms has also been published [38, 40]. The dopant atom serves as a donor in each of these instances by replacing the Zn atom in the crystalline structure [37]. The dopant from group III contains an extra electron than Zn which allows it to easily ionize and generate a conduction electron in the material. The group IV elements may theoretically provide two electrons by substitution however it has been discovered that these dopants actually exist in the form of trivalent ions which provides one electron in the conduction band [40]. However, an element from Group VII, such as F can be used to replace oxygen [41]. Because F has one more valence electron than O, it may also donate an electron to the conduction band [38].

1.4   OPTICAL PROPERTIES

The optical characteristics of any material are determined by its band gap, the energy levels created by defects and impurities within the bandgap. ZnO has an energy gap of 3.37 eV, making it transparent in the visible range of radiation. The energy gap, refractive index, extinction coefficient and geometry all influence the optical properties of thin films. These parameters are impacted by the material's structure and chemical

composition. The thickness of the thin film, its uniformity and its roughness are all part of the geometry. The optical transparency is determined by the absorption edge as well as the plasma edge. The absorption edge corresponds to the band gap absorption and the plasma edge is associated with free electron plasma absorption.

The Fermi level is found in the middle of the band gap in intrinsic semiconductors. Doping in the semiconductors creates additional energy levels within the forbidden gap near the conduction band and valance band. The charge carriers are introduced in the conduction band of semiconductors by these additional energy levels. The increase in the electron concentration causes the shift in Fermi level E_F towards the conduction band given by equation

$$E_F - E_C = \frac{\hbar^2}{2m_e^*} \frac{\hbar^2}{2m_h^*} (3\pi^2 n_e)^{\frac{2}{3}} \tag{1.1}$$

Where E_C, m_e^* and n_e are the lowest energy of CB, the effective mass of electron and concentration of electron respectively. The Fermi level shifts into the conduction band because of the large concentration of electrons caused by native defects and external doping and the semiconductor is referred to as a degenerate semiconductor. The Burstein-Moss effect refers to this phenomenon. The existence of the Fermi level in the conduction band implies that the bottom states are filled in the conduction band. The band gap of a semiconductor increases as a result of the Burstein-Moss effect. The shift in the band gap is given by

$$\triangle E_{BM} = \frac{\hbar^2}{2m_e^*} (3\pi^2 n_e)^{\frac{2}{3}} \left(\frac{1}{m_h^*} - \frac{1}{m_e^*} \right) \tag{1.2}$$

The increase in the band gap due to a high electron concentration is beneficial for the transparent conductive oxide (TCO) properties of the material, as it shifts the absorption edge to a lower wavelength, expanding the transparent spectral region. Advances in deposition techniques for the fabrication of nano-dimensional structures have generated increased interest in nanostructures/nanoparticles [42–46]. The nano-dimensional thin films have applications in future optoelectronic applications due to their high transmittance in visible & NIR region, low resistivity, high chemical & physical stability [47]. The optical characteristics of ZnO films like the forbidden band gap, photoluminescence spectrum, optical transmittance and excitonic recombination can be tailored by changing the doping element and doping concentration.

1.5   ELECTRICAL PROPERTIES

ZnO is an electronically specialized wide band gap semiconductor. One of the most important characteristics of ZnO semiconductor material is its ability to be manipulated to alter its electrical, optical and electronic properties. For the application of ZnO as TCO and in optoelectronic devices, the electrical resistivity should be of the order of $\sim$ 10^{-4} Ωcm. The resistivity of pure or undoped ZnO is too high to be employed in any device. Controllable n-type doping may be achieved by substituting Zn with group-III elements and oxygen with group-VII elements [48]. The electrical conductivity of most semiconductors is given by

$$\sigma = ne\mu_e + pe\mu_h \tag{1.3}$$

The movement of carriers is principally hindered by the scattering of ionized impurities at high concentrations of electrons. The decrease in carrier mobility leads to a decrease in both conductivity and optical transmission near the infrared edge. Intrinsically, ZnO mobility and conductivity are limited by ionized impurities scattering for carrier levels exceeding 10^{20} cm^{-3}. Its vital to keep in mind, however, that the mobility not only depends on ionized impurities scattering but also on electron scattering with the lattice, neutral impurity, electron and impurity. Its still challenging to get consistent p-type doping in ZnO. This issue occurs when the p-type dopants are not sufficiently soluble and are subjected to n-type impurities, resulting in limited solubility of p-type ZnO. This impairs its ability to be used in electrical, optoelectronic and semiconductor applications, which typically require the use of p-n junctions. In a sol-gel dip coating method, *Keh-moh Lin et al.* reported a thin film of Al doped ZnO with an electrical resistivity of 7.08×10^{-3} Ωcm [49]. *Hua Wang et al.* [50] used sol-gel method with rapid thermal annealing to synthesize an Al doped Zinc oxide film and obtained resistivity of 1.2×10^{-3} Ωcm. Ga doped Zinc oxide films were prepared by *Chien-Yie Tsay et al.* [51] using sol-gel spin deposition technique on glass and found a lowest average resistivity of 2.8×10^{2} Ωcm. The magnetron sputtering technique was used by Mahdhi et al. [52] to deposit Ga-doped zinc oxide films. The minimal resistivity obtained was 2.2×10^{-3} Ωcm. Elements from group IV have also been employed as efficient donors to improve the optoelectronic characteristics of zinc oxide films. The electrical resistivity of zinc oxide films that were doped with 3% Si, synthesized by spray pyrolysis, was measured to be 3.7×10^{-3} Ωcm, as reported by *Nazanin Rashidi et al* [53]. *Zhong Yan et al.* [54]

produced Ge-doped zinc oxide thin films using a PLD method, yielding a resistivity of 6.10×10^{-4} Ωcm. *Mejda Ajili et al.* [55] achieved an electrical resistance of 8.32×10^{-2} Ωcm for Sn-doped Zinc oxide films produced using the spray pyrolysis approach.

1.6 MECHANICAL PROPERTIES

Young's and bulk modulus, piezoelectric constants, stiffness and hardness, are all examples of mechanical characteristics of a material. External forces cause solids to deform and the resulting deformation is measured as strain. The internal mechanical restoring force system that resists deformation and attempts to revert the solid to its original state is described by stress. Within the elastic limit, stress (σ) is proportional to strain (ε) and full recovery from strain is obtained by eliminating stress. According to Hooke's law, the components of the stress tensor are the linear functions of the strain tensor and are given as

$$\sigma_{ij} = C_{ijkl} \cdot \varepsilon_{kl} \tag{1.4}$$

where C_{ijkl} are the elastic stiffness coefficients. Since both stress and strain are symmetric with respect to an interchange of the suffixes and the elastic coefficients form symmetric fourth-rank tensors, there exist 21 independent elastic coefficients. In hexagonal wurtzite crystals, due to symmetry, there remain only five independent stiffness constants given as C_{11}, C_{33}, C_{44}, C_{12} and C_{13}. The elastic constants C_{11} and C_{33} correspond to longitudinal modes. The bulk modulus in terms of elastic constants can be expressed as [56]

$$B = \frac{(C_{11} + C_{12})C_{33} - 2C_{13}^2}{C_{11} + C_{12} + 2C_{33} - 4C_{13}} \tag{1.5}$$

For an isotropic approximation of structure, Young's modulus (Y), shear modulus (G) and Poisson's ratio can be written as

$$Y = 3B(1 - 2v), \quad G = \frac{Y}{2(1+v)}, \quad and \quad v = \frac{C_{13}}{(C_{11} + C_{12})} \tag{1.6}$$

Table 1.2 gives a brief overview of useful and well accepted parameters describing the mechanical properties of ZnO. As seen from the table, ZnO is a relatively soft material, with a hardness of ~ 5 GPa at a plastic penetration.

ZnO is a somewhat soft substance with a hardness of around 4.5 Mohs [57]. The elastic constants of ZnO are lower than those of other III-V group compounds, such as GaN.

Table 1.2: Mechanical properties of *c*-axis oriented Wurtzite ZnO

Sr. No.	Parameter	Values	Theoretical Value
1	Bulk Young's modulus, Y (GPa)	111.2±4.7	
2	Bulk hardness, H (GPa)	5.0±0.1	
5	Bulk modulus, B (GPa)	142.4	156.8
11	C_{11} (GPa)	209	246
12	C_{33} (GPa)	216	246
13	C_{12} (GPa)	120	127
14	C_{13} (GPa)	104	105
15	C_{44} (GPa)	44	56
16	e_{33} (Cm^{-2})	0.96	1.19
17	e_{31} (Cm^{-2})	-0.62	-0.55
18	e_{15} (Cm^{-2})	-0.37	-0.46

Ceramics are well suited to benefit from the properties of Zinc Oxide (ZnO), such as its high heat capacity, heat conductivity, low thermal expansion and high melting temperature [58]. Because of the orientation of the basal planes, there are several crystal orientations of ZnO that affect mechanical characteristics [59]. Bulk Zinc oxide with an a-axis orientation with just a hardness of roughly 2 GPa, is substantially softer than c-axis material.

1.7   PIEZOELECTRICITY

Piezoelectricity is also a significant mechanical characteristic. Among the tetrahedrally tied semiconductors, ZnO possesses the greatest piezoelectric characteristics [60]. This property makes it an important material for many applications that need a high level of electromechanical resonance. In the presence of stress, electrical polarization (P_i) is generated in piezoelectric crystals. The piezoelectric strain coefficients e_{ijk} and the piezoelectric stress coefficients d_{ijk} are connected to electric polarization as

$$P_i = e_{ijk}\varepsilon_{jk} = d_{ijk}\sigma_{jk} \tag{1.7}$$

Where d_{ijk} are known as electromechanical constants. Mechanical strain can also be produced if an electric field E_k is applied to a crystal, as $\varepsilon_{ij} = d_{ijk}E_k$. In ZnO hexagonal wurtzite structure, due to symmetry piezoelectric tensor has three components denoted as e_{31}, e_{33} and e_{15} [61]. The piezoelectric constants e_{33} and e_{31}, are the measure of polarization generated along the c-axis and basal plane respectively by a strain along

these axes and is given by relation [62]

$$P_z^{\text{piezo}} = e_{33}\varepsilon_z + e_{31}\varepsilon_\perp \tag{1.8}$$

where the strains along the c-axis and basal planes are denoted by ε_z and $\varepsilon_\perp$ respectively. The third piezoelectric constant e_{15} is generated by shear strain. The wurtzite form of ZnO has low degree of symmetry and therefore it yields spontaneous polarization along the c-axis. ZnO has the greatest piezoelectric tensor among tetrahedrally linked materials, even bigger than GaN and AlN, indicating that it is a good choice for device applications needing significant electromechanical coupling. This feature makes it a crucial material for many piezoelectrical systems that need a high electromechanical correlation. The three piezoelectric stress coefficients, e_{ik} for wurtzite ZnO [63, 64], have been determined via theoretical and experimental research and a selection of these values, as well as the elastic constants c_{hk}, are presented in Table 1.2.

1.8   VIBRATIONAL PROPERTIES

Table 1.3: Phonon mode frequencies of ZnO measured from Raman Spectroscopy and theoretically calculated value

Sr. No.	Phonon Modes	Frequency (Cm^{-1})	
		Raman Spectroscopy	**Theoretical Calculation**
1	$A_1(TO)$	380	382
2	$E_1(TO)$	409	316
3	$A_1(LO)$	574	548
4	$E_1(LO)$	587	628
5	E_2^{low}	102	98
6	E_2^{high}	438	433
7	B_1^{low}		261
8	B_1^{high}		552

The vibrational properties of ZnO can be explored by Raman scattering technique. There are a total of 12 phonon modes in the hexagonal wurtzite structure of ZnO. These include six TO modes, three LO, two TA and one LA. Group theory predicts that for hexagonal ZnO there are 8 ($2A_1$, $2B_1$, $2E_1$, $2E_2$) normal phonon modes at Γ point out of which A_1 & E_1 are acoustic and 6 (A_1, $2B_1$, E_1, $2E_2$) optical phonon modes. E_2 mode at Γ point is denoted as E_2^{high} representing the higher frequency branch and E_2 mode at

low frequency is termed as E_2^{low}. The vibration of the Zn lattice is related with the low-frequency E_2^{low} mode, whereas the oxygen atoms are involved in the high-frequency E_2^{high} mode. A_1 and E_1 phonon modes are both Raman and infrared active while E_2 phonon modes are only Raman active. B_1 modes are inactive modes. Only $A_1(LO)$ and E_2 modes are seen for normal incidence of light to the surface in strongly oriented ZnO thin films, whereas other modes are forbidden. Table 1.3 shows the comparison of phonon Mode frequencies of ZnO measured from Raman spectroscopy and infrared spectroscopy with theoretically calculated values.

1.9   PROBLEM STATEMENTS

ZnO is a material that has a lot of potential for its applications in optoelectronic semiconductor devices. The fabrication of optoelectronic devices such as LEDs and LASERs requires both n-type and p-type semiconductors. As we know n-type ZnO can be easily obtained. Even the Native defects, such as Zn interstitials and Oxygen vacancies, without any extrinsic n-type doping, can produce n-type ZnO. However, doping ZnO with p-type to make highly conducting p-type ZnO is very challenging. This might be owing to the p-type dopants' limited solubility in ZnO. As a result, the fundamental constraint to the manufacturing of ZnO-based devices is the lack of acceptable p-type ZnO. In 1997, the first report on p-type ZnO was published; however, the mobility and hole concentration were both found to be too low. *J. G. Lu et al.* [65] achieved p-type doping of ZnO using a Li-N dual acceptor doping, which was deposited via pulse laser deposition. They achieved the resistivity of 0.93 Ωcm, Hall mobility of 0.75 cm^2/Vs and a hole concentration of 8.92×10^{18} cm^{-3}. *Rajib Sahu et al.* [66] prepared the B and N co-doped Zinc oxide films by PLD method and achieved 3×10^{18} cm^{-3} of hole concentration and mobility of 10 cm^2/Vs for p-type conductivity. *Kong Chun-Yang et al.* [67] fabricated p-type Zinc oxide films by co-doping of In and N using the magnetron sputtering method together with direct implantation of nitrogen acceptor dopants and reported hole mobility and concentration of 2.19 cm^2/Vs and 1.22×10^{18} cm^{-3} respectively. Although p-type ZnO were reported with appreciable hole concentration, mobility and resistivity, but still the reported resistivity is not up to the desired level. Stability, reproducibility and durability over long time periods remain challenges to be addressed in the future.

1.10 RESEARCH OBJECTIVES:

- To prepare Zinc Oxide (ZnO) thin films by different deposition methods.

- To prepare doped ZnO thin films by various method viz Thermal evaporation method, Sol-Gel method, Spray pyrolysis method etc.

- To find the best doping elements to have maximum transmittance and lowest resistivity to be used as TCO.

- To optimize doping levels to find maximum transmittance and lowest resistivity.

- To optimize the thickness of ZnO thin films prepared by different methods to have best TCO properties.

- To determine optical and electrical parameters like dielectric constant, absorption coefficient, refractive index and resistivity experimentally as well as theoretically and compare both the results.

- To calculate and study, electronic band structure and density of states (DOS) for various doped ZnO films.

- By getting all the parameters experimentally and theoretically, efficient & effective results will be used for future applications in various devices.

In this work undoped, doped and co-doped ZnO thin films are fabricated by sol-gel route utilizing spin coating method at 1000, 2000, 3000, 4000, 5000 and 6000 rpm rotating speed. For this we have chosen many elements Al, Mn, Co and Ni for doping in ZnO host matrix. Ni-Al & Mn-Ni were selected for co-doping in ZnO films synthesized by sol-gel method using spin coating approach. The effect of doping and co-doping is studied on optical, micro-structural, surface morphology, vibrational and luminescence characteristics of ZnO films. The effect of annealing temperature has also been studied on Mn-Ni co-doped ZnO films.

The thesis is organized in the following manner. The first chapter covers the basics of undoped and doped Zinc Oxide (ZnO) thin films, as well as their many properties and applications. The second chapter reviews the literature on the characterization of undoped and doped zinc oxide thin films deposited using various procedures. The third chapter focuses into the materials, deposition process and characterization techniques employed in this study. The proposed experimental work of synthesis, characterization

and outcome of undoped ZnO thin films is presented in the fourth chapter. The fifth chapter details the fabrication, characterization and results of Ni, Al, Co and Mn doped ZnO thin films. The sixth chapter describes the preparation of co-doped thin films using the pair of dopants Ni-Al and Mn-Ni, as well as their characterization and findings. The seventh chapter discusses the conclusions of the work as well as the future scope of work.

CHAPTER 2

LITERATURE SURVEY

2.1 INTRODUCTION

Lately, zinc oxide semiconductor materials have become more and more popular, as seen by an increase in publications. Its potential for optoelectronic applications is attributed to its huge forbidden band gap ($E_g \sim 3.37$ eV) which is what drives ZnO's interest in optoelectronics. ZnO has the potential to be used as a substitute for GaN because of the additional advantages of large excitonic binding energy (~ 60 meV), abundance and low cost [68]. Moreover, ZnO-based devices are cheaper due to simpler crystal-growth techniques such as sol-gel. Additionally, ZnO is more radiation stable and more adaptive for space applications over other large energy gap materials. Moreover, extrinsic doping is able to enhance the electrical properties of zinc oxide while retaining its optical transparency simultaneously. This makes it suitable for transparent conducting oxide which has applications in displays and solar cells [69–71]. A novel material called dilute magnetic semiconductor (DMS) emerges from wide band gap semiconductors such as ZnO when doped with magnetic atoms. DMS exhibits high-temperature ferromagnetism and has potential applications in spintronics and opticomagnetics [72–74]. The next dimension in the electronic industry is transparent electronics which will be the base for the new generation of optoelectronic devices. Thin film transistor based on Si has some limitation like sensitivity to visible light while ZnO transistors are transparent to visible light and hence the protective layer required for the prevention of light can be abolished [31, 75].

Studies of optical properties are concerned with how light interacts with a material. The intrinsic properties of ZnO directly correlate with the interaction of charge carriers present in the conduction band, the valence band and the defect states within the band

gap. Extrinsic optical properties directly relate to the position and nature of the discrete energy levels created in the band gap by intentional doping. The optical properties of ZnO can be studied by absorption, transmission, reflection and emission spectroscopy. Photoluminescence is one of the best technique used for the analysis of the optical behaviour of ZnO. The ultra-violet emission is predominantly observed in the photoluminescence (PL) of ZnO thin films and is attributed to a near band edge transition. Additionally, a green emission band is present, which is attributed to interstitials, anti-sites, vacancies, and their combinatorial complex defects [76–78].

Dye sensitized solar cells (DSSCs) has been evolved as the alternative to traditional Si-based solar cells which operates on the principle of photo voltaic effect. The popularity of dye sensitized solar cells is supported by their low cost, eco-friendly and simple fabrication process. Dye sensitized solar cells mainly made up of a semiconductor layer with dye, an electrolyte coat and a conducting counter electrode. A large band gap semiconductor with a porous structure and high mobility is the core element of DSSC. Till date TiO_2 nano-particles layer has been used as the photoanode because of its large surface area and high efficiency. Other oxides such as ZnO, SnO_2, $BiVO_4$, In_2O_3, Nb_2O_5 are also used as photoanode but ZnO has presented its candidature to replace the TiO_2 due to low cost, lower recombination rate and low resistance. The main hindrance for the ZnO is the low conversion efficiency of DSSC, which can be enhanced by increasing the light absorption ability of the photoanode and increasing the recombination time. Understanding the creation and recombination of photoexcited carriers in DSSCs is required for photoelectric transformation. In ZnO-based DSSCs, doping, surface morphology and heterostructure play a key role in the performance. Doping is a powerful method for altering the electrical and optical characteristics of ZnO nanostructures and thereby increasing their efficiency [79–82].

Conventional solar cells work on p-n junction of silicon and are mostly used due to their efficiency and reliability but high cost limits their application. Organic and hybrid solar cells are new generation solar cells which are comprehensively explored because of their low cost, flexibility and solution based processing. In a hybrid solar cell, organic p-type semiconductors and inorganic n-type semiconductors are utilized as active layers. ZnO has been identified as an ideal n-type semiconductor layer for use in hybrid solar cells, due to its non-toxicity, low cost and ease of fabrication using simple techniques [83]. Moreover, thin film solar cells use CdS as the layer of buffering which is toxic and not eco-friendly. ZnO can substitute the CdS buffer layer in solar cells as it is non-toxic and has other suitable properties [84]. It has been established that thin films

of zinc oxide could be used for making Resistive Random Access Memory (RRAM) devices, a viable alternative to charge-based flash memory [85]

ZnO is often suggested as a GaN substitute for device applications because of its cheaper production cost and improved optical characteristics. ZnO may be considered a promising material for the fabrication of LED in the ultraviolet range owing to its high excitonic binding energy. Reproducible and stable p-type Zinc oxide is still an obstacle for ZnO-based semiconductor devices. Therefore many devices which do not require p-type ZnO were fabricated. ZnO has numerous applications based on electrical, optical and other properties.

2.2   LIGHT EMITTING DIODES

An LED is a semiconducting diode, which when biased converts electrical energy into light energy. This is done by the recombination of a hole and an electron. The frequency of light is computed by the forbidden band gap of the semiconductor. ZnO exhibits similar characteristics to those of the other common semiconductor materials used for LED emission, such as GaN and ZnS, which are employed for green and UV emission, respectively [86]. The first Zinc oxide-based heterostructure LED was synthesized in 1968 employing Cu_2O as the p-type material [87]. Due to the lack of p-type Zinc oxide, p-n homojunction LEDs based on ZnO cannot be realized. This problem can be resolved by using n-type ZnO and other p-type materials like Si, GaN, Cu_2O, NiO, CdTe, SiC to form p-n heterostructure for LEDs fabrication. *Ricky W. Chuang et al.* [88] fabricated heterostructure of Zinc oxide on GaN utilizing the vapor cooling condensation system. They fabricated two heterojunction LEDs of structures *p*-GaN/*n*-ZnO:In (*p-n*) and *p*-GaN/*i*-ZnO/*n*-ZnO:In (*p-i-n*). Both heterojunction (*p-n* and *p-i-n*) light emitting diodes show rectifying behaviour. Peak emission of electroluminescence at 385 nm wavelength was observed due to ZnO layer. Heterojunction light emitting diode of *n*-ZnO/*p*-AlGaN was fabricated by Ya. I. Alivov et al. [89] on n 6H-SiC substrates. *p*-type AlGaN was grown using hydride vapor phase epitaxy and the n-type Zinc oxide layer was grown by CVD method. A stable UV emission with a peak at 389 nm was perceived in forward biased with a threshold voltage of 3.2 volts originated from recombination within the ZnO. *Daotong You et al.* [90] fabricated n-ZnO/AlN/p-GaN heterojunctions light-emitting devices and observed ultraviolet emission at 387 nm wavelength. LEDs based on ZnO p-n homojunction were also fabricated by many researchers. Do-Kyun Kwon et al. [91] successfully fabricated LEDs with n-type ZnO

nanorods/Ag-doped p-type ZnO NRs by low-temperature solution process. The homo-junction LED shows rectifying behaviour and has a turn on voltage of 3.5 V. The LED emitted a broad yellow emission peak at 645 nm at a forward bias of 9 V.

2.3   TRANSPARENT CONDUCTING OXIDES (TCO)

Transparent Conducting Oxides (TCO) are technologically of great importance due to their high transparency in the visible spectrum and low electrical resistivity. This class of material has applications in the semiconductor industry in transparent electrodes, transparent contact for solar cells, liquid crystal devices, optoelectronic devices, displays, and touchscreens. Indium doped tin oxide (ITO) is widely utilized as TCO in the industry because of its low electrical resistivity and high transparency in the visible spectrum. But the high cost, toxicity and scarce resources of Indium are the drawbacks of Indium doped tin oxide (ITO). ITO cannot fulfil the growing demand for thin film transparent electrodes; therefore a suitable alternative for TCO material is required. ZnO based transparent Conducting Oxide (TCO) could be a good alternative to ITO because of its high transparency and low resistivity in the visible spectrum, low processing temperature, good etch-ability and high reproducibility. The synthesis of zinc oxide transparent conductive oxide (TCO) films has been achieved with a range of dopants; however, Al-doped and Ga-doped ZnO films have proven to possess the highest levels of conductivity and carrier concentration. *Hideaki Agura et al.* [92] grown the Al-doped Zinc oxide thin film on glass by PLD technique and obtained the low resistivity value of 8.54×10^{-5} Ω.cm. *Sang-Moo Park et al.* [93] synthesized Ga-doped ZnO films by PLD technique. The films exhibit low resistivity of 8.12×10^{-5} Ω.cm and 1.46×10^{22} cm^{-3} carrier concentration. *Amaresh Das et al.* [94] fabricated undoped ZnO films by sol-gel method. The films have been implanted with Al ions. The films exhibit resistivity of 6.81×10^{-2} Ω.cm, electron concentration of 1.29×10^{19} cm^{-3} with mobility of 7.08 cm^2/Vs.

2.4   THIN FILM TRANSISTOR

Metal oxide semiconductor field effect transistors (MOSFET) are what thin film transistors (TFTs) are. TFTs are made by the deposition of an active semiconductor layer, a dielectric layer and metallic contacts on an insulating substrate. There is the widespread use of thin film transistors in displays, liquid crystal displays and smartphones. ZnO has been investigated as an active channel layer for transparent thin film transistors.

Organic TFTs have been shown to deteriorate under atmospheric circumstances, while amorphous silicon TFTs have been shown to have some optical application constraints, such as sensitivity to light, light deterioration and opacity [95]. In contrast, ZnO TFTs have good chemical and thermal stability, as well as strong field effect mobility, decreased light sensitivity and excellent transparency within the visible light spectrum. As a result, thin films based on ZnO show potential to be used for TFTs. Because of the large band gap, ZnO TFTs do not interact with visible light and their properties do not deteriorate by exposure of visible light, while amorphous Si TFTs do. *Jyh-Liang Wang et al.* [96] synthesized Zinc oxide based TTFT by hydrothermal technique. The aluminium-doped ZnO seed layer was used to grow the ZnO active channel laterally. By annealing in an oxygen environment, good field-effect mobility of 9.07 cm^2/Vs, 2.25 V of threshold voltage, 10^6 on/off current ratio and leakage current of less than 1 nA were obtained. Transparent ZnO-based TFTs were fabricated with optical transparency of 75% in the visible region of radiation by R L Hoffman et al [97]. Excellent drain current saturation, 10^7 on/off current ratio and n-channel enhancement mode TFT were all indicated by V-I measurements. *Young Hwan Hwang et al.* [31] created a TFT using a simple and cost friendly solution method for growing the ZnO channel layer. The TFT operated in depletion mode, exhibits n-type character, high transparency ($>$90%), mobility of 9.4 cm^2/Vs and on/off current ratio of 10^5.

2.5   SENSORS

A gas sensor is an electronic nose that can smell (detect) the various gas or liquid molecules present in the environment. It is usually used for industrial and environmental applications due to small size, cost-effectiveness and user friendly operation. The sensor's gas detecting method includes ambient oxygen adsorption on the oxide surface, which removes electrons from the semiconducting material, resulting in a change in carrier density and conductivity. Adsorbed oxygen concentration and hence conductivity change when interacting with oxidizing or reducing gases. A measure of gas concentration is the change in conductivity. The use of nanostructured materials is predicted to improve gas sensing properties since the gas sensing process involves a surface response [98, 99]. The sensor takes use of the increased surface area seen in all nanoscale materials, including ZnO nanorods. Changes in the characteristics of nanorods, such as luminescence, conductivity, frequency of vibration and mass, can be used to identify molecule adsorption. The most basic and widely used approach

involves passing an electrical current through nanorods and observing how it changes when exposed to the gas. *Kim et al.* [100] produced ZnO nanowires with Platinum and Palladium functionalization's. The sensors were set to self-heat in order to lower the operational temperature. At ambient temperature, Pt-functionalized nanowires have a maximum sensing response of 2.86 for 50 ppm toluene, whereas Pd-functionalized nanowires have a maximum sensing response of 2.20 for 50 ppm benzene. The development of a Schottky barrier, which offers additional adsorption sites on the sensor surface, might be the sensing process. *Chen et al.* [101] used a hydrothermal technique to grow Pd nanoparticles functionalized ZnO nanowires with (0, 1, 2 and 5% Pd) and used them for NO_2 gas sensing. At 100 ^{o}C, the sensor had a quick response time for 1 ppm and a high sensing response of 13.5. The combined impact of chemical and electrical processes resulted in improved sensing.

2.6 DILUTED MAGNETIC SEMICONDUCTORS

Since the 1970s, researchers have been focused on the transition metal doped metal oxide semiconductor. The addition of the local magnetic moment to the systems by substituting transition metals on a host element paves the way for spintronics or spin electronics. As a result, dilute magnetic semiconductors (DMSs) are known to occur in existing semiconductors with magnetic impurities. The fundamental issues of spintronic materials are that I they should keep their ferromagnetic properties above room temperature and (ii) they should offer potential improvements over current technologies. The discovery of giant magnetoresistance (GMR) was the catalyst for spintronic device research. Because of the extraordinary optical and magnetic characteristics of transition-metal oxides (TMOs), the design and development of TMO-based spintronic devices is rapidly rising in contrast to non-oxide semiconductors. ZnO-based DMS materials have already garnered a lot of attention due to their ease of band gap tailoring with the right dopants. With the potential to produce and regulate spin-polarized charge carrier transport, ZnO-based spintronic devices may be effectively realized. Despite the fact that a significant number of studies are being conducted throughout the world, obtaining a higher transition temperature remains a difficult challenge. Theoretical efforts, such as first-principles studies, provide some insight into the underlying physics of these events. Substrate effects, the role of post-annealing on secondary phase development and the effect of dopants are among the key aspects to be considered while analyzing growth parameters. *D. Anbuselvan et al.* [102] grew Ni-doped ZnO nanopar-

ticles to better understand the influence of Ni-doped ZnO nanoparticles on the ferro-magnetic property of ZnO, especially at room temperature. Magnetic properties of 3% Ni-doped ZnO nanoparticles show an intense ferromagnetic property at room temperature. *Dandan Wang et al.* [103] synthesized Nd-doped ZnO nanowire arrays with stable room temperature ferromagnetism and a high coercivity of 780 Oe. *R. Elilarassi et al.* [104] used sol-gel auto-combustion technique to successfully produce DMS ($Zn_{1-x}Fe_xO$) nanoparticles with various doping concentrations. At room temperature, magnetic measurements revealed that all of the samples are ferromagnetic.

2.7   VARISTORS

A varistor is an electrical device which has diode like non-linear current voltage behaviour. Varistors can be used to protect sensitive components from electrical surges. ZnO varistors exploit the resistance and capacitance characteristics of grains and grain boundaries of polycrystalline pellets. At low voltages, current transport is dominated by the inter-granular regions, with a breakdown voltage of 2-3 V per grain. At higher voltages, barrier height narrows and electron tunnelling occurs, accompanied by a large increase in the current flow. The density of grain boundaries in the varistor and the inclusion of dopants that migrate to the grain boundary, modify the barrier height may all be used to regulate the breakdown voltage [105]. A typical grain size and device thickness of a varistor is $\sim$10 μm and 1.6 mm respectively. The current may change up to 11 orders of magnitude with a variation of voltage of around a factor of 3.

2.8   PIEZOELECTRIC DEVICES

ZnO shows excellent piezoelectric properties having piezoelectric strain coefficient, d_{33} $\sim 10 \times 10$ CN^{-1}[60]. Piezoelectricity can be employed in several devices like a surface acoustic wave and piezoelectric devices [106]. SAW devices are used in cell phones and telecommunication stations. These have applications as torque and pressure sensors in the automotive industry, chemical sensors in the medical industry. SAW devices have high sensitivity, low cost and high weariblity. Some sensors can now be integrated without a power source. An electrical contact on insulating ZnO film induces a mechanical deformation. The insulating wave is detected by a metal finger contact as it travels at the speed of sound along the ZnO film surface. With a typical wave velocity of 3 km/s, signals with high frequency (10 MHz - 10 GHz) can be transformed to SAW [107].

MATERIALS, DEPOSITION TECHNIQUE AND CHARACTERIZATION TOOLS

3.1 INTRODUCTION

This chapter deals with the materials, fabrication technique and characterization tools used in the experimental study of undoped, doped, and co-doped Zinc Oxide thin films fabricated by sol-gel technique. A description of the instruments UV-Vis spectrophotometer, Raman spectrometer, X-ray diffractometer, spectrofluorometer and scanning electron microscope is provided in the following sections.

3.2 MATERIALS: SOURCES AND PURITY

Table 3.1 lists the chemicals utilized in the fabrication of undoped ZnO, doped ZnO (Ni, Al, Mn and Co) and Ni-Al, Mn-Ni co-doped ZnO thin films.

3.3 DEPOSITION TECHNIQUE

3.3.1 Sol-Gel Method

Sol-gel is a solution-based chemical process for fabricating thin films, solid powders, ceramics and other materials. This technique is mainly used for the formation of metal oxides. It entails the formation of a colloidal solution (sol) from organic and inorganic precursors, which evolves into a diphasic system with both liquid and solid phases, known as a gel. Metal alkoxides and alkoxysilanes are the popular precursors for the formation of sol in organic or aqueous solvents. Obtained sol gets polymerized with time to form the gel. During the sol formation, the parameters like pH, temperature,

Table 3.1: Source of procurement and purity of the chemicals used

Sr. No.	Chemicals	Source	Purity(%)
1	Zinc Acetate Dihydrate $(Zn(CH_3COO)_2 . 2H_2O)$	Molychem	99.5
2	Nickel Acetate Tetrahydrate $(Ni(CH_3COO)_2 . 4H_2O)$	Molychem	98.0
3	Aluminium Chloride Hexahydrate $(AlCl_3.6H_2O)$	Thomas Baker	99.5
4	Cobalt Acetate Tetrahydrate $(CH_3COO)_2.Co.4H_2O$	Thomas Baker	99.0
5	Manganese acetate tetrahydrate $(CH_3COO)_2.Mn.4H_2O$	Molychem	99.5
6	2-methoxy ethanol $CH_3O.CH_2.CH_2.OH$	Molychem	99.5
7	Monoethanolamine C_2H_7NO	Thomas Baker	99.5
8	Diethanolamine $[CH_2(OH)CH_2]_2NH$	Thomas Baker	99.5

concentration, reaction time and ageing time for gel formation can control the structural, electrical and optical properties of the end material. Many techniques can be utilized to convert the final gel to desired solid material like aerogel, zerogel, nanopowder, or nanostructured thin film. To fabricate the thin film on substrates using sol-gel, spray pyrolysis, dip and spin coating method can be utilized. For the fabrication of thin films using the spin coating method, the sol solution is dropped by dropper on the rotating substrate. In this process the substrate is uniformly coated with the sol. In the subsequent steps the film is dried to remove the organic solvents from the material and then annealed at a desired temperature to finally get the required film. Film thickness, annealing time and temperature decide the crystallinity and properties of the obtained thin film. Dip-coating, in which the dipped substrate is taken out of the solution at a steady speed, is the simplest approach for the production of thin films. The solution spreads on both sides of the substrate homogeneously due to the effect of viscosity and surface tension. The rest of the steps are the same as those employed in the spin coating method. Another technique for the fabrication of thin films is spray pyrolysis. In this method, the sol is uniformly sprayed with the help of a nozzle on the substrate maintained at a constant temperature.

Various methods are available for fabricating thin films, including sputtering, pulse laser deposition, CVD and thermal evaporation. The major advantages of sol-gel technique of thin film fabrication over other techniques are as

a. Simple processing technique

b. High purity of precursors

c. Low temperature processing

d. Low temperature sintering

e. Ease of synthesis of homogeneous stoichiometric films

f. Control of chemical composition and microstructure

g. High purity

h. Low cost

i. Ability to coat large and complex substrate

j. No need of expensive equipment's.

The sol-gel process also has some shortcomings. It is not a very clean process as it is a wet chemical process. As it involves chemical reaction in solution, contamination of some undesired atoms and molecules is possible. Cost of precursor chemicals, shrinkage of wet gel upon drying, precipitation of a particular oxide in multicomponent glasses during the sol formation and residual porosity are some of the drawbacks of sol-gel method.

3.3.2   ZnO Thin Films Deposition by Sol-Gel Process

Zinc oxide thin films can be prepared by numerous deposition techniques but sol-gel method offers simple processing, low cost, low processing temperature and high crystallinity over the other methods. Sol-gel is a chemical method which involves the following steps: a) Hydrolysis or Alcoholysis b) condensation and polymerization c) growth of particles d) formation of gel. Thin film deposition by sol-gel method includes mainly 3 steps: a) formation of sol-gel b) deposition of solution on substrates by spin coating or dip coating technique c) drying and annealing of deposited film. The details of sol-gel approach and its components are discussed in the next section.

3.3.3 Precursors

The mostly used precursors for ZnO fabrication are Nitrate, chloride, alkoxide and acetate dihydrate. Zinc acetate dihydrate is the most frequently used salt for the ZnO thin film preparation. The synthesis of ZnO from zinc acetate involves two phases of hydrolysis and condensation. Hydrolysis of zinc acetate occurs as

$$\text{Zn(OH)}(\text{CH}_3\text{COO})_2 + \text{OH}^- \rightarrow \text{Zn(OH)}_2 + (\text{CH}_3\text{COO})^- \tag{3.1}$$
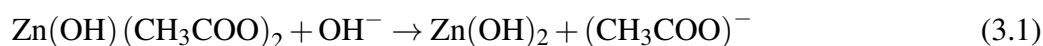
Two Zn(OH)_2 molecule condensation can be given as

$$\text{HO} - \text{Zn} - \text{OH} + \text{HO} - \text{Zn} - \text{OH} \rightarrow \text{HO} - \text{Zn} - \text{O} - \text{Zn} - \text{OH} + \text{H}_2\text{O} \tag{3.2}$$
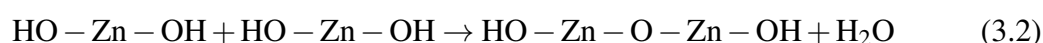
Final product HO-(Zn-O-Zn)$_n$-OH is obtained after water evaporation by the condensation of n molecules. Condensation happens uniformly throughout the substrate's plane. Annealing results in the formation of ZnO thin films.

3.3.4 Solvents

We know that the solvents with higher dielectric constant can dissolve the inorganic salts. Some of the most commonly utilized solvents include 2-methoxyethanol [108], Methanol [109], 1-butanol [110], ethanol [111], 1-propanol [112] and 2-propanol [113, 114]. The texture of the deposited films is also affected by the solvents. *Wang et al.* [115] showed that raising the concentration of ethanol in an aqueous-ethanolic solution causes the crystal orientation to change from perpendicular to roughly parallel to the substrate's surface.

3.3.5 Stabilizers

As stabilizers, chemical species containing at least one functional group can be used. Alkali metal hydroxide, carboxylic acid, alkanolamines, alkylamines, acetylacetone and polyalcohols are some of the stabilisers used to deposit ZnO [116]. They are used for a variety of purposes, including assisting in the dissolution of zinc salt in alcoholic solvents in some situations. Zinc acetate dihydrate is commonly regarded for not entirely dissolving in alcohols such as ethanol or 2-propanol. This problem can be remedied by adding stabilisers like monoethanolamine or diethanolamine [109]. Another function of stabilisers is to stabilize ligands, inhibiting zinc hydroxide precipitation and therefore assisting in the production of stable sols [116]. A transparent solution can be pro-

duced by adding monoethanolamine to zinc acetate solution [**c3r10**]. The most frequent stabilisers used in ZnO sol-gel deposition are monoethanolamine or diethanolamine. These stabilisers decrease contamination of ZnO films while also posing fewer health and environmental concerns [117].

3.3.6 Substrate Preparation

All the ZnO thin films are fabricated on soda lime glasses slides of thickness 1.3 mm. Glass substrates are cut in the 2.5 cm × 2.5 cm size. The glass substrate must be cleaned before depositing the thin films since it may contain dirt, oil, or grease deposits on its surface. Cleaning a substrate eliminates pre-deposits such as hydrocarbons and other particles or contaminants before the thin film deposition. The cleaning procedure increases adherence to the substrate, resulting in improved coating performance. Cleaning also enhances the thin film's optical or electrical properties, which might be degraded by contaminants. Inconsistencies in thin film uniformity can be caused by any type of surface contamination. In the cleaning process, the glass substrates are first cleaned with detergent by rubbing the cotton pads on the glass manually to remove any dirt, oil, grease and any hydrocarbon deposits. The glass substrates were then rinsed and washed many times with deionized water (DI) and acetone. Just before film deposition, they are ultrasonically cleaned with acetone, methanol and deionized water (DI). The glass slides were dried in an oven at 150 °C for 30 minutes.

3.3.7 Thin Film Deposition

Spin coating and dip coating are the two most prevalent techniques for the synthesis of ZnO films. Aged or fresh sol can be utilized at room temperature of around 60 °C. In this study ZnO thin films have been deposited with the help of the spin deposition technique. The undoped, doped and co-doped ZnO thin films are deposited at a substrate rotation speed of 1000rpm, 2000rpm, 3000rpm, 4000rpm, 5000rpm and 6000rpm. Most of the researchers has reported the ZnO film deposition by spin deposition technique at 3000 rpm substrate rotation speed because the best results regarding physical properties and microstructure are obtained at this optimized rotation speed. The sol solution is dropped by dropper on the spinning soda lime substrate to deposit thin layers using the spin coating technique. The substrate is uniformly coated with the sol in this procedure. The film is then dried at hot plate at 100 °C to evaporate the organic solvents from the material. To achieve the necessary thin film thickness, the deposition and drying cycle

is repeated numerous times. Finally, the films are annealed at various temperatures in a tube furnace to enhance the microstructure and crystallinity of the films.

3.3.8   Pre and Post Heat Treatment

When it comes to heat treatment, a two-step approach is preferable. The solvent and organic substances are removed in the first step known as pre-heat treatment, at temperatures ranging from 40 to 500 degrees Celsius. The first step is to deposit thin films by dropping the sol with the help of a dropper on the spinning substrate. After the deposition the film is dried at 150 °C on the hot plate to evaporate the solvent organic substances. This deposition and drying procedure is repeated numerous times to get the appropriate thickness. Finally the thin film is given post-heat treatment known as "*annealing*". Annealing is necessary to improve the crystallinity of the films while also decomposing organic by-products. Depending on the substrates utilised, the annealing temperature might range from 250 to 900 °C. In this work, the annealing of all film is done at 350 °C except for the case in which the effect of annealing temperature is studied.

3.4   CHARACTERIZATION TOOLS

In this section characterization tools and techniques used for the analysis of the synthesized ZnO film will be discussed. UV visible analysis of the thin film samples is carried out by Labman Scientifics, UV visible double beam spectrophotometer (LMSP-UV 1900S). Raman Spectrophotometer (EnSpectr R532) is used for the analysis of the vibrational study. The structural study has been done by X-ray diffractometer (Rigaku Ultima IV). Luminescence spectra are obtained using Spectrofluorometer (FluoroSENS Camlin Photonics). SEM was used to do topographical analysis on the thin films.

3.4.1   UV-Visible Spectrophotometer

Labman Scientifics, UV visible double beam spectrophotometer (LMSP-UV 1900S) was used to record the UV-visible spectra of undoped and doped ZnO thin films. The image of the instrument used is given in Figure 3.1.

Figure 3.1: Actual photograph of UV visible double beam spectrophotometer (LMSP-UV 1900S, Labman Scientific)
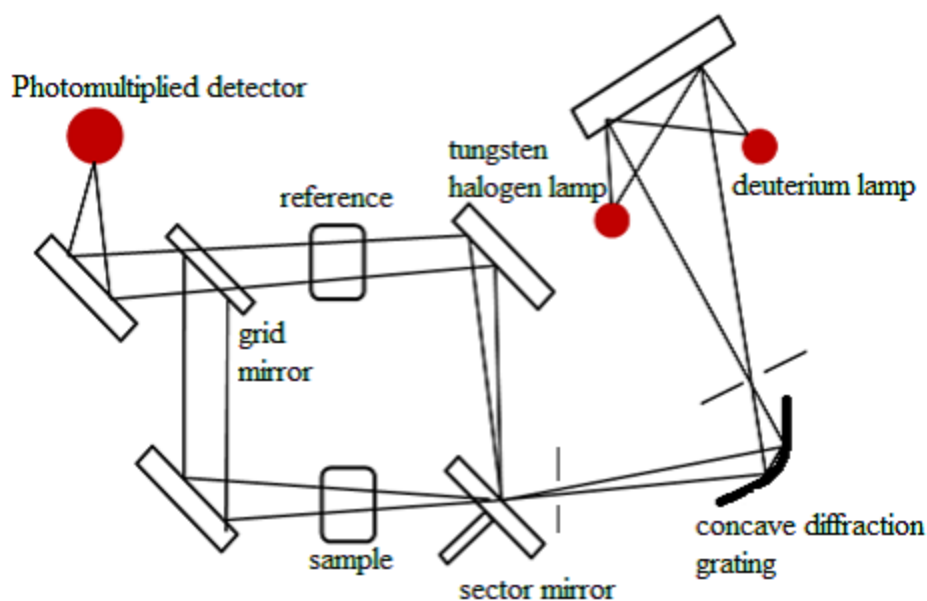
Figure 3.2: Block Diagram of the Spectrophotometer

A light beam is incident on the sample to transmit through it and the wavelength of the light reaching the detector is measured. The measured wavelength provides important quantitative and qualitative information about the sample. Information may be obtained as transmittance, absorbance or reflectance of radiation in wavelength range [118, 119]. The electrons jump to excited states or the anti-bonding orbitals by absorption of incident light photons when the energy of the light photon matches the energy gap between the initial and final state. This process is known as absorption and is the basic operating principle of absorption spectroscopy. The spectrophotometer consists of five parts:

1) Light source (Halogen or deuterium lamps)

2) Monochromator

3) Sample compartment

4) Detectors

5) Display or Recorder

In spectrophotometer, the light from the lamp is incident on the monochromator's entry slit, where the collimating mirror sends the beam onto the grating in a spectrophotometer. The grating disperses the light beam to generate the spectrum, with a collimating mirror focusing a portion of it on the monochromator's output slit. The beam is then transmitted via one of the filters to a sample compartment. The beam is transmitted to the silicon photodiode detector after exiting the sample chamber, causing the detector to generate an electrical signal that is shown on the digital display. The block diagram of a UV visible spectrophotometer is displayed in Figure 3.2.

3.4.2   Raman Spectrophotometer (EnSpectr R532)

Raman spectroscopy has been used to do the vibrational investigation of the deposited thin films. The Raman spectrum is analyzed by Enspectr Raman spectrometer at a wavelength of 532 nm. When light photons interact with molecules, the scattered photons may have a different frequency than the incident photons. Stokes radiation refers to photons with a lower frequency, whereas anti-stokes radiation refers to photons with a higher frequency. Because anti-Stokes scattering requires the molecules to be in an excited state, the intensity of anti-Stokes scattering is often less than that of Stokes radiation. As a result, just the Stokes radiation is typically recorded. Figure 3.3 depicts a Raman scattering energy level diagram.

A rotation or vibration must change the electric dipole of the molecule in order to be infrared or microwave active. Raman activity requires a change in the molecular polarizability associated with molecular rotation or vibration. Figure 3.4 shows a schematic illustration of a traditional Raman spectrometer.

EnSpectr is an easy-to-use instrument that can be operated by a user without any special technical training. The test sample is exposed to 532 nm laser, the light scattered from the films is investigated simultaneously. In the device, the scattered light is filtered. The filtered emission gets onto the diffraction grating and then onto the CCD-line. An actual optical image of Raman Spectrometer (EnSpectr R532) is shown in Figure 3.5. The
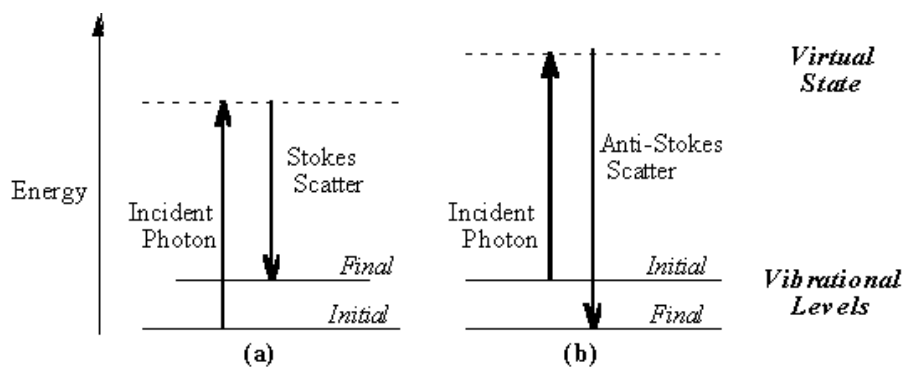
Figure 3.3: Energy level diagram for Raman Scattering; (a) Stokes scattering (b) Anti Stokes scattering
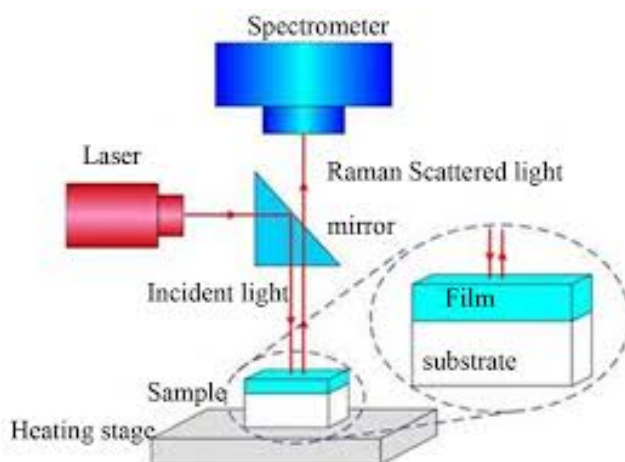
Figure 3.4: Schematic diagram for conventional Raman spectrometer

substance subjected to laser emission is identified by analysis of the spectrum using the computer program. The device consists of a laser source, a Czerny-Turner spectrometer and an analysis system. A built-in USB controller provides PC connection and access to the data measured. The diffraction grating spectrometer has no moving parts and is rigidly fixed to the laser assembly, so it can be used for the control of substances in workrooms and field conditions. The measured spectral range of the EnSpectr device covers molecular vibration regions as well as most visible-range electron transitions of organic and inorganic compounds.

Figure 3.5: Actual optical image of Raman Spectrometer (EnSpectr R532)

In a matter of seconds the device performs measurement and analysis of the spectrum of an unknown substance, determines the spectral position and relative intensities of the Raman and luminescence spectral lines, the "fingerprints" of the substance in question. Comparison of the "fingerprints" to the spectral database of known substances enables to identify the sample as an individual substance or a mixture of substances.

3.4.3 Fluorescence Spectrometer (Fluorosens Camlin Photonics)

The photoluminescence spectra of the ZnO samples has been analyzed by Fluorescence Spectrometer (FluoroSENS Camlin Photonics). Fluorescence is a three-phase process which occurs in the orbits of electron of specific compounds known as fluorophores or fluorescent dyes. The simplified energy state Jablonski diagram in Figure 3.6 depicts the process. These three stages are:

    i. **Excitation:** A photon of energy $h\nu_{ex}$ when incident from an external source is absorbed by the fluorophore. After gaining this energy electron goes from a lower

state (E_0) to a higher state (E_1). The process of absorption takes approximately 1 fs = 10^{-15} s.

ii. **Non-radiating transitions:** The electron remains in the excited state for a life-time of typically one to ten nanoseconds. During this time, the fluorophore losses its energy within the vibrational states known as vibrational relaxation. This results in the singlet excited state which gives rise to fluorescence emission.

iii. **Fluorescence emission:** The fluorescence emission from the singlet excited state to ground state E_o occurs by the emission of photon of energy $h\nu_{fl}$ and fluorophore returns to its ground state E_o. Due to the dissipation of energy in vibrational relaxation in an excited state, the energy of this emitted photon is less than the incident photon. Therefore emitted photon has a greater wavelength than the incident photon. The difference in wavelengths between the absorption and emission maximum defines the Stokes shift given as:

$$\Delta\lambda_{Stokes} = \Delta\lambda_{Max.\ emission} - \Delta\lambda_{Max.\ absorption} \tag{3.3}$$
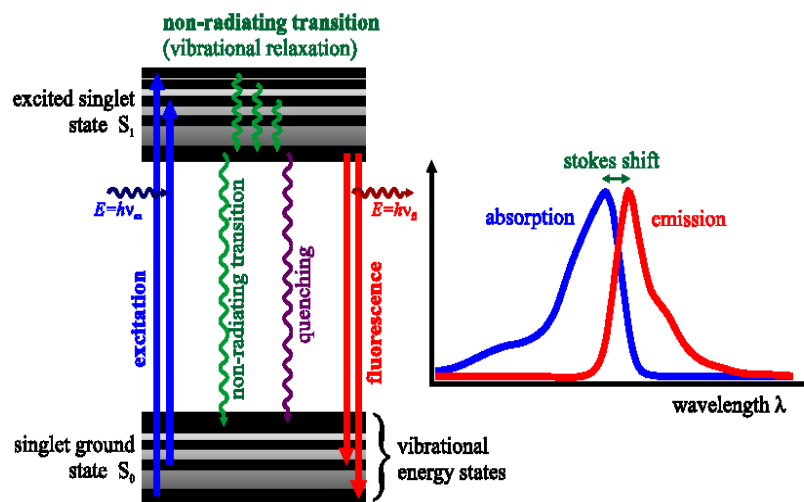
Figure 3.6: Jablonski diagram involving optical absorption and subsequent emission of fluorescence.
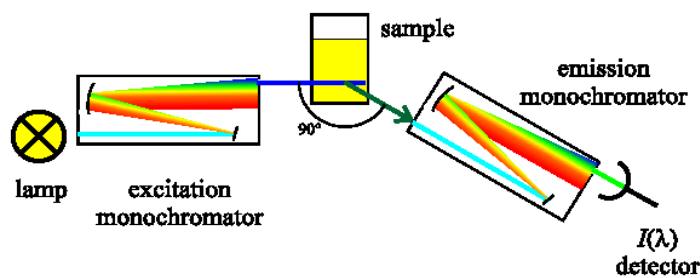
Figure 3.7: Principle of a fluorescence spectrometer

The block diagram of a fluorescence spectrometer is depicted in Figure 3.7. A monochromatic excitation light source and a detection channel are the parts of a fluorescence spectrometer, which may be used to analyze fluorescence spectra. The detection channel is perpendicular to the excitation to prevent as much detection of the emission light as possible.

Figure 3.8: Optical image of Spectrofluorometer (FluoroSENS Camlin Photonics)

Actual photograph of fluorescence spectrometer (fluoroSENS Camlin Photonics) is demonstrated in Figure 3.8. The fluoroSENS instrument is a versatile bench top fluorometer with a high resolution performance allowing for fine line structures to be easily distinguished. The single photon counting sensitivity provides an excellent signal to noise ratio of greater than 3000:1 for a water Raman peak at 397 nm. The source light is provided by an internal tunable light source (TLS) consisting of a 150W Xenon lamp and a 300mm focal length monochromator. Slits are fully adjustable and can be set to allow through a particular bandwidth of light. The output from the excitation

monochromator is directed through an adjustable iris and onto a beam splitter where the majority of light is transmitted and a small percentage is reflected onto a silicon photo-diode which is used as a reference detector. The excitation signal that is transmitted is then focused on the centre of the sample. Perpendicular to the excitation optics is the collection optics for the fluorescent signal. This is a standard arrangement as it reduces stray light and excitation light which may be transmitted through the sample. Fluorescent light from the sample is then directed through a six position filter wheel containing 5 different high pass filters and one empty slot for 100% transmission. The resultant emission data is collected by a 300 mm focal length monochromator with a photo-multiplier tube (PMT) module attached to the exit slit. This is then processed by a high speed single photon counting data acquisition board. All control electronics are internally housed. Correction data files are provided allowing both real-time and post measurement correction. This reduces the effect of any artefacts or imperfections that may be caused by the optical performance of the instrument optics or the detector response. The fluoroSENS employs a range of single photon counting detectors allowing it to cover a broad spectral range of effectively 185 to 1100nm.

3.4.4   X-Ray Diffraction

X-ray diffraction (XRD) is a special characterization tool utilized to measure the solid structure, preferred growth direction, lattice constants, crystallite sizes and quality of the crystal. In XRD X-rays of a particular wavelength is incident on the sample at a particular angle θ. The intensity of diffracted X-rays is measured with respect to the diffraction angle. The crystalline structure of the material is revealed in this way. The diffraction angle (θ), interplaner spacing of the crystal lattice (d_{hkl}) and the wavelength (λ) are related by Bragg's law [120].

$$2d_{hkl}\sin\theta = n\lambda \tag{3.4}$$

where n is diffraction order. Interplaner distance (d_{hkl}) can be calculated if the wavelength is known.
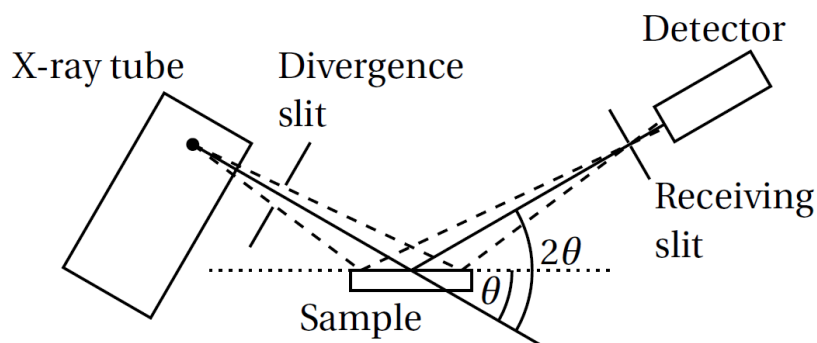
Figure 3.9: Bragg-Brentano geometry used in XRD

The Miller indices, denoted by (hkl), represent the orientation of the crystallographic plane. Various different geometries can be used in XRD, but the Bragg-Brentano geometry is most popular for $\theta/2\theta$ scans [121]. Figure 3.9 illustrates this geometry schematically. The angle of incidence (θ) between incidence and the sample surface is varied in this geometry and the detector is moved accordingly to keep the angle 2θ between detector and incident ray. When scanning a film with $\theta/2\theta$ scan, only planes which are parallel to the surface are investigated. In the case of a textured thin film, only a few peaks will be visible since the planes parallel to the surface belong to the same family. The parallel beam arrangement, which is less susceptible to misalignment of sample height than the Bragg-Brentano geometry, can be used instead of Bragg-Brentano geometry [122].

Several variables determine the breadth of a diffraction peak. Instrumental parameters such as the emission characteristics of the X-ray source or the specifications of the X-ray optics used provide the first factor of broadening. The second truth is that microstrains cause widening. Localized crystal lattice distortions, such as dislocations, are microstrains. Changes in the lattice parameter lead the diffraction peak to expand as a result of these distortions. The crystallite size constraint is the third component that leads to peak widening. The peaks are wider when the crystallites are smaller. Peak broadening analysis is particularly relevant when dealing with nanoparticles, as the Scherrer equation may be used to quantify particle size D [123].

$$D = \frac{K\lambda}{\beta \cos\theta} \tag{3.5}$$

In equation 3.5, β is FWHM and K is a constant having value of approximately 0.9. Le-Bail and Pawley refinement technique can be utilized for the determination of lattice parameters of ZnO hexagonal lattice [124]. The lattice parameter of the ZnO hexagonal

system can be determined by the equations-

$$\alpha = \frac{\lambda}{\sqrt{3}\sin\theta} \tag{3.6}$$

$$c = \frac{\lambda}{\sin\theta} \tag{3.7}$$

3.4.5   Scanning Electron Microscopy

The texture, surface morphology and chemical composition of thin films may all be studied using a scanning electron microscope (SEM). This technology can capture highly magnified pictures of the sample surface in the order of nanometers. The technique can also analyze the local chemical composition of material with an analytical probe [125, 126].
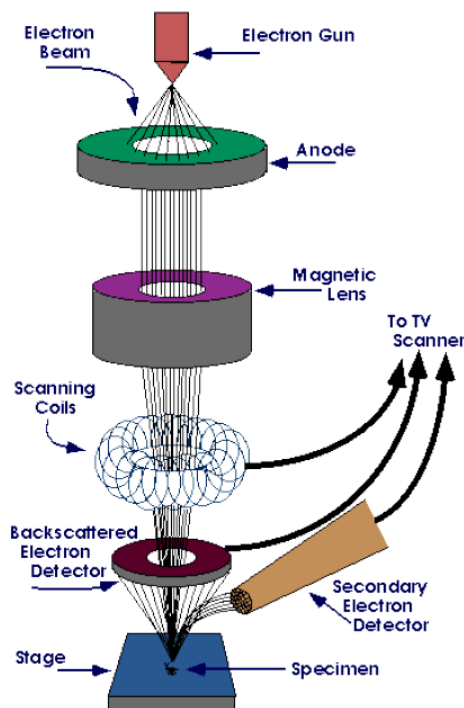
Figure 3.10: Schematic diagram of SEM

A voltage of the order of kV accelerates an electron beam in a scanning electron microscope (SEM). The beam is then focused on a tiny area on the sample's surface and scanned over it. Secondary electrons, backscattered electrons and X-rays are all produced when electrons interact with the sample. These signals are captured by electronic

detectors, which are then utilized to recreate the surface image of the sample. Incident primary electrons when interact with sample, the atoms ionize and secondary electrons are generated. Because the energy of secondary electrons is quite low, they are released from near the surface. As a result, secondary electrons reveal surface morphology [127]. Backscattered electrons have energies of more than 50 eV, whereas secondary electrons have energies of less than 50 eV. Backscattered electrons are elementary electrons that collide elastically with the sample's atoms. As the mass of the scattering atoms increases, backscattering becomes more likely; consequently, larger atoms result in a higher number of backscattered electrons. As a result, the chemical contrast is represented by these electrons. The elemental composition of a sample is determined using the EDX (energy dispersive X-ray spectroscopy) technique. To get EDX spectra, a sample is exposed to an electron beam within a scanning electron microscope. The electron beams collide with the orbital electrons of the sample to eject them from their orbits. X-rays are emitted when higher-energy electrons arrive at these vacant sites. The chemical composition of the sample is found by analyzing the emitted X-rays. EDX is a critical instrument for determining the composition of any type of material. The Schematic of the interaction of the primary electron beam with the sample surface in SEM is depicted in Figure 3.10.

Elastic scattering is the sole way to get backscattered electrons. The whole system must be vacuum shielded to avoid electron scattering by air molecules. The incoming electrons are focused on the sample using an electromagnetic lens. These lenses are used to concentrate beam spots that range in size from a few nanometers to 10 nanometers. After that, the region of interest is raster scanned, dispersed signals are captured and an image is created. In morphological research, secondary electrons are commonly employed. The SEM technique is commonly used for morphological research because it reveals extremely small objects in the nm range with greater resolution. It is also essential since it enables you to perceive little objects in three dimensions.

CHAPTER 4

FABRICATION OF UNDOPED ZnO THIN FILMS AND ITS CHARACTERIZATION

4.1   INTRODUCTION

ZnO is considered as a substance of importance now a day because of its multi dimensional applications in semiconductor industry. It has the potential to be used in a variety of optoelectronic and future applications. The future of ZnO can be seen in the shape of planer thin films formed on suitable substrates and in the form of nano-structured devices. The study of pure or undoped ZnO thin films (UZOTF) is essential in order to compare the properties of these films to those of doped ZnO films and understand the extent to which doping impacts the properties of ZnO. In this chapter, deposition, characterization and results of pure or undoped ZnO films are discussed. Sol gel spin deposition technique was used to deposit undoped Zinc oxide thin films on a glass substrate using Zinc Acetate inorganic precursors. The optical, vibrational and fluorescence properties of a ZnO thin film fabricated on glass have been studied using UV-visible, Raman and fluorescence spectroscopy. Results from the study provide insight into the properties of the thin film.

4.2   EXPERIMENTAL DETAILS

The solution is processed by using the zinc acetate dihydrate (ZAD), 2-methoxyethanol (2ME) and monoethenolamine (MEA) as starting chemicals. The solvent used is 2ME while MEA is used as the stabilizer. The 0.5 M undoped ZnO sol is prepared by dissolving ZAD in 2ME using magnetic stirrer at 70 °C for 30 minutes. The solution became hazy, therefore MEA was added drop by drop to stabilize it by fixing the Zn^{2+}/MEA
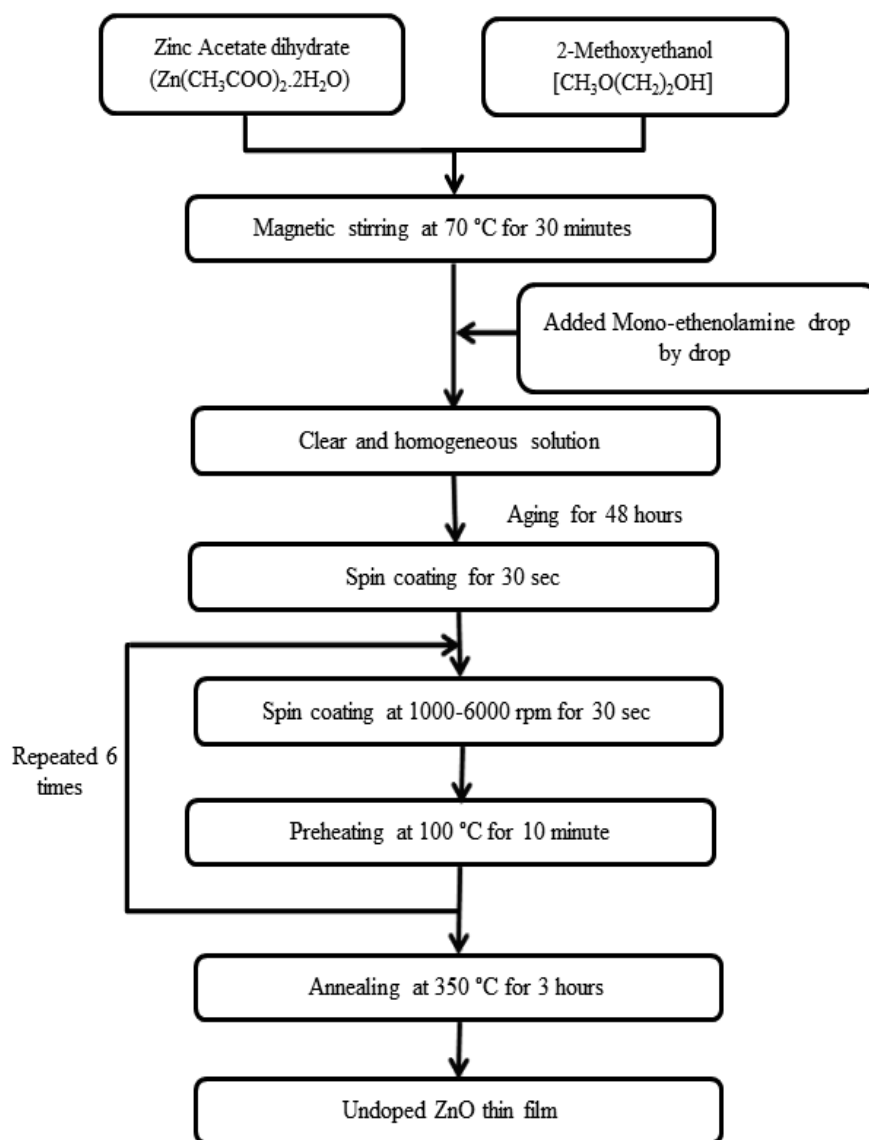
Figure 4.1: Flow chart for fabricating undoped ZnO thin films

molar ratio to 1:1. This caused the residual mass of ZAD to dissolve and the solution to become transparent. The solution is further stirred for 2 hours at 70 °C using stirrer to obtain a clear and uniform solution. In the next step the prepared sol is aged for 48 hours at ambient temperature in air tight bottles. Figure 4.1 represents the process map for the preparation of undoped ZnO thin films. Soda lime glass substrate (2.5cm × 2.5cm) is cleaned by the steps as already described in chapter 2. Glass substrates are ultrasonically cleaned with acetone and DI water before being dried in an oven at 150 °C for 30 minutes before being deposited with thin films. The aged solution is utilized for fabrication of UZOTF on pre cleaned glass substrates. Spin deposition technique has been utilized for fabrication of films. The films are fabricated by dropping the sol with the help of dropper on spinning glass substrate. The substrate is uniformly coated

with the sol in this procedure. Thin films are deposited at substrate spinning speed of 1000 to 6000 rpm. The film is then dried at hot plate at 100 °C to evaporate the organic solvents from the material. To achieve the necessary thin film thickness, the deposition and drying cycle is repeated six times. Finally, the films are annealed for 3 hours in a tube furnace at 350 °C to enhance the microstructure and crystallinity.

4.3   RESULTS AND DISCUSSION

UV-visible spectra, Raman spectra and fluorescence spectra of undoped ZnO thin films has been observed. A dual beam UV visible spectrophotometer is used to study the absorption spectra in the wavelength range of 300-1100 nm. The Raman spectrum is studied by Enspectr Enhanced Spectrometry at a wavelength of 532 nm. The fluorescence spectrum was examined by Fluorescence Spectrometer in the wavelength range of 350-650nm.

4.3.1   UV Visible Spectra

The film homogeneity as well as the depositing of crack and void free films are dependent on the rotation speed. To investigate the impact of spinning speed, thin films were synthesized at various rotating speed ranging from 1000-6000 rpm to find out the optimized rotating speed to get the best results. The absorbance spectra of UZOTF grown at 1000-6000 rpm rotation speed are shown in Figure 4.2. The absorption spectrum of the films indicates low absorbance in the visible and near-infrared regions, but strong absorbance in the ultraviolet region. The highest absorption peaks exist in absorption spectra at around 358nm for all thin films. The absorption begins to increase with a drop in wavelength at 374 nm, which is known as the adsorption edge and corresponds to the thin film's forbidden band gap. The absorbance decreases as the spin coating speed increases as seen from Figure 4.3 and Table 4.1.

 The rotational speed of the substrate has a direct influence on the properties and homogeneity of thin films. Table 4.1 shows that there is maximum absorption at the lowest rotating speed (1000 rpm) and minimum absorption at the highest rotating speed (6000 rpm). At the lowest rotating speed (1000 rpm), discontinuities in the films are likely due to the lack of sufficient centrifugal force, while at higher speeds, discontinuities may be caused by excessive centrifugal force which rapidly distributes the liquid and results in non-uniform films.

 Figure 4.4 and 4.5 illustrates the variation of optical transmittance of undoped ZnO thin
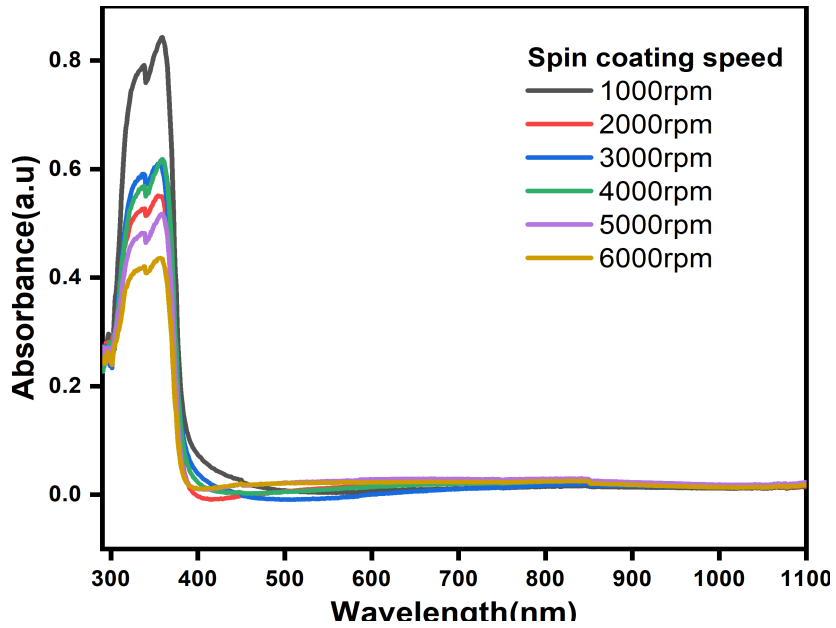
Figure 4.2: Absorption spectra of undoped ZnO thin film synthesized at 1000-6000 rpm
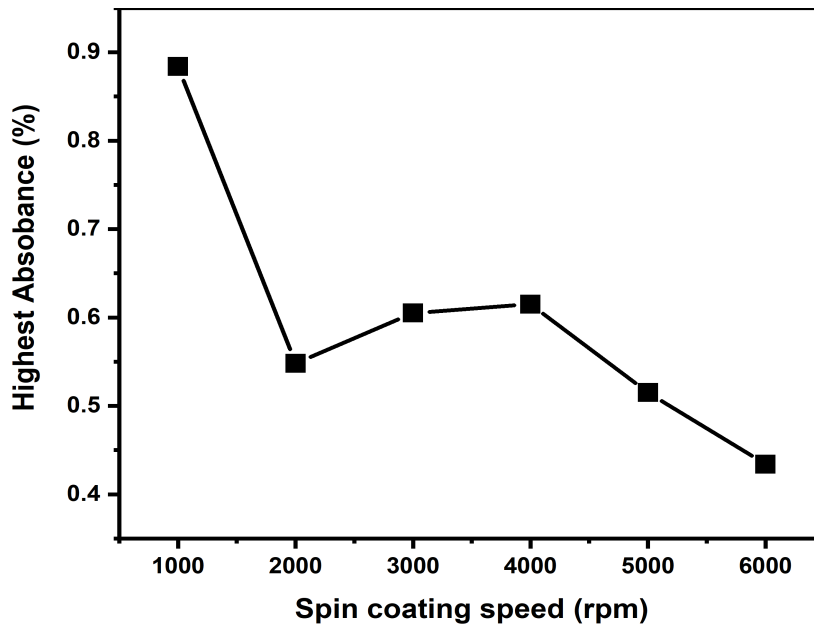
Figure 4.3: Variation of highest absorbance of undoped ZnO thin films with spin coating speed
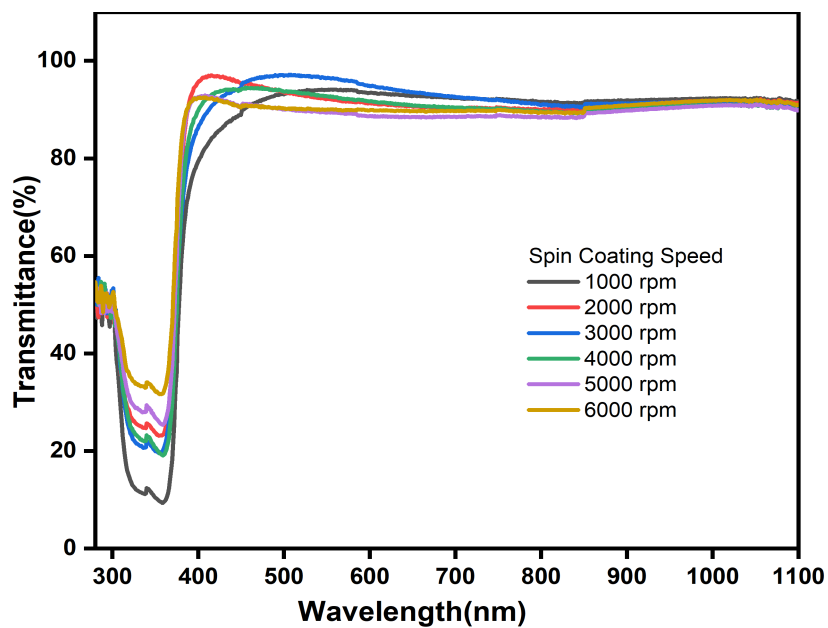
Figure 4.4: Transmission spectra of undoped ZnO thin film synthesized at 1000-6000 rpm
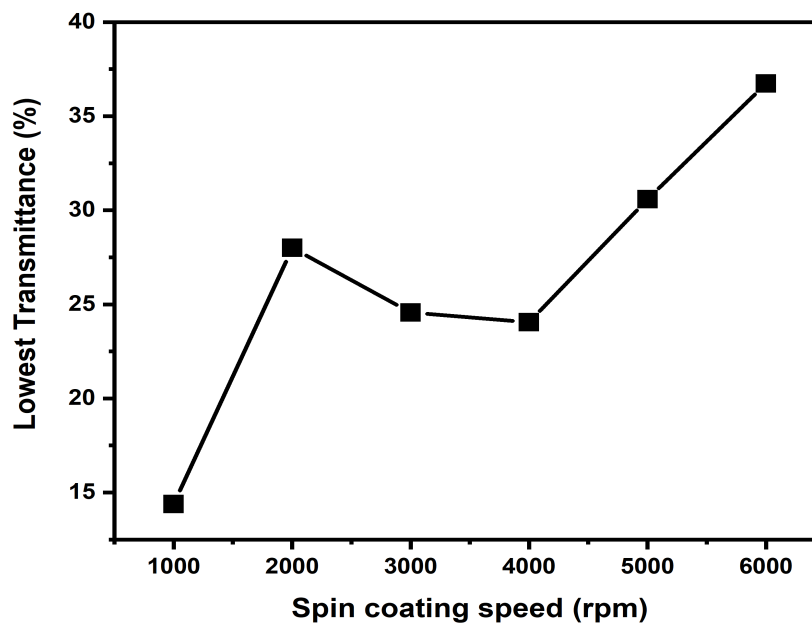
Figure 4.5: Variation of lowest transmittance of undoped ZnO thin films with spin coating speed

Table 4.1: Variation of peak absorbance of undoped ZnO thin films with spin coating speed

Sr. No.	Spin Coating Speed (rpm)	Peak Absorbance value (a.u.)
1.	1000	0.884
2.	2000	0.548
3.	3000	0.605
4.	4000	0.615
5.	5000	0.515
6.	6000	0.434

Table 4.2: Variation of lowest transmittance of undoped ZnO thin films with spin coating speed

Sr. No.	Spin Coating Speed (rpm)	Peak Absorbance value (a.u.)
1.	1000	14.38
2.	2000	28.00
3.	3000	24.57
4.	4000	24.05
5.	5000	30.59
6.	6000	36.73

films synthesized at 1000-6000 rpm obtained using double beam UV spectrophotometer from 300-1100 nm. It has been observed that the transmittance value of the films are less at short wavelengths (<370 nm) and high at long wavelength (>420 nm). All thin films have a transmittance of more than 85% in the visible and near-infrared spectra. This implies that at longer wavelengths, the films act like a transparent material. Figure 4.5 shows that the transmittance of all thin films is lowest at around 358nm. The value of lowest transmittance is minimum 1000 rpm while its value is highest at 6000 rpm of substrate rotation speed and it almost increases with the spin coating speed as shown in Figure 4.5 and Table 4.2.

Figure 4.4 and Figure 4.5 reveal that the value of the lowest transmittance increases from 3000 rpm to 6000 rpm and its value for all thin films is greater than 85% in the visible spectrum of radiation which makes the thin films a good candidate for transparent conducting oxide for optoelectronic devices [128]. But in the case of 1000 rpm, the transmission value is lowest which can be explained by the interference pattern in the transmission spectra. As *D. A. Ajadi et al*. [129] explains, interference through the film occurs when light reflects from the top at one wavelength and from the bottom at a different wavelength.
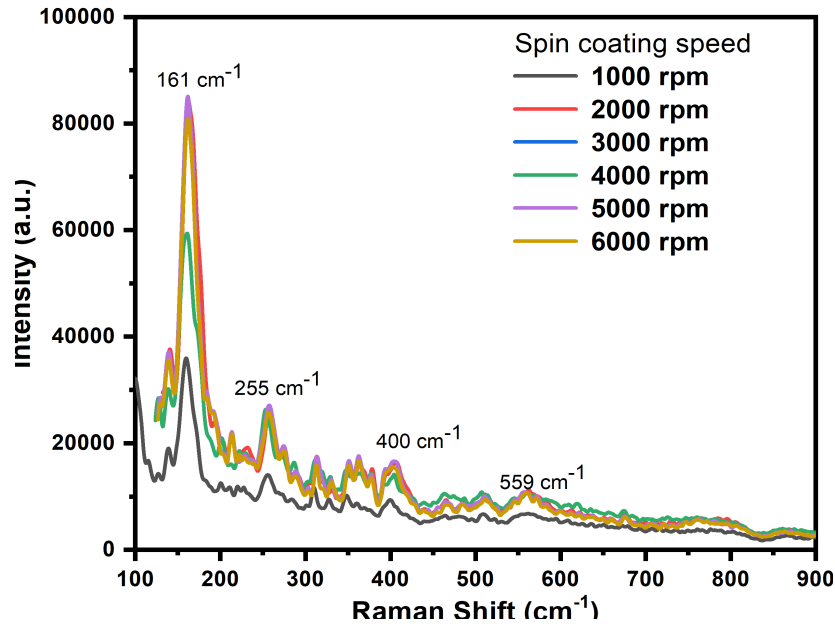
Figure 4.6: Raman spectra of undoped ZnO thin film synthesized at 1000-6000 rpm

4.3.2   Raman Spectra

Figure 4.6 illustrates the Raman spectra of undoped ZnO thin film at 1000 rpm - 6000 rpm rotation speed, fabricated by the sol-gel technique, is reported herein. The crystal structure of ZnO is wurtzite, which belongs to the C_{6V}^4 (P6$_3$ mc) space group [130, 131]. The phonon modes are predicted to correspond to the 2E$_2$, 2E$_1$, 2A$_1$ and 2B$_1$ symmetries by group theory. Raman active symmetry modes are 2B$_1$. The theory of group predicts the occurrence of the following optical modes at the Γ point of brillouin zone: Γ_{opt} =A$_1$+2B$_1$+E$_1$ +E$_2$. The B$_1$ (low) and B$_1$ (high) silent modes have been determined to have frequencies of 260 cm^{-1} and 540 cm^{-1}, respectively. Furthermore, since A$_1$ and E$_1$ are both infrared active, they branched into longitudinal and transverse optical components (LO and TO) [132, 133].

The Raman spectra of UZOTH manufactured at the substrate spinning speed of 1000 rpm to 6000 rpm are depicted in Figure 4.6. The Raman peaks are located at the frequencies 161 cm^{-1}, 255 cm^{-1}, 400 cm^{-1} and 559 cm^{-1} as shown in Figure [134]. The Raman peak at 161 cm^{-1} in the low-frequency domain is attributable to TA phonon overtones near the M point [135]. 2TA, E$_1$ (TO) and A$_1$ (LO) modes are responsible for the maxima at 255, 400 and 559 cm^{-1} [136, 137]. The presence of a peak at about 559 cm^{-1} (A$_1$ (LO) modes) can be attributed to the presence of lattice defects, such as oxygen vacancies or zinc interstitials, or a combination of the two.

4.3.3 Photoluminescence Spectra

Fluorescence spectroscopy is a great intense method for studying a material's precise band edge transition levels. A well-defined photoluminescence (PL) spectrum of the UZOTFs synthesized at spinning speed varying from 1000 to 6000 rpm is depicted in Figure 4.7.
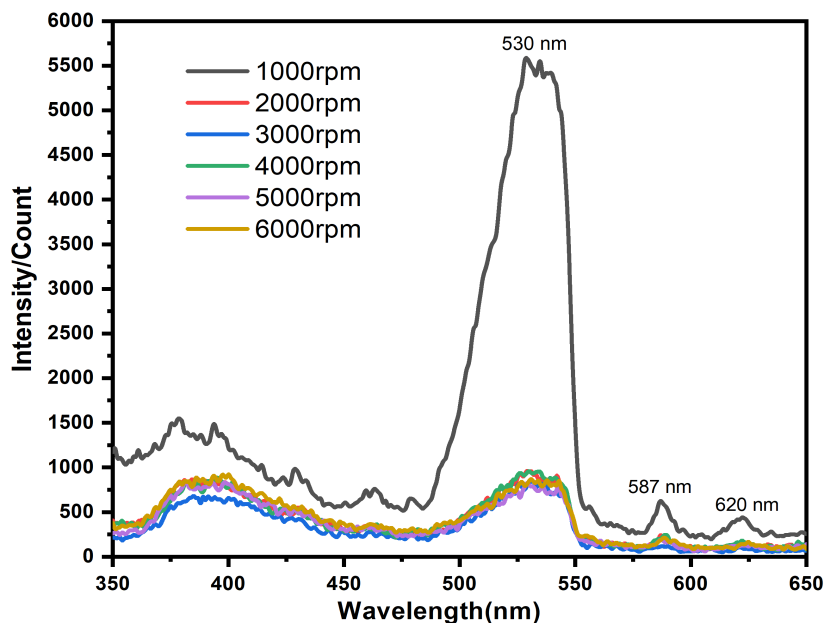
Figure 4.7: Fluorescence spectra of undoped ZnO thin film synthesized at 1000-6000 RPM

The photoluminescence spectrum in Figure 4.7 spectacles an emission peak in the ultraviolet region at about 385 nm for rotational speeds of 2000 to 6000 rpm, while for a film deposited at 1000 rpm, the peak occurs at 378 nm. The exciton recombination associated with ZnOs near band edge transition (NBE) produced these UV peaks [138, 139]. In compared to other thin films, the UV peak at 1000 rpm speed is blue shifted, which corresponds to a change in the thin film's band gap. The visible emission peak at about 530 nm corresponds to the green emission. The oxygen vacancies (V_o) and antisite oxygen (O_{zn}) are responsible for the green emission peak [140–142]. The weak yellow emission peaks observed at 587 nm and 620 nm are attributed to the presence of intrinsic defects in the material, likely arising from Zn vacancy and oxygen interstitials in the ZnO due to its non-stoichiometry [143–145].

4.3.4 Density of States and Electronic Band Structure

When it comes to transitions between CB and VB, the density of states (DOS) is significant. The DOS is not persistent, in the sense that it is not a natural quantity, but it

may be changed to improve device performance. The density of states (DOS) in solid state physics refers to the number of energy levels per unit volume that are accessible for electrons in a small energy range from E to E+dE. In other words, the density of states is represented by the first derivative of the number of energy states in terms of energy per unit volume.

$$(D(E) = \frac{1}{V} \cdot \frac{dN(E)}{dE})$$
(4.1)
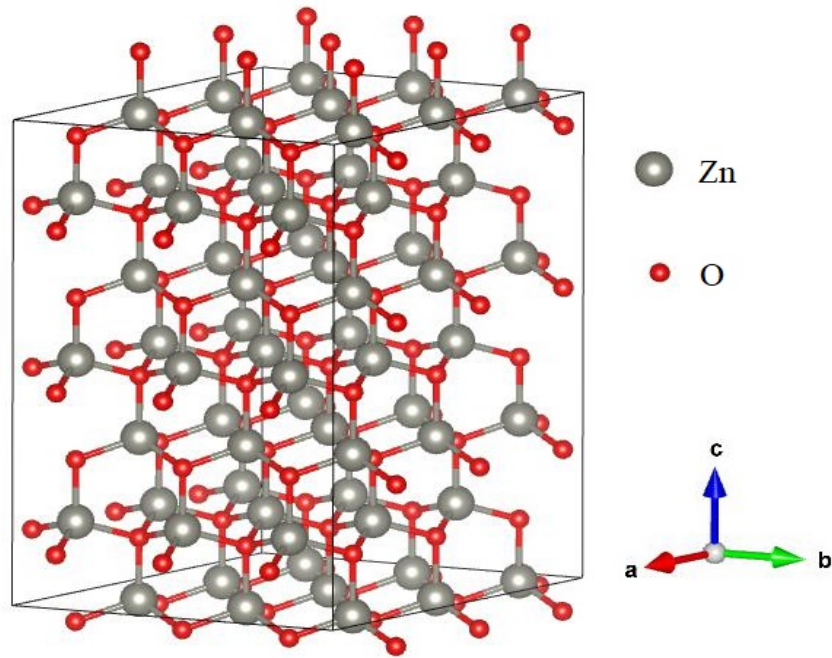
Figure 4.8: 2×2×2 super cell of ZnO generated using VESTA software
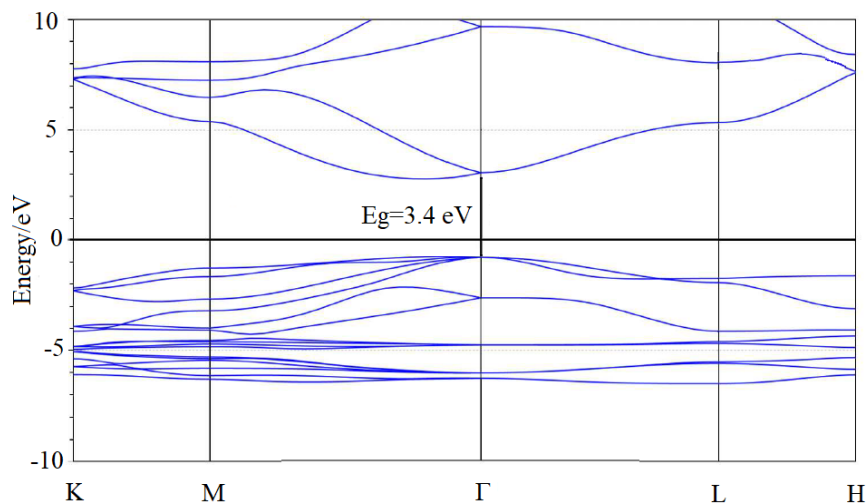
Figure 4.9: Energy band structure of ZnO
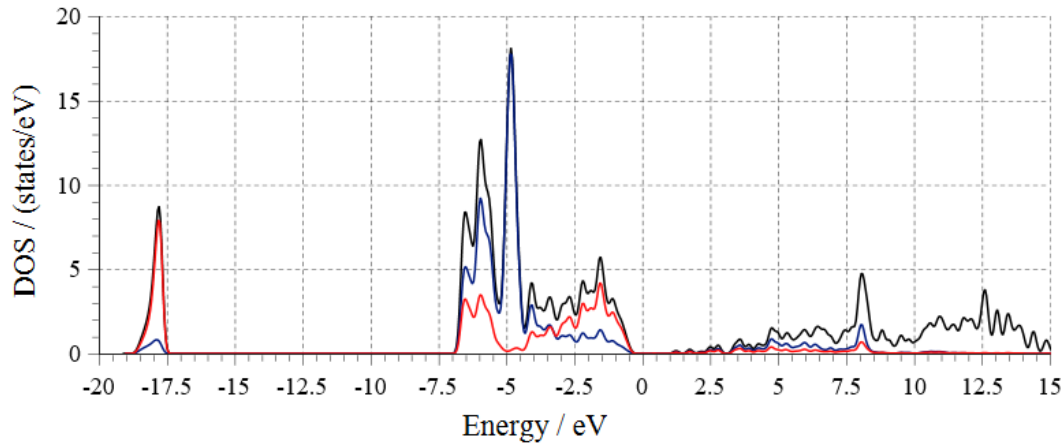
Figure 4.10: Density of states (DOS) for ZnO Calculated from Burai and Quantum Espresso

The electronic structure and density of states of ZnO have been calculated using a 2×2×2 super cell constructed from the ZnO unit cell. The computation based on the Density Functional Theory was done with the Quantum Espresso tool. Figure 4.8 depicts the 2×2×2 super cell created with the VESTA software.

The electronic band structure and density of states are calculated using the Burai software application. The band structure is a model that may be used to describe key physical phenomena of semiconductors and other materials. Figure 4.9 depicts the electronic structure of ZnO as calculated. The density of states (DOS) for ZnO was calculated using Burai and Quantum Espresso software as shown in Figure 4.10.

<div align="right">

CHAPTER **5**

</div>

FABRICATION OF Ni, Al, Co AND Mn DOPED ZnO THIN FILMS AND THEIR CHARACTERIZATIONS

5.1 FABRICATION OF Ni-DOPED ZnO THIN FILMS AND ITS CHARACTERIZATION

5.1.1 Introduction

Zinc oxide (ZnO) is astounding semiconducting material due to its properties such as high excitonic binding energy, high transparency in the visible region, and good conductivity. Additionally, by controlling extrinsic doping with elements such as Mn, Ni, Co, and Fe, its characteristics can be adapted to the needs of various devices [146]. Furthermore, one of its marvellous property as a dilute magnetic semiconductor (DMS) can be induced by doping of transition metal elements like Mn, Ni, Co, Fe etc. This can be accomplished by randomly replacing the host Zn atom with a transition metal element that induces magnetic behaviour above room temperature, such as paramagnetism, ferromagnetism, or antiferromagnetism [102, 147–150]. Due to its multi-functionality in opticomagnetic applications, doped zinc oxides are among the finest choices for DMS. Due to properties like as transparency in the visual region and piezoelectricity, ZnO-based DMS have caught the scientific community's attention as a possible candidate for the fabrication of spin transistors and spin-polarized light-emitting diodes. In ZnO, Ni is a key dopant for inducing magnetic characteristics. Ni^{++} and Zn^{++} have the same valance as well as the radius of $Ni^{++} \sim 0.69$ Å is comparable with the radius of Zn^{++} ~ 0.74 Å, so Ni^{++} is likely to substitute Zn^{++} in Zinc oxide structure making it easily

adaptable. To prepare DMS, Sol Gel is a superior technique than other methods [151–153].

The inorganic precursor Zinc Acetate Dihydrate is used in this work to develop Ni-doped ZOTFs on a glass substrate using a sol gel spin coating technique. UV-visible spectroscopy, Raman spectroscopy and fluorescence spectroscopy were used to investigate the ZnO thin film formed on glass substrate. The thin film's optical, vibrational, electrical and fluorescence characteristics are scrutinized.

5.1.2 Experimental Details

Zinc acetate dihydrate (ZAD), Nickel acetate tetrahydrate (NATH), 2-methoxyethanol (2ME) and monoethenolamine (MEA) are utilized as initial chemicals for the formation of 0.5M 1 at% Ni-doped sol. As a solvent and a stabilizer, 2ME and MEA are utilized. The sol is prepared by dissolving ZAD and NATH in 2ME using magnetic stirrer at 70 °C for 30 minutes. After 30 minutes, MEA was added drop by drop to stabilize the solution, with the Zn^{2+}/MEA molar ratio set at 1:1. Upon adding the MEA, the undissolved residual mass of ZAD is dissolved and the solution becomes transparent. The solution is further stirred for 2 hours at 70 °C using a stirrer to obtain a clear and uniform solution. In the next step the prepared sol is aged for 48 hrs at ambient temperature in air tight bottles. The flow chart for the deposition of UZOTFs is shown in Figure 5.1.

Soda lime glass substrates (2.5cm × 2.5cm) are cleaned by the steps as already described in chapter 2. Glass substrates are ultrasonically cleaned with acetone and DI water before being dried in an oven at 150 °C for 30 minutes before being deposited with thin films. The aged solution has been utilized for fabrication of UZOTFs on pre cleaned glass substrates. Spin deposition technique has been utilized for fabrication of films. The films are fabricated by dropping the sol with the help of dropper on spinning glass substrate. The substrate is uniformly coated with the sol in this procedure. Thin films are deposited at substrate spinning speed of 1000 to 6000 rpm. The film is then dried at hot plate at 100 °C to evaporate the organic solvents from the material. To achieve the necessary thin film thickness, the deposition and drying cycle is performed six times. Finally, the films are annealed for 3 hours in a tube furnace at 350 °C to enhance the microstructure and crystallinity.
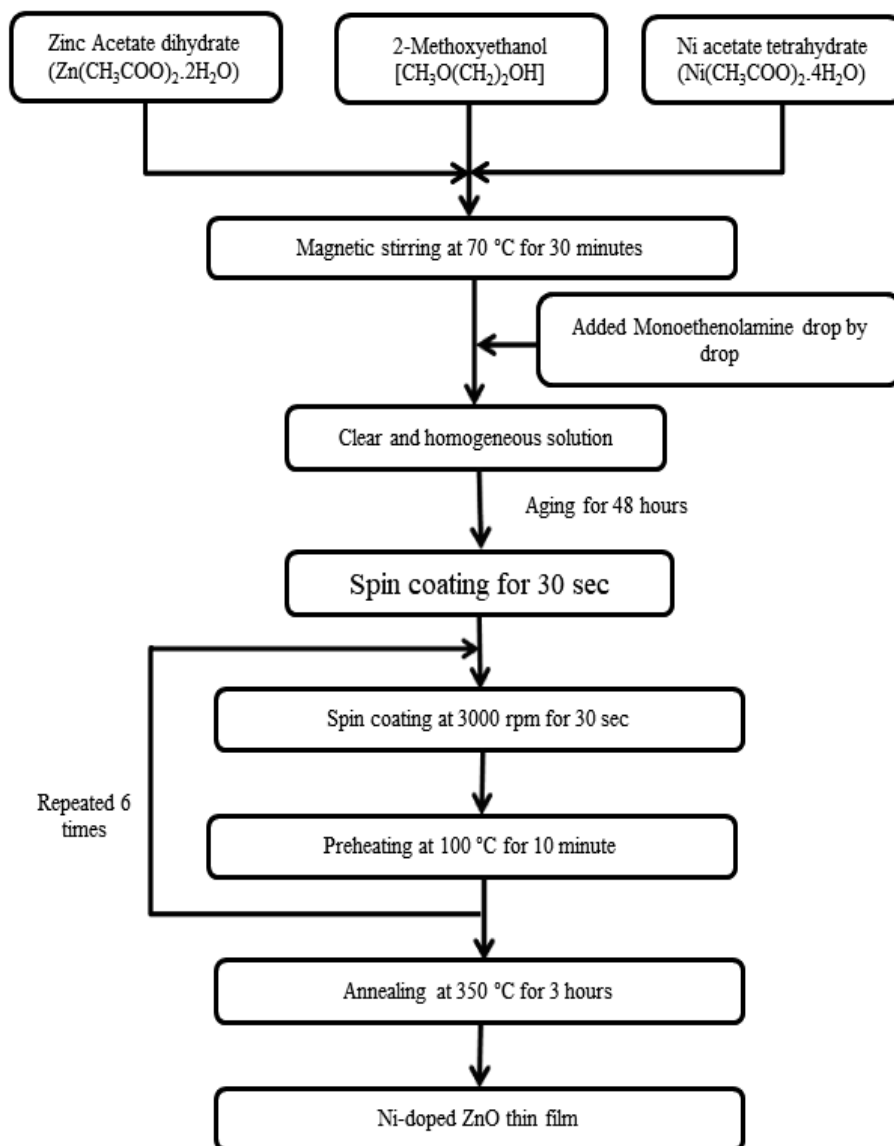
Figure 5.1: Flow chart for fabricating Ni-ZnO thin films

5.1.3   Results and Discussion

The double beam UV visible spectrophotometer is used to determine the absorption and transmission spectrum of the sample, while Enspectr enhancement spectrometry is used to obtain the Raman spectrum of the sample at 532 nm. Photoluminescence spec-
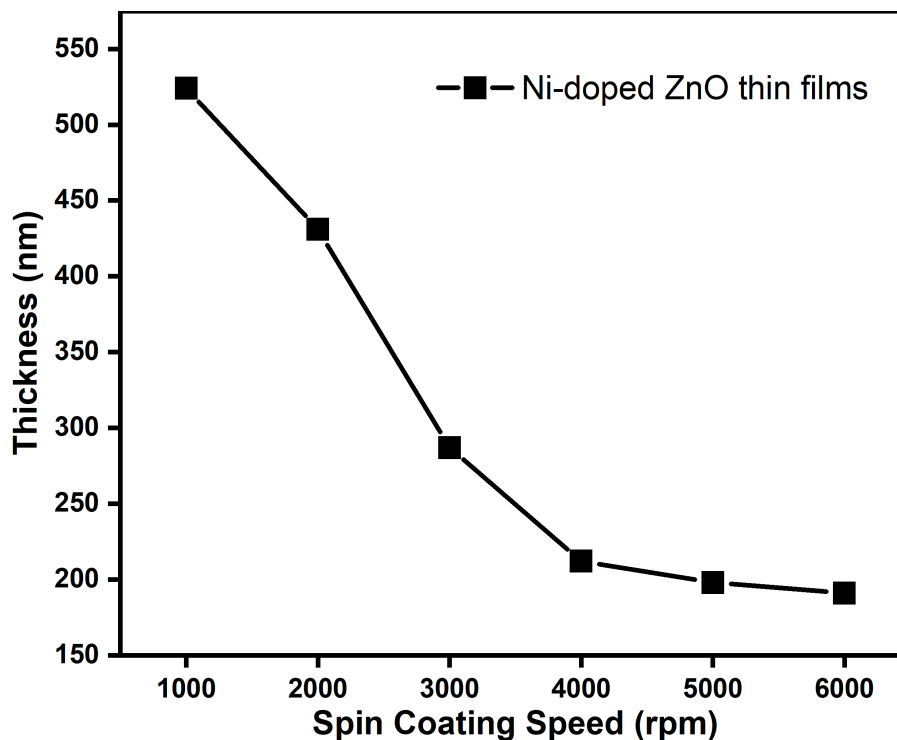
Figure 5.2: Variation of thickness of Ni-doped ZnO thin film with spin

tra were measured between 350 and 650 nm with a Spectrofluorometer (FluoroSENS Camlin Photonics). The resistivity of the samples is evaluated using the Vander-pauw four point probe method. SEM micrographs were used to inspect the cross section view of thin films to extract information about their thickness. Figure 5.2 depicts the variation in thickness of Ni-doped ZnO thin films. The thickness of the thin film decreases with increase in spin coating speed. Thickness of thin film is highest at 1000 rpm because the centrifugal force is lowest. The centrifugal force rises as the spin coating speed increases and hence the thickness reduces.

5.1.3.1   UV Visible Spectra

The absorbance spectra of the synthesized Ni-doped ZOTFs at different rotating speed from 1000-6000 rpm were investigated in the wavelength range from 300-1100 nm as shown in 5.3. It is observed that the rotating speed affects the quality as well as the uniformity of the thin films. The value of highest absorbance occurs at about 339 nm for
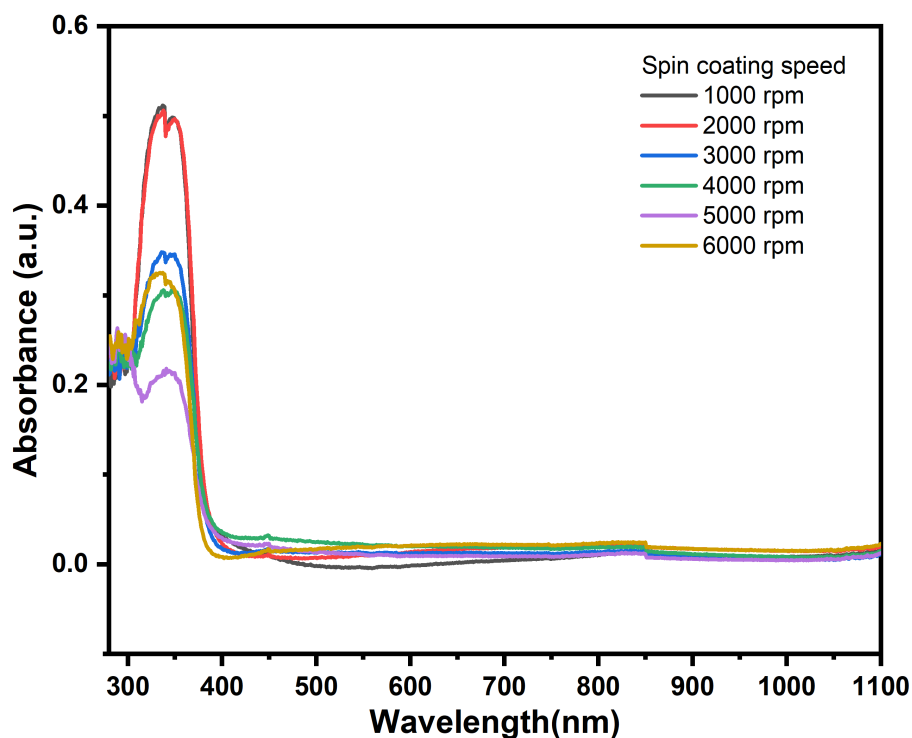
Figure 5.3: Absorption spectra of Ni doped ZnO thin film at synthesized at 1000-6000 rpm

Table 5.1: Variation of peak absorbance of Ni doped ZnO thin films with spin coating speed

Sr. No.	Spin Coating Speed (rpm)	Highest Absorbance
1.	1000	0.512
2.	2000	0.502
3.	3000	0.346
4.	4000	0.302
5.	5000	0.215
6.	6000	0.323

all thin films. Absorbance starts increasing with decrease in wavelength below 387 nm (absorption edge) for all thin films which corresponds to the band gap. The maximum and minimum absorptions are observed at rotating speed of 1000 rpm and 5000 rpm respectively as demonstrated by Figure 5.4 and Table 5.1. At the lowest rotating speed (1000 rpm) there is a discontinuity in the films due to the lack of enough centrifugal force while at higher speed the discontinuity is possibly due to the excessive centrifugal force which spreads out liquid instantly and causes non uniform films. The absorbance of Ni-doped ZOTFs decreases as the spin deposition speed increases as shown in Figure 5.4 and Table 5.1.

The optical transmittance spectra of Ni-doped ZOTFs manufactured at various rotational speeds from 1000 to 6000 rpm were studied in the wavelength range of 300-1100 nm, as shown in Figure 5.5. The transmittance spectra and the variation of lowest trans-
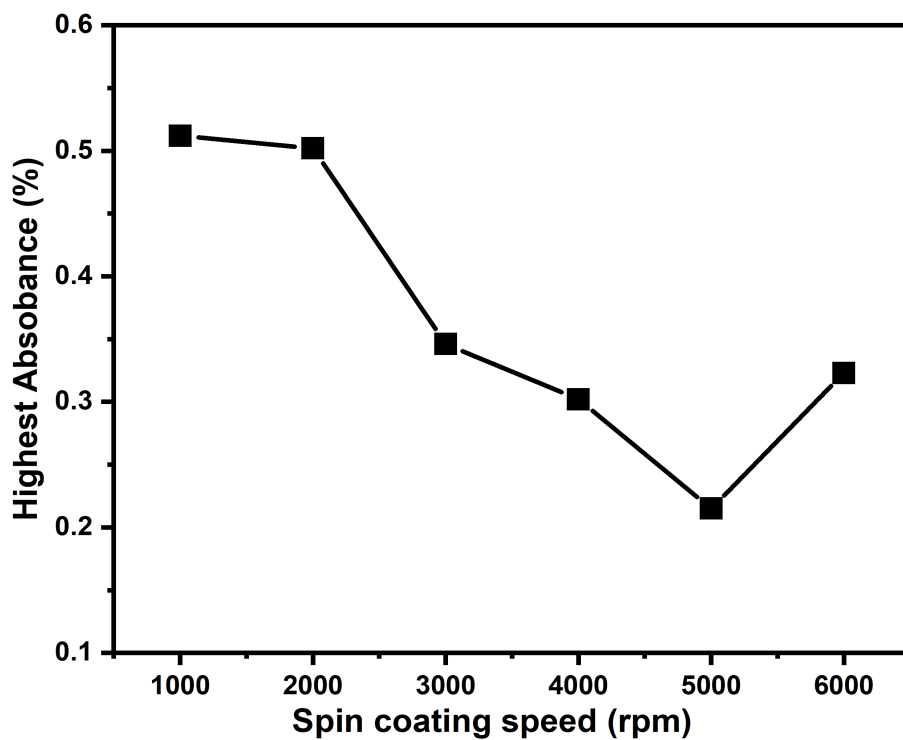
Figure 5.4: Variation of highest absorbance of Ni-doped ZnO thin films with spin coating speed
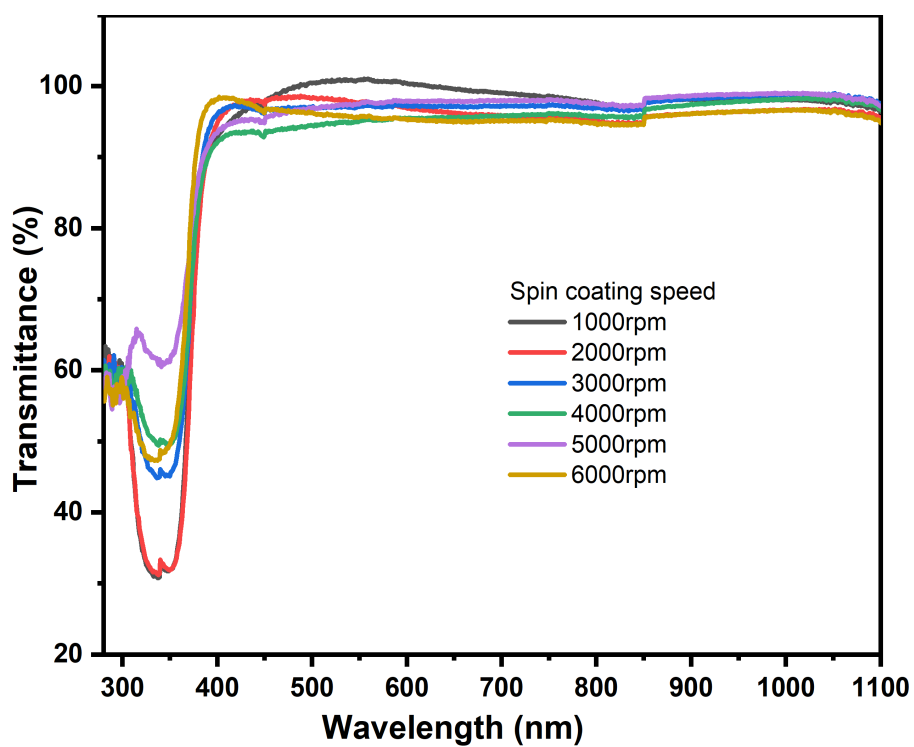
Figure 5.5: Transmission spectra of Ni doped ZnO thin film at synthesized at 1000-6000 rpm
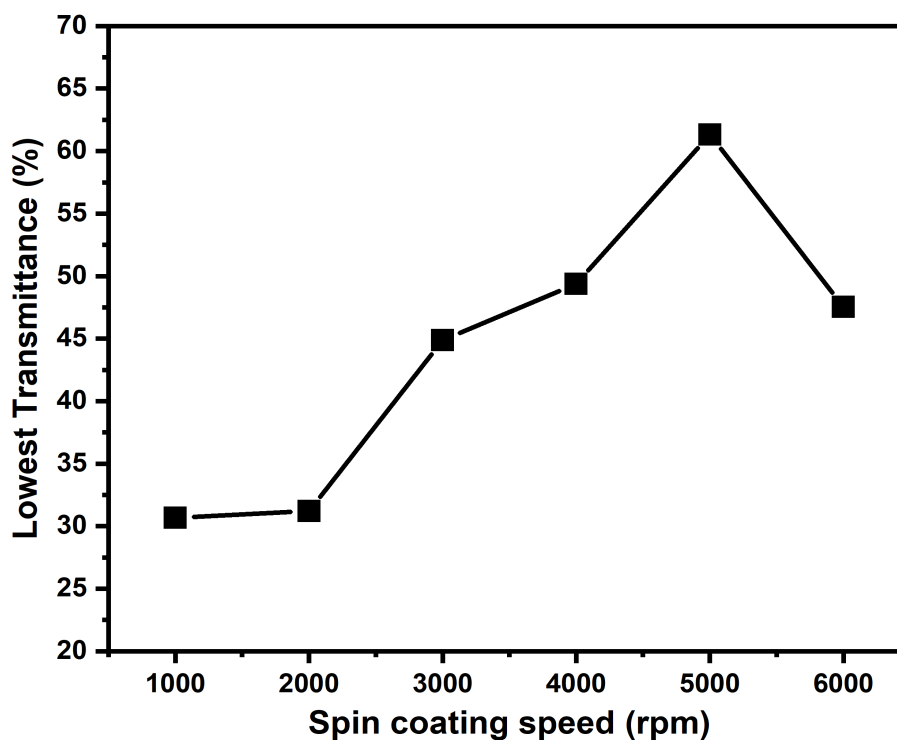
Figure 5.6: Variation of lowest transmittance of Ni-doped ZnO thin films with spin coating speed

Table 5.2: Variation of lowest transmittance of Ni doped ZnO thin films with spin coating speed

Sr. No.	Spin Coating Speed (rpm)	Lowest Transmittance value (%)
1.	1000	30.67
2.	2000	31.21
3.	3000	44.88
4.	4000	49.39
5.	5000	61.33
6.	6000	47.53
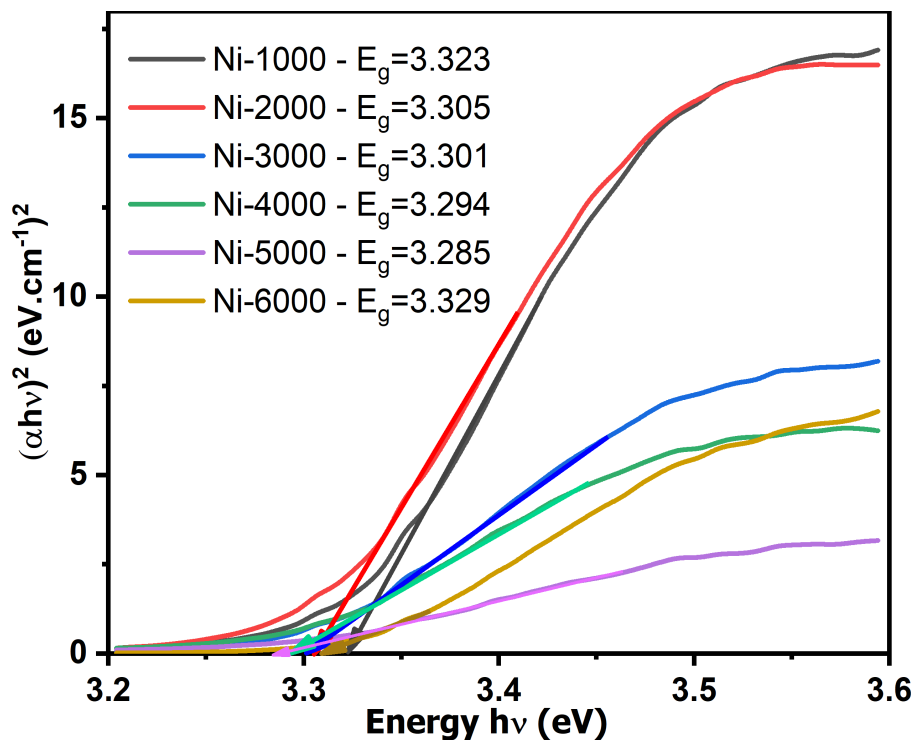
Figure 5.7: Tauc's plot for Ni-doped ZnO thin films

mittance of the deposited thin films are depicted in Figure 5.5 and Figure 5.6. The value of lowest transmittance increases as the rotation speed of deposition increases from 1000 rpm to 5000 rpm and then it declines for the film deposited at 6000 rpm. Figure 5.5 shows that all thin films are indeed highly transparent in the visible and NIR region of the spectrum, indicating that they may be employed as transparent conducting oxide in optoelectronic devices [16, 154]. The lowest transmittance is observed at 339 nm for all thin films and it almost increases with the spin coating speed as shown in Figure 5.6 and Table 5.2. The optical Band gap of Ni-doped ZOTFs fabricated at the substrate rotation speed of 1000-6000 rpm has been measured using Tauc's plot between $(\alpha h\nu)^2$ and energy $h\nu$ making use of equation $\alpha h\nu = A(h\nu - E_g)^{1/2}$. The band gap of a direct band gap semiconductor may be calculated using this equation [155, 156]. In this equation α, $h\nu$ and E_g are the absorption coefficient, photon energy and energy gap of semiconductor respectively. The intercept on the energy axis of extrapolation of the linear part of the the $(\alpha h\nu)^2$ versus energy $(h\nu)$ yields the band gap. Figure 5.7 portrays the Tauc's plot for the Ni-doped ZOTFs. The variation of the optical band gap with spinning speed is shown in Figure 5.8. It is observed that the band gap decreased when the rotation speed was increased from 1000 rpm to 5000 rpm, and then increased again at 6000 rpm. This shift in the absorption edge in the absorption spectra was consistent with the change in the optical band gap.
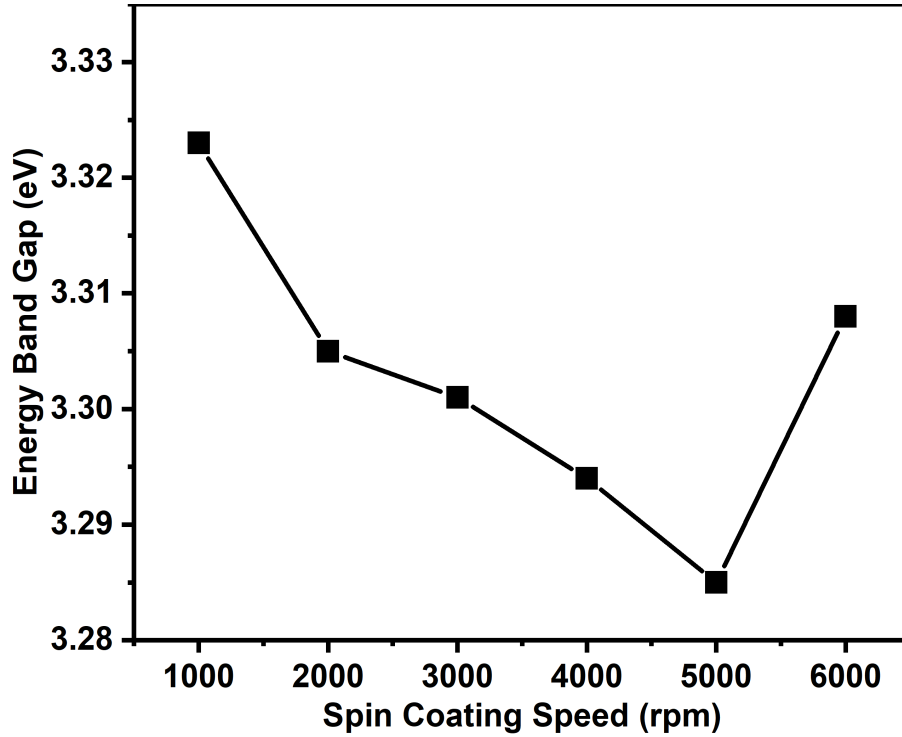
Figure 5.8: Variation of band gap with substrate rotation speed

5.1.3.2   Refractive Index and Dielectric constant

The refractive index (RI) is an essential optical constant for the materials to be used in the designing of an optical device. It provides information about local fields, polarization and phase velocity of light in propagating material. Therefore, it is significant to determine the RI of the Zinc oxide films. When light traverses through a film, some part is absorbed, some is reflected and the rest is transmitted. The absorbed part is taken into account by the complex refractive index (n*) given by

$$n^* = n + i\,k \tag{5.1}$$

here n is the refractive index and k is the extinction coefficient.

The refractive index of Zinc oxide thin films has been computed using the expression [157, 158]

$$n = \left(\frac{1+R}{1-R}\right) + \sqrt{\left(\left(\frac{4R}{(1-R)^2} - k^2\right)\right)} \tag{5.2}$$
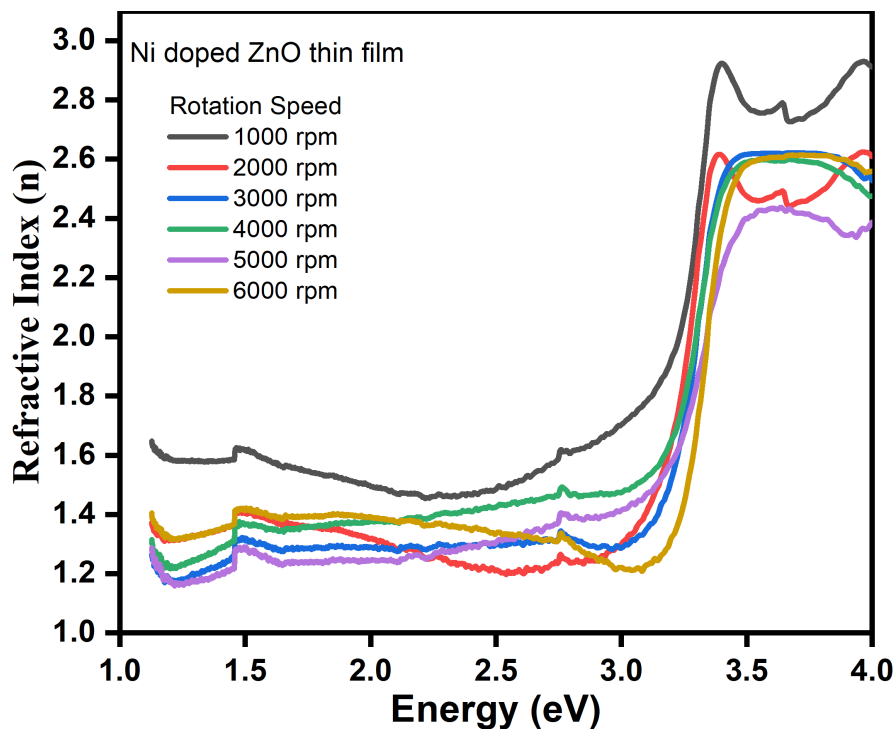
Figure 5.9: Variation of refractive index of Ni-doped thin films with energy
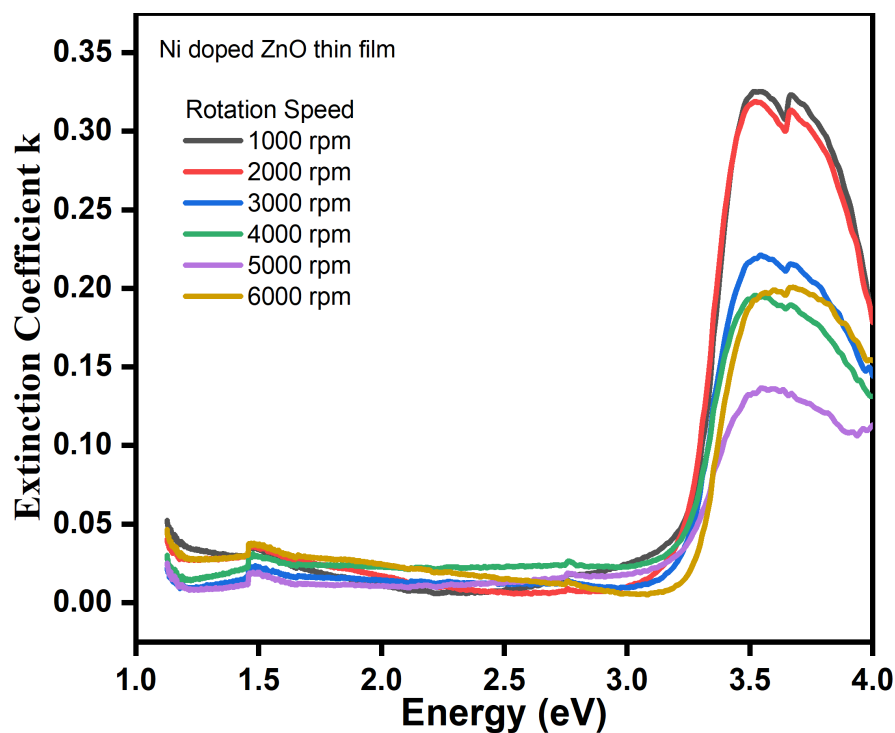
Figure 5.10: Variation of extinction coefficient of Ni-doped thin films with energy

The extinction coefficient (k) is a measurement of the proportion of light lost per unit distance of the participating material owing to scattering and absorption. The extinction
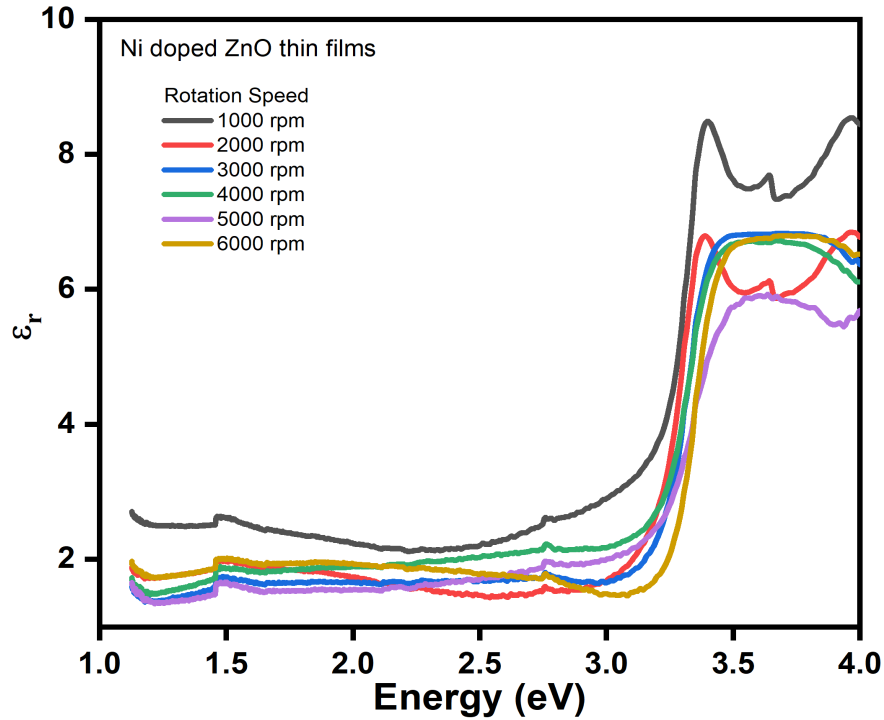
Figure 5.11: Variation of real part (ε_r) of dielectric constant with energy

coefficient k is calculated as follows:

$$k = \frac{\alpha\lambda}{4\pi} \tag{5.3}$$

where $\alpha = (1/d)ln(1/T)$ is the absorption coefficient [159, 160]. In Figure 5.9 and Figure 5.10, the extinction coefficient and refractive index spectral distributions are illustrated respectively. Figure 5.9 shows that a peak of refractive index (RI) is present for all films studied. It was found that the highest refractive index (2.92) was observed for the film deposited at 1000 rpm, while the minimum refractive index (1.70) was observed for the films deposited at 5000 and 6000 rpm. Moreover, the peak refractive index (3.39 eV) was observed for the films deposited at 1000 and 2000 rpm, whereas the peak refractive index (3.46 eV) was observed for the other films. The refractive index of Ni-doped ZnO thin films varied in the range from 1.12 to 2.92 between energy 1.1 eV to 4 eV. These findings regarding RI are consistent with the reported values by *Fahrettin Yakuphanoglu et al* [161]. There is a modest change in the value of the extinction coefficient from 1.1 eV to 3.15 eV, after this its value increases sharply from 3.15 eV and gains a maximum at 3.50 eV. The value of extinction coefficient then decreases from 3.50 eV to 4.0 eV. With decreasing energy, the refractive index and extinction coefficient rise. The usual dispersion behavior of the material is shown by the rise in the value of the RI with energy. The extinction coefficient increases as energy declines,
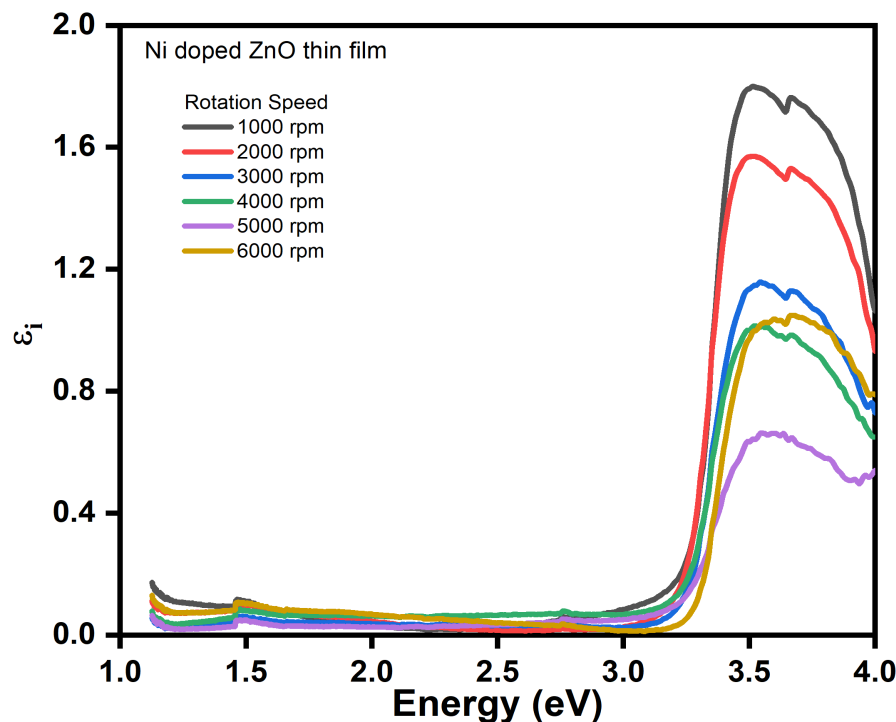
Figure 5.12: Variation of imaginary part (ε_i) of dielectric constant with energy

indicating that the percentage of light lost owing to scattering and absorption decreases. Using the relationship, $\varepsilon_r = n^2 - k^2$ and $\varepsilon_i = 2nk$, the real part (ε_r) and imaginary (ε_i) components of the dielectric constant (DC) were computed. Dielectric constant's real part (ε_r) gives the reduction in the velocity of light in the material and the imaginary part (ε_i) gives the energy absorption by electric field due to dipole motion [158].

Variation of real part (ε_r) and imaginary (ε_i) parts of DC for Ni-doped ZOTFs deposited at substrate rotation speed 1000-6000 rpm, with energy is shown in Figure 5.11 and 5.12 respectively. The values of the real component are greater than those of the imaginary part, as seen in the figure. The value of real part (ε_r) of DC is found to be highest at 3.39 eV, which decreasing with decrease in energy. The imaginary (ε_i) part of DC also decreases with decrease in the energy. No appreciable variation was noticed in real and imaginary part of DC before 3 eV.

5.1.3.3 Raman Spectra
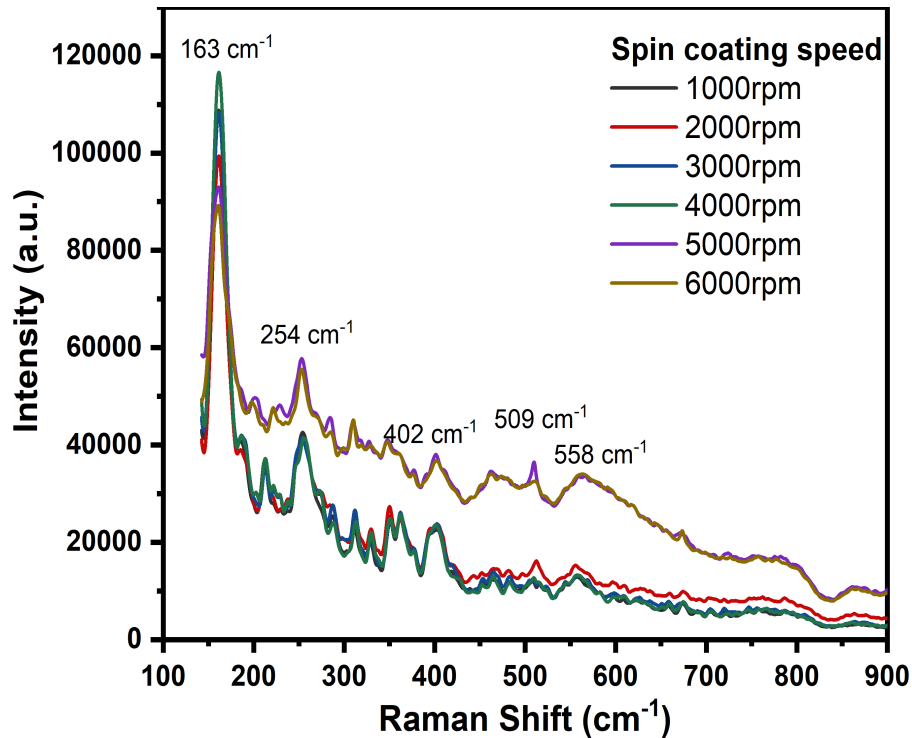
Figure 5.13: Raman spectra of 1 at% Ni doped ZnO thin film at synthesized at 1000-6000 rpm

The Raman spectra of Ni-doped ZOTFs deposited at 1000 rpm to 6000 rpm speed of rotation of substrate is obtained using Raman Spectrophotometer (EnSpectr R532) and is revealed in Figure 5.13. The Raman peaks are observed at the frequencies of 163 cm^{-1}, 254 cm^{-1}, 402 cm^{-1}, 509 cm^{-1} and 558 cm^{-1}. Overtones of TA phonons around the M point are responsible for the Raman peak seen at frequency 163 cm^{-1} [135]. The 254 cm^{-1} Raman peaks is attributed to B1(low) mode disorder caused scattering [162]. The peaks perceived at 402 cm^{-1} and 558 cm^{-1} may be attributed to E_1 (TO) and A_1 with LO overtone [163]. The peak at 558 cm^{-1} (A1 (LO) modes) could be due to lattice defects, such as oxygen vacancies, zinc interstitials, or a combination of the two.

5.1.3.4 Photoluminescence Spectra

Spectrofluorometer (FluoroSENS Camlin Photonics) was utilized to examine the photoluminescence spectra of Ni-doped ZOTFs fabricated at spin coating speeds ranging from 1000 to 6000 rpm. In Figure 5.14, the photoluminescence spectrum has been exhibited. The photoluminescence spectrum showed an emission peak at about 385nm, originated from the recombination transition from CB to VB known as the NBE transition of ZnO [138, 139]. The visible emission band witnessed between 490nm to 550nm
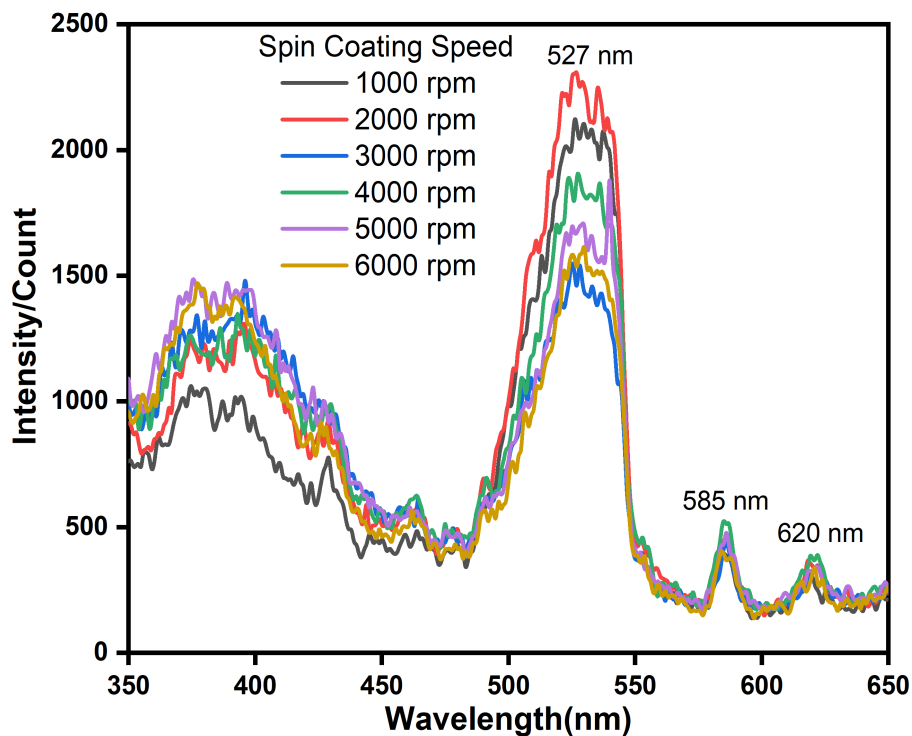
Figure 5.14: Fluorescence spectra of 1 at% Ni doped ZnO thin film at synthesized at 1000-6000 rpm

corresponds to the green emission and has a peak maximum at 527 nm. The oxygen vacancies (V_o) and antisite oxygen (O_{zn}) are responsible for the green emission band [140–142]. The emission peak at 527 nm is assumed to be caused by oxygen vacancies in ZnO. At 585 nm, the emission corresponds to oxygen interstitials (O_i). The transition from complicated V_oZn_i defects to zinc vacancies defects is responsible for the emission at 620 nm. [143–145].

5.1.3.5 Resistivity

Transparent conductor is one of the most common applications of ZnO thin films. The electrical property of thin films is also an vital factor for its performance in devices. So, resistivity of thin films is accessed by using Vander Pauw measurements. The sheet resistance is calculated using the formula

$$R_s = \frac{\pi R}{ln\ 2} \tag{5.4}$$

The electrical resistivity of thin films is computed by using the following formula

$$\rho = R_s.t \tag{5.5}$$
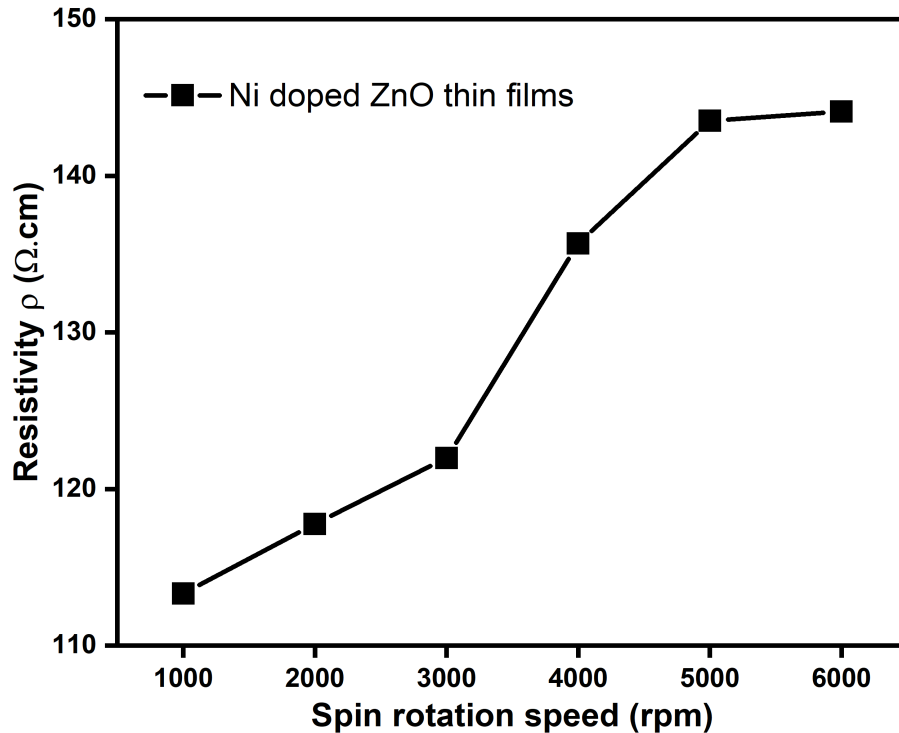
Figure 5.15: Variation of resistivity of Ni-doped ZnO thin films with spin coating speed

Vander Pauw technique was employed to evaluate the resistivity of Ni-doped ZOTFs deposited at spin revolution speed of 1000 rpm to 6000 rpm. The resistivity of thin films was observed to rise from 113 to 177 Ωcm. as the spin rotation speed was increased from 1000 rpm to 6000 rpm. *Shuqun Chen et al*. [164, 165] also observed a drop in resistivity as layer thickness increased. The resistivity of Ni-doped ZOTFs deposited at different spin rotation speeds is demonstrated in Figure 5.15.

5.2 FABRICATION OF Al-DOPED ZnO THIN FILMS AND ITS CHARACTERIZATION

5.2.1 Introduction

Photovoltaic devices, flat panel displays and many other applications have requirement of TCO coatings, which have been the focus of numerous studies for decades [166]. The most frequently utilized TCO in industry are indium tin oxides (ITOs). High cost and limiting resources of Indium promoted the development of TCOs alternatives. Doped ZnO has emerged as the most suitable alternatives for ITO. Al-doped ZnO is a potential material for use as a TCO because of its low resistivity and great transparency in the visible range [167]. Zinc oxide is a semiconductor with a direct and huge band gap that

has a wide range of uses in the semiconductor industry [168, 169]. Moreover doped ZnO can be deposited by low temperature simple chemical sol-gel route [170, 171]. Al-doped ZOTFs grown on glass substrate through acetate dihydrate, aluminium chloride hexahydrate inorganic precursors using the sol-gel spin coating process are described in this section. The UV-visible, Raman and fluorescence spectroscopy were utilized to characterize the deposited films and optical, vibration and fluorescence properties of the thin film are critically discussed.

5.2.2 Experimental Details

The 0.5M 1% Al doped ZnO solution was prepared by dissolving zinc acetate dihydrate and aluminum chloride hexahydrate in 2-methoxy ethanol and stirring for 30 minutes at 70 °C. When the solution became cloudy, monoethanolamine (MEA) was added drop by drop to stabilize it by keeping the Zn^{2+}/MEA molar ratio to unity. After preparing the sol solution, it is kept for aging in airtight bottles at room temperature for 48 hours. The glass substrate (2.5cm × 2.5cm) was cleaned and dried in an oven at 150 °C for 30 minutes before fabricating the thin films, as described in earlier chapters. The aged solution has been used for fabrication of Al-doped ZOTFs on pre cleaned glass. Spin deposition technique has been utilized for fabrication of films. The films are fabricated by dropping the sol with the help of dropper on spinning glass substrate. Thin films are deposited at substrate revolution speed of 1000 rpm to 6000 rpm. The film is then dried at hot plate at 100 °C to eradicate the organic solvents from the material. To achieve the necessary thin film thickness, the deposition and drying cycle is repeated six times. Finally, the films are annealed for 3 hours in a tube furnace at 350°C to enhance their microstructure and crystallinity. Figure 5.16 depicts the flow chart for the synthesis of Al-doped ZOTF.

5.2.3 Results and Discussion

5.2.3.1 UV Visible Spectra

Films of 1 at% Al-doped ZnO have been synthesized on glass substrate using spin deposition sol-gel technique at the speed of substrate rotation varying from 1000 rpm to 6000 rpm. Figure 5.17 shows the absorbance spectra of synthesized films in the range of wavelength of 300-1100 nm. Figure 5.17 illustrates that the absorbance is lowest between 400 nm and 1100 nm and then it increases with a decrease in wavelength and
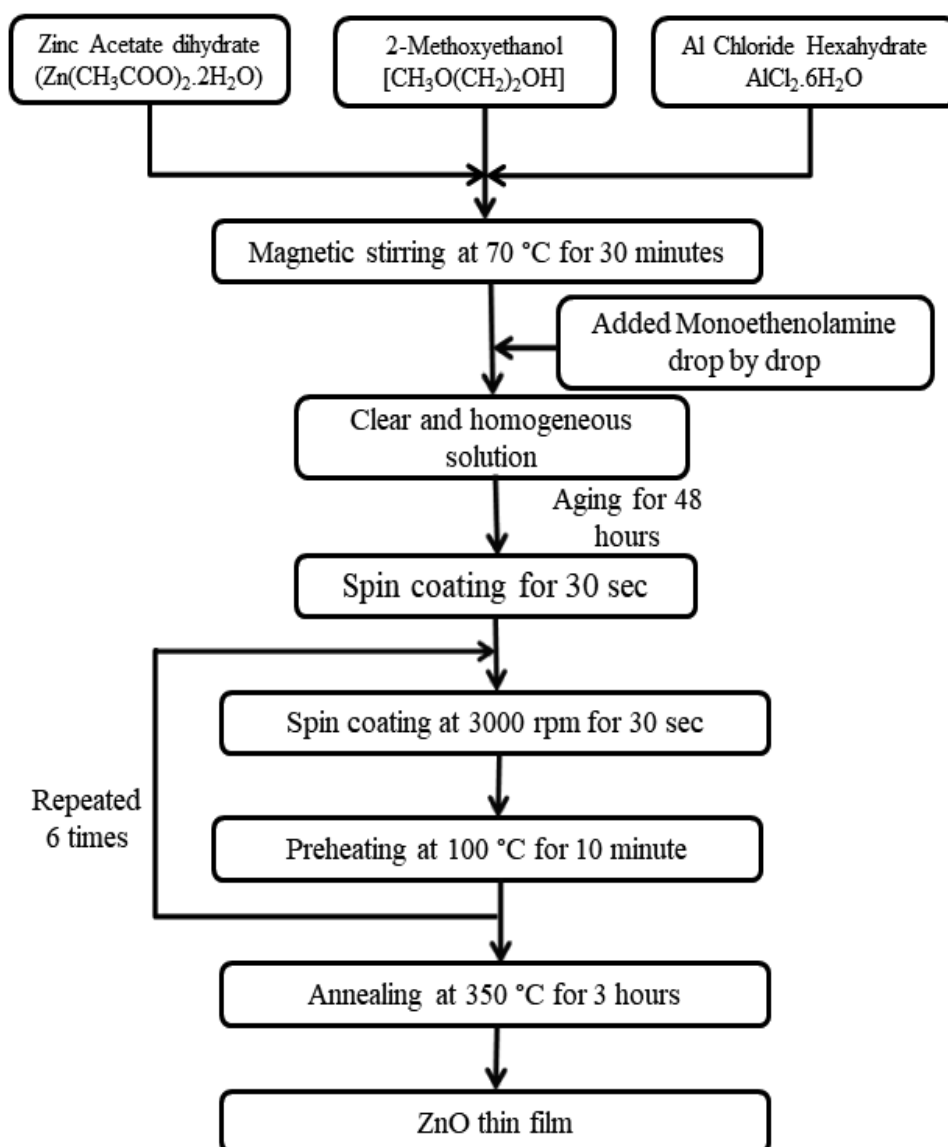
Figure 5.16: Flow Chart for fabricating 1 at% Al doped ZnO thin films
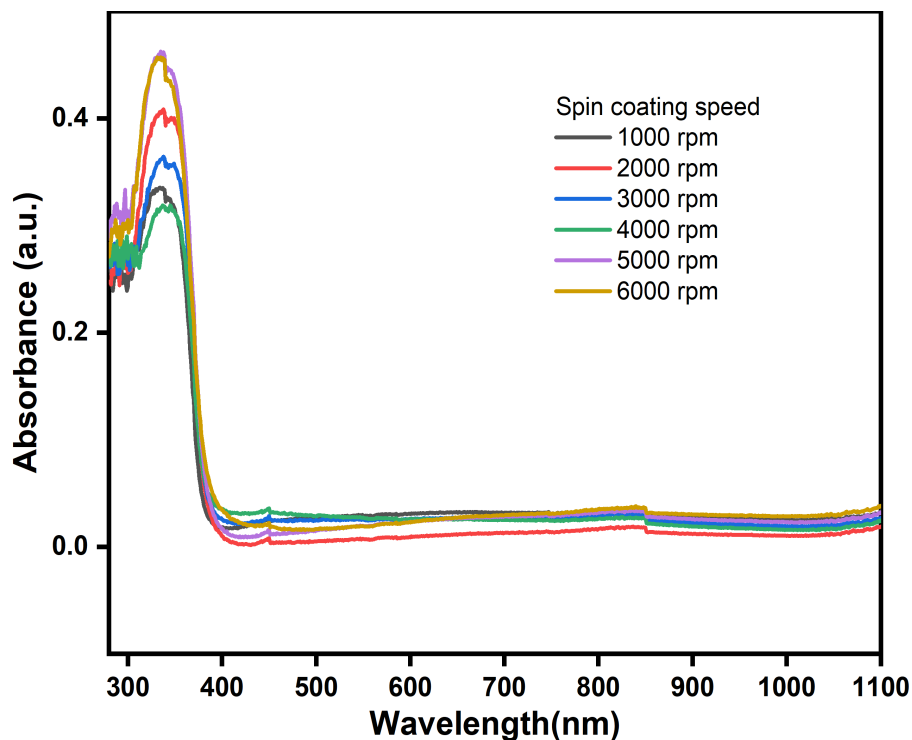
Figure 5.17: Absorption spectra of 1 at% Al doped ZnO thin film synthesized at 1000-6000 rpm

Table 5.3: Variation of peak absorbance of Al doped ZnO thin films with spin coating speed

Sr. No.	Spin Coating Speed (rpm)	Peak Absorbance value (a.u.)
1.	1000	0.313
2.	2000	0.397
3.	3000	0.352
4.	4000	0.308
5.	5000	0.452
6.	6000	0.445

touches its maximum value at 336 nm. Absorbance starts increasing with a decrease in the wavelength at the absorption edge about 385nm, which is related to the band gap of thin films [172–174]. The films show low absorbance in the visible and near-infrared regions, but strong absorbance in the ultra violet domain, as per the absorption spectrum. Figure 5.18 shows the variation in highest absorbance as a function of spin coating speed from 1000 to 6000 rpm.

Figure 5.19 displays the variation of optical transmittance of Al-doped ZOTFs synthesized by spin deposition process at 1000 rpm to 6000 rpm using double beam UV-spectrophotometer in the wavelength range 300 nm to 1100 nm. It has been perceived from the figure that the transmittance is greater than 90% in the long wavelength larger than 400 nm [175–177]. High transmittance in the visible spectrum of radiation is the
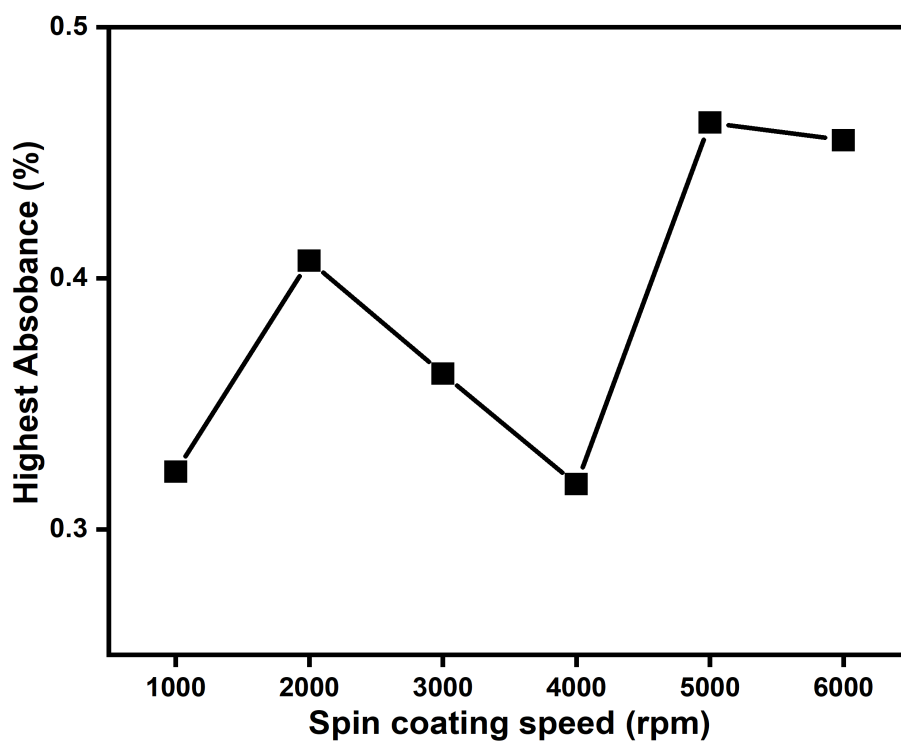
Figure 5.18: Variation of highest absorbance with spin coating speed from 1000-6000 rpm
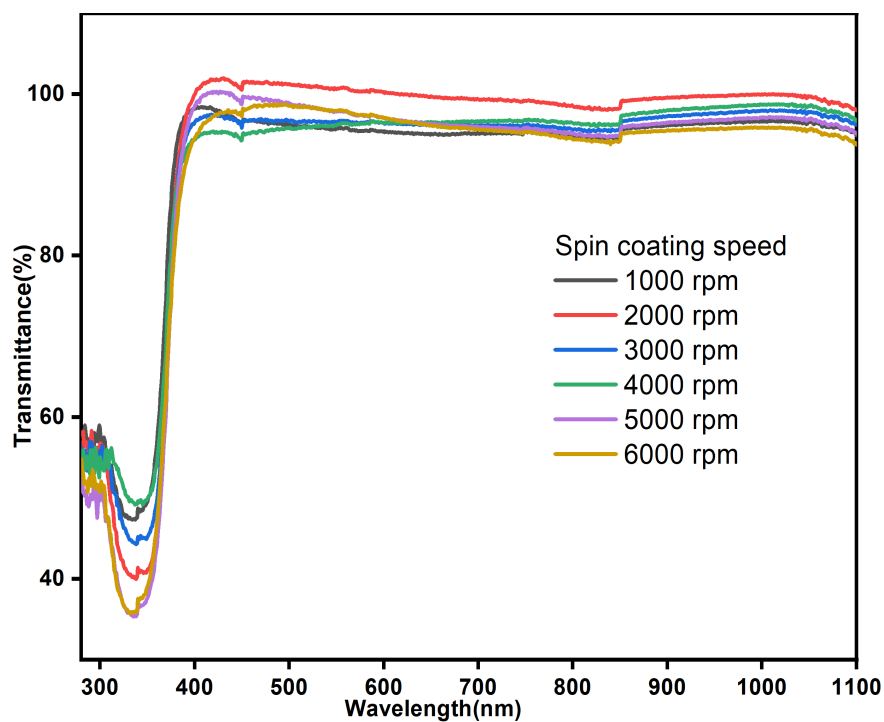
Figure 5.19: Transmission spectra of 1 at% Al doped ZnO thin film synthesized at 1000-6000 rpm
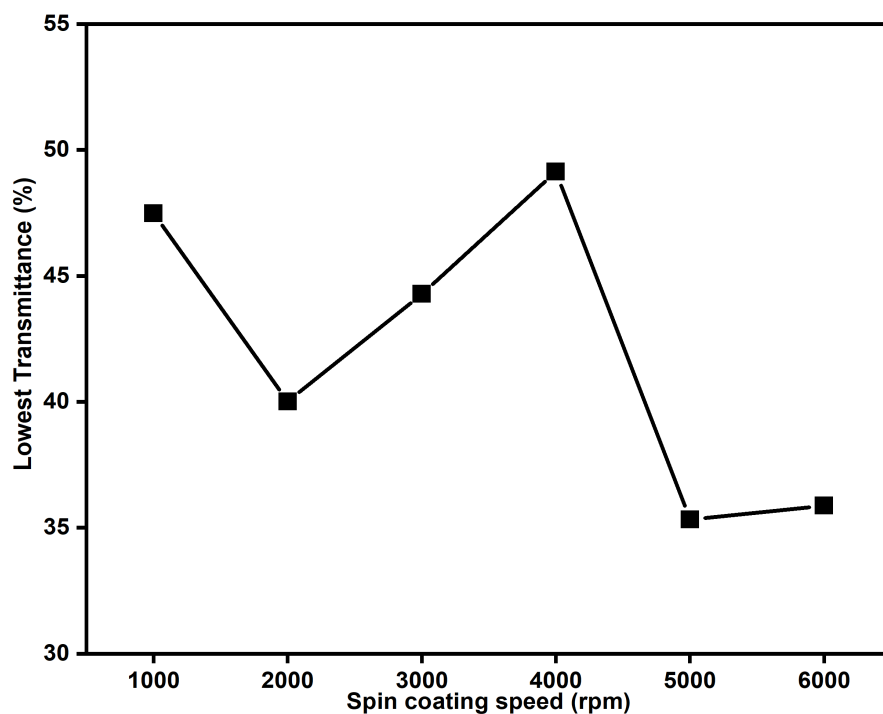
Figure 5.20: Variation of lowest transmittance with spin coating speed from 1000-6000 rpm

Table 5.4: Variation of lowest transmittance of Al doped ZnO thin films with spin coating speed

Sr. No.	Spin Coating Speed (rpm)	Lowest Transmittance value (%)
1.	1000	47.48
2.	2000	40.01
3.	3000	44.28
4.	4000	49.13
5.	5000	35.33
6.	6000	35.87

key property for the application of the films in TCOs. Figure 5.20 reveals the variation of the lowest transmittance of the films synthesized at the glass spinning speed of 1000 rpm to 6000 rpm. The lowest transmittance values were observed to be highest for 4000 rpm and minimum for spinning speeds of 5000 rpm and 6000 rpm. This unveils that the films behave as transparent material in visible and NIR regions of the spectrum.

5.2.3.2   Raman Spectra

The Raman spectra of Al-doped ZnO thin film fabricated on glass substrate at the revolution speed of 1000 - 6000 rpm by spin coating route using sol-gel is reported herein. The vibrational Raman spectra of the thin films are illustrated in Figure 5.21.
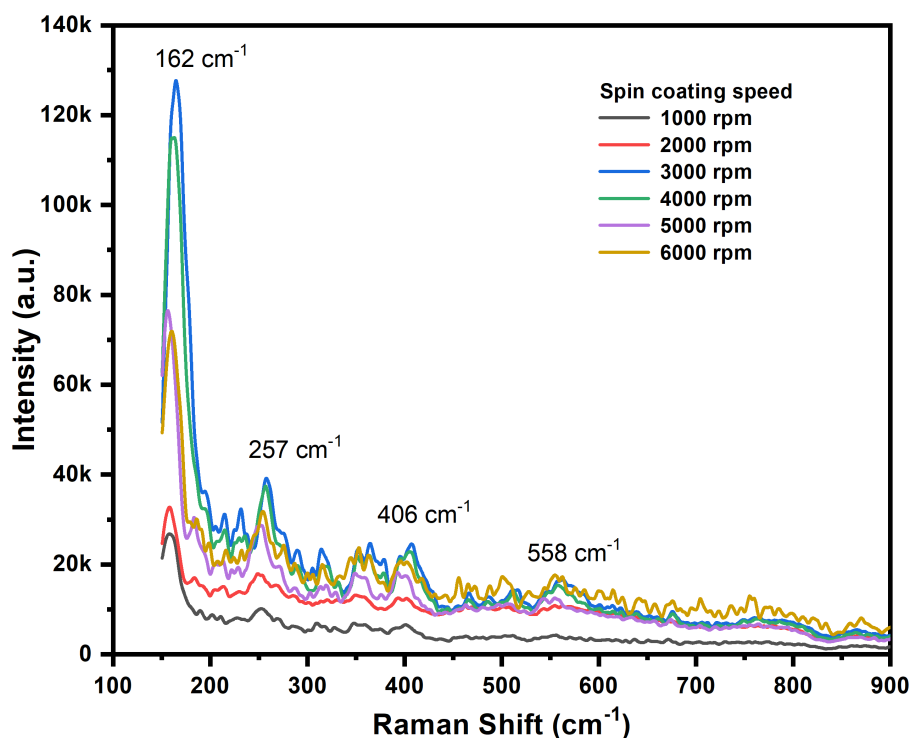
Figure 5.21: Raman spectra of 1 at% Al doped ZnO thin film synthesized at 1000-6000 rpm

The Figure 5.21 demonstrates the appearance of Raman peaks at frequencies 162 cm^{-1}, 258 cm^{-1}, 406 cm^{-1} and 558 cm^{-1}. Overtones of TA phonons around the M point may be responsible for the peak appearing at 162 cm^{-1} [135]. The presence of peak at 258 cm^{-1} is attributed to 2TA mode [162]. The occurrence of Raman peak at 406 cm^{-1} and 558 cm^{-1} is due E_1 (TO) and A_1 (LO) modes. The peak at the frequency of 561 cm^{-1} (A_1 (LO) modes) is caused by lattice defects, such as oxygen vacancies and zinc interstitials or a combination of these [163].

5.2.3.3   Photoluminescence Spectra

Fluorescence spectroscopy is a good in-depth method for determining a material's specific band edge transition levels. A well-defined fluorescence spectrum of the synthesized ZnO thin films ranging from 1000 to 6000 rpm is depicted in Figure 5.22.
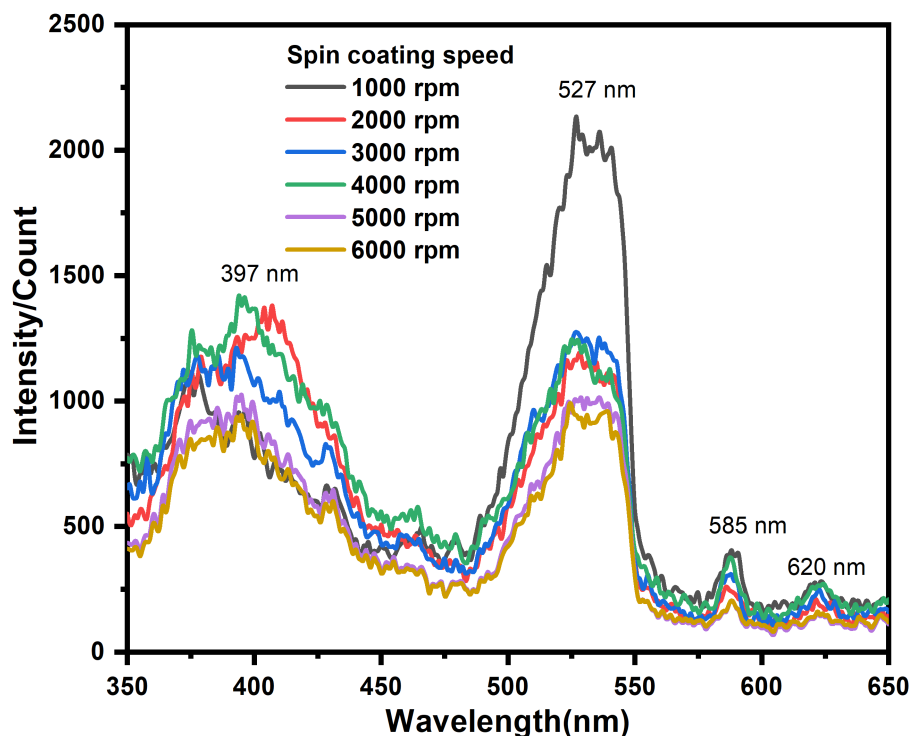
Figure 5.22: Fluorescence spectra of 1 at% Al doped ZnO thin film synthesized at 1000-6000 rpm

The photoluminescence of Al-doped ZOTFs prepared on glass at substrate spinning speed of 1000 rpm to 6000 rpm using sol-gel chemical route, has been measured by Spectrofluorometer (FluoroSENS Camlin Photonics). The UV emission peak at about 397 nm corresponds to the near band emission transition from lower edge of CB to upper edge of VB [138, 139]. The UV peak is characterized by the band gap of the thin films. The green emission peak in visible region at about 527 nm is credited to the O_2 vacancies (V_o) and antisite oxygen (O_{zn}) [140–142]. At 585 nm, the emission corresponds to oxygen interstitials (O_i). The transition from complicated V_oZn_i defects to zinc vacancies defects is responsible for the emission at 620 nm. [143–145].

5.3   FABRICATION OF Co-DOPED ZnO THIN FILMS AND ITS CHARACTERIZATION

5.3.1   Introduction

ZnO is recognized as astounding semiconductor material as for use in various opto-electronic, SAW and spintronics devices. Doping of extrinsic impurity elements is an effective approach to modify its various properties for multi-functional applications [178–182]. ZnO has the potential to replace all wide band gap semiconductors like GaN which are widely used in UV, blue, green emission, photo-detector, solar cells and LEDs [183–187]. Doping of transition metal elements like Co, Mn, Fe induces magnetic properties in ZnO thin films which have enormous applications in spintronics devices [188–190]. Co is among the important metallic element doped in ZnO lattice since it can modify the structure, luminescence, optical and magnetic characteristics of ZnO [191–193]. Several techniques have been utilized for the deposition of Co-doped ZOTFs e.g. electrochemical deposition [194], sputtering [195], PLD [196], spray pyrolysis [197] and sol-gel [198, 199]. Among these techniques sol-gel method for thin film fabrication is ingenious, low cost, low temperature and ease of adding dopants. In this section of work, the synthesis of Co-doped ZOTFs on glass using an ingenious economical wet chemical based sol-gel spin deposition technique is discussed. The thin films have been deposited at the substrate spinning speed of 1000 rpm to 6000 rpm. Optical, Vibrational and luminescence properties of the synthesized films have been discussed by making use of UV visible spectroscopy, Raman spectroscopy and fluorescence spectroscopy.

5.3.2   Experimental Details

Zinc acetate dihydrate (ZAD), cobalt acetate tetrahydrate (CATH) and 2-methoxy ethanol (2ME) are used as starting material for the preparation of 0.5M 1 at% Co-doped solution by simple chemical based sol-gel technique. In the first step, ZAD and CATH are dissolved in 2ME at 70 °C for 30 minutes using a stirrer. After 30 minutes the solution becomes murky and then drop by drop, monoethanolamine (MEA) has been added to stabilize it by keeping the molar ratio of Zn^{2+}/MEA to unity. The solution turns transparent and homogeneous. The formed solution is further stirred for 2 hours at 70 °C using a magnetic stirrer. The obtained solution is filled in air-tight glass bottles to age it for 48 hours at ambient temperature. The flow chart for the preparation of Co-doped
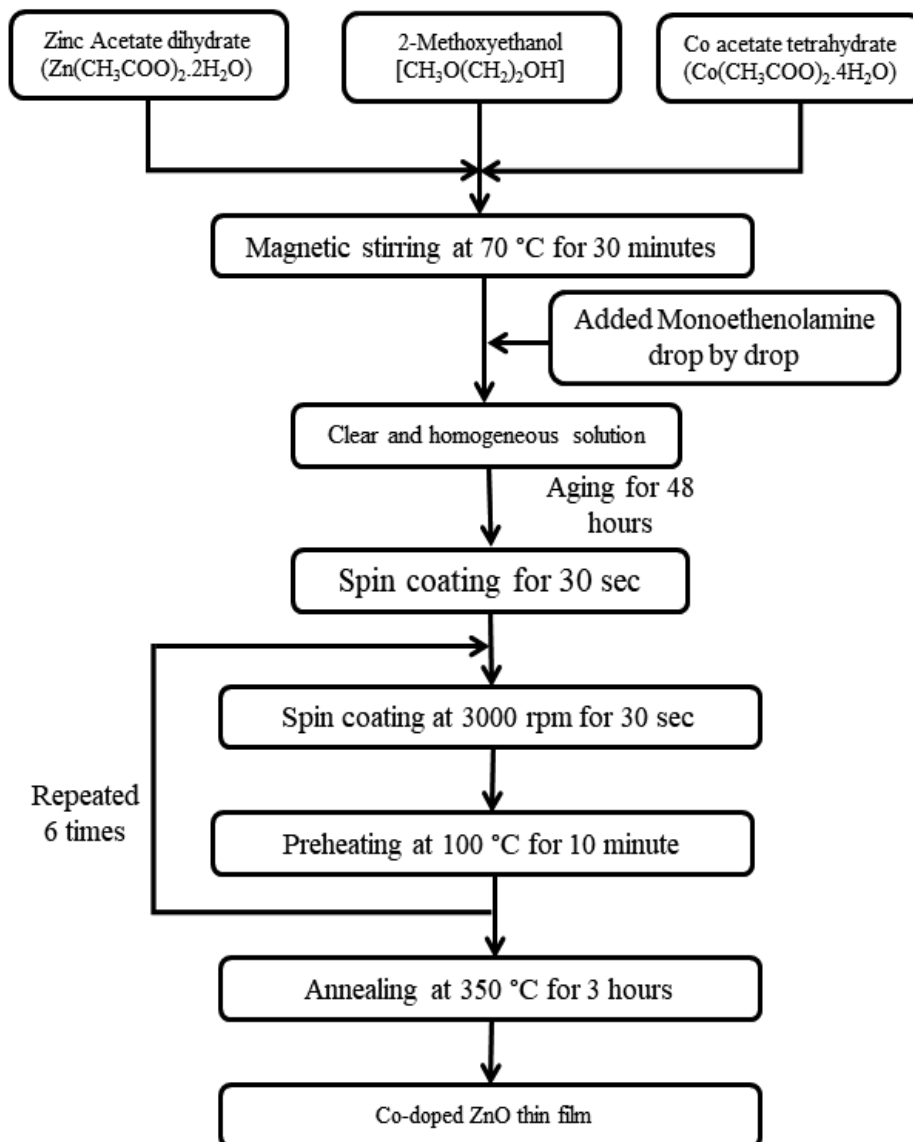
Figure 5.23: Flow Chart for fabricating 1 at% Co-doped ZnO thin films

ZOTF is shown in Figure 5.23. Before being coated with thin films, glass substrates are ultrasonically cleaned with acetone and DI water and then dried for 30 minutes at 150 °C. On pre-cleaned glass substrates, the aged solution was utilized to fabricate undoped ZnO thin films. The spin deposition process was used to fabricate the films. The films are fabricated by dropping the solution onto a rotating glass substrate with the use of a dropper. In this technique, the substrate is consistently coated with the sol. Thin films are deposited at speeds ranging from 1000 to 6000 revolutions per minute over a rotating substrate. The films are then dried on a hot plate at 100 degrees Celsius to eliminate the organic solvents. To achieve the necessary thin film thickness, the deposition and drying step is repeated six times. Finally, the films are annealed for 3 hours in a tube furnace at 350°C to enhance their microstructure and crystallinity.

The absorption and transmission spectrum of Co-doped ZOTFs fabricated by spin coating using sol-gel technique are examined by double beam UV visible spectrophotometer in the wavelength range from 300 nm to 1100 nm. The vibrational study is carried out by Enspectr Enhanced Raman Spectrometry at a wavelength of 532 nm. The Photoluminescence emission analysis is done with Spectrofluorometer (FluoroSENS Camlin Photonics) in 300-750 nm range of wavelength.

5.3.2.1   UV Visible Spectra

The absorbance spectra of the synthesized 1 at% Co doped ZOTFs at rotating speed from 1000-6000 rpm were investigated in 300 nm to 1100 nm range of wavelength as depicted in Figure 5.24. The absorbance is observed to increase for all thin films from 300 nm and reaches the maximum value at 355 nm and then it decreases sharply up to 420 nm. The films exhibit low absorbance in the visible and near-infrared regions, but strong absorbance in the ultraviolet domain, according to the absorption spectrum. The highest absorbance is found to decrease with spin revolution speed as shown by Figure 5.25 and Table 5.5.

The optical transmittance spectra of 1 at% Co-doped ZOTFs fabricated at rotating speed from 1000-6000 rpm were investigated in 300 nm to1100 nm range of wavelength and presented in Figure 5.26. Short wavelengths (<370 nm) have a low transmission value, whereas long wavelengths (>420 nm) have a high transmission value. The figure shows that the thin films optical transmittance is higher than 85% in the visible and NIR region of the spectrum, this means that the films behave as a transparent material at longer wavelengths. High transmittance in the visible region is a requirement for TCOs. It is also observed from Figure 5.27 and Table 5.6 that the lowest transmittance increases
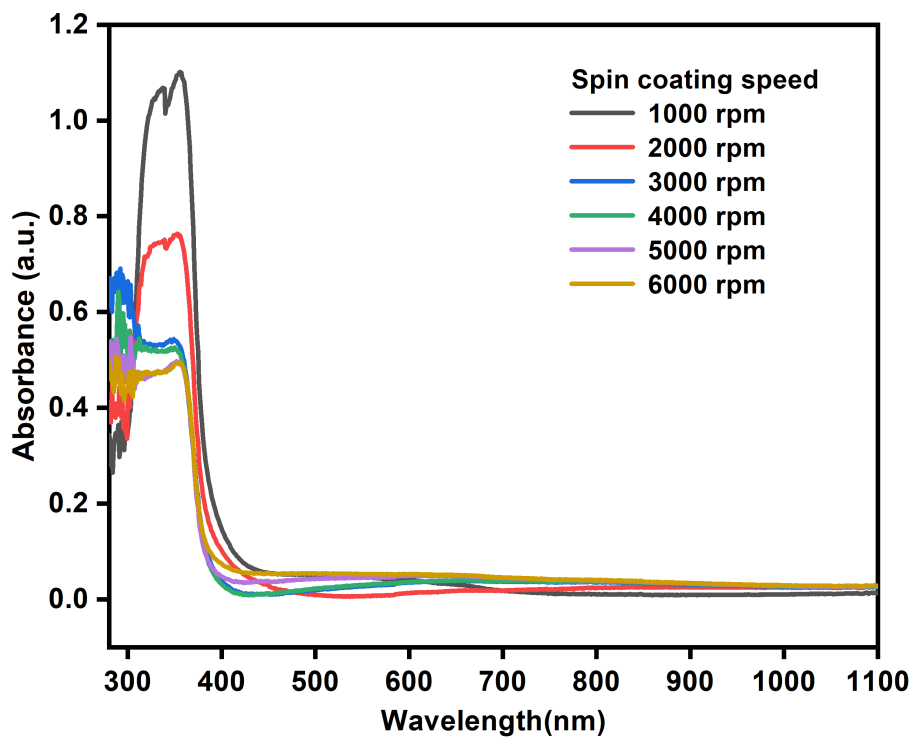
Figure 5.24: Absorption spectra of 1 at% Co-doped ZnO thin film at synthesized at 1000-6000 rpm
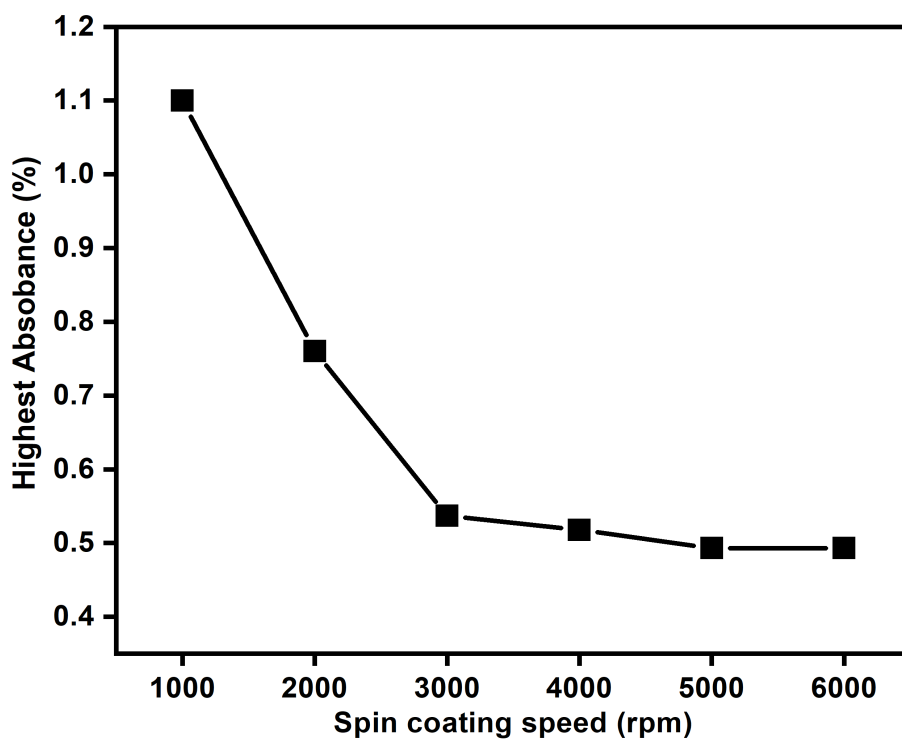
Figure 5.25: Variation of highest absorbance with spin coating speed of Co doped ZnO thin films
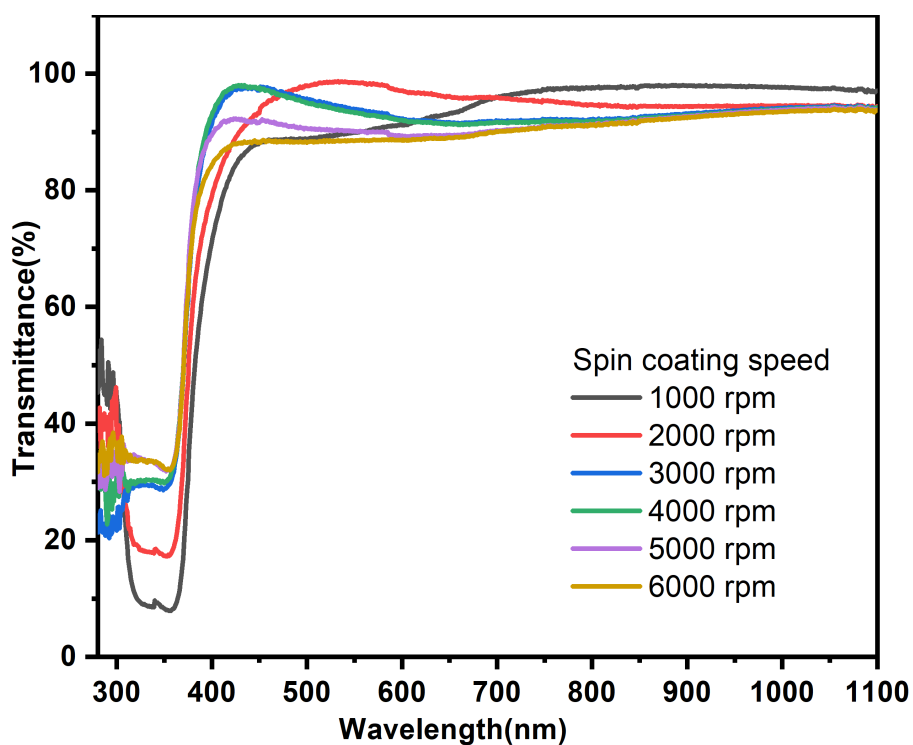
Figure 5.26: Transmittance spectra of 1 at% Co doped ZnO thin film at synthesized at 1000-6000 rpm
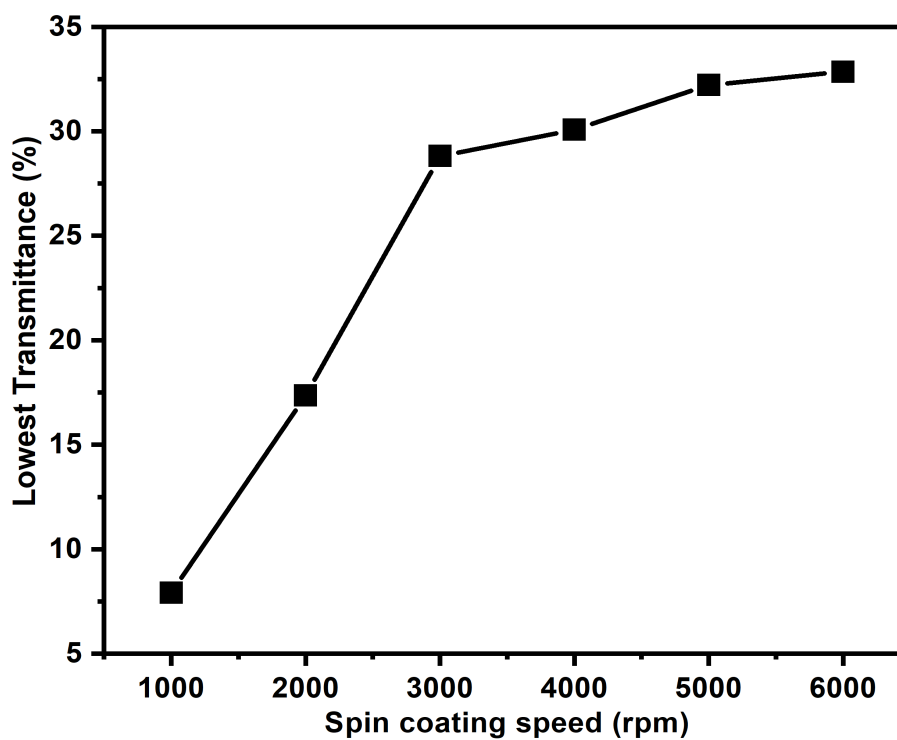
Figure 5.27: Variation of Transmittance versus spin coating speed of Co doped ZnO films

Table 5.5: Variation of peak absorbance of Co doped ZnO thin films with spin coating speed

Sr. No.	Spin Coating Speed (rpm)	Peak Absorbance value (a.u.)
1.	1000	1.10
2.	2000	0.76
3.	3000	0.537
4.	4000	0.518
5.	5000	0.493
6.	6000	0.493

Table 5.6: Variation of lowest transmittance of Co doped ZnO thin films with spin coating speed

Sr. No.	Spin Coating Speed (rpm)	Lowest Transmittance value (%)
1.	1000	07.91
2.	2000	17.35
3.	3000	28.81
4.	4000	30.07
5.	5000	32.21
6.	6000	32.84

with as the spin coating speed is increased.

5.3.2.2   Raman Spectra

Figure 5.28 depicts the Raman spectra of Co-doped ZOTFs fabricated at 1000 rpm - 6000 rpm rotation speed by the sol-gel spin coating process. The wurtzite structure of ZnO belongs to the C_{6V}^4 (P6$_3$ mc) space group. The phonon modes are predicted to belong to the 2E$_2$, 2E$_1$, 2A$_1$ and 2B$_1$ symmetries by group theory. Raman active symmetry modes are 2B$_1$ [200, 201].
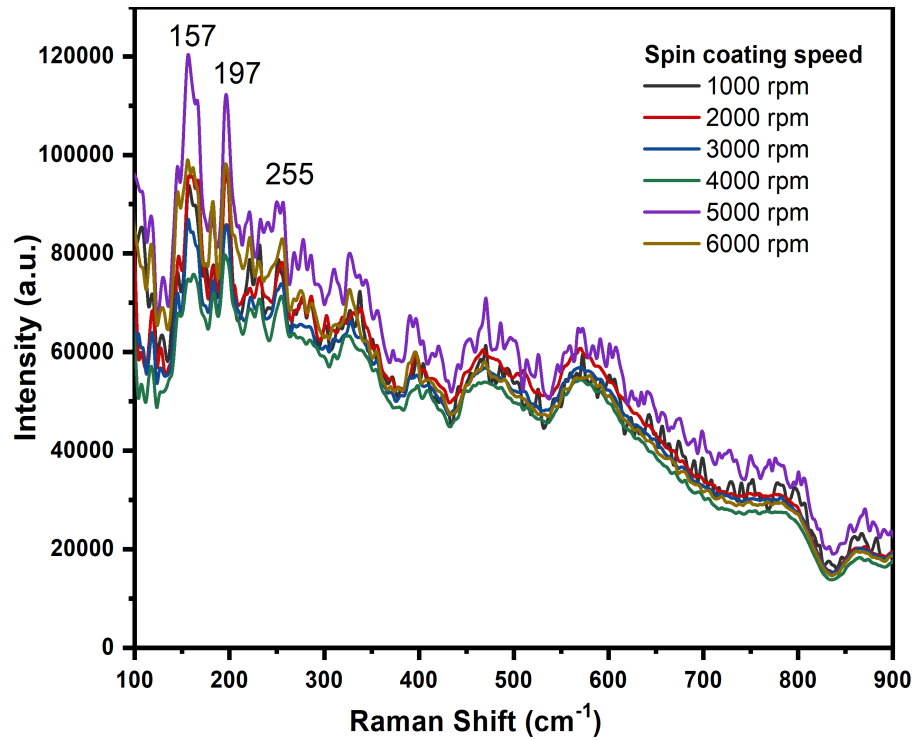
Figure 5.28: Raman spectra of 1 at% Co-doped ZnO thin film at synthesized at 1000 rpm to 6000 rpm

The Raman spectra of Co-doped ZOTFs deposited at 1000 rpm to 6000 rpm speed of rotation of substrate are obtained using Raman Spectrophotometer (EnSpectr R532) and are depicted in Figure 5.28. The Raman peaks are observed at the frequencies of 161 cm^{-1}, 255 cm^{-1}, 410 cm^{-1} and 557 cm^{-1} [134]. Overtones of TA phonons around the M point are responsible for the Raman peak at frequency 163 cm^{-1} [135]. The peaks at 255, 410 and 557 cm^{-1} may be ascribed to 2TA, E_1 (TO) and A_1 (LO) modes [136, 137]. The presence of a peak at roughly 559 cm^{-1} attributed to A_1 (LO) modes might be due to oxygen vacancies or zinc interstitials, or their combination of defects.

5.3.2.3 Photoluminescence Spectra

The Photoluminescence spectrum of Co-doped ZOTFs deposited at spin revolution speed from 1000 to 6000 rpm is depicted in Figure 5.29. The figure reveals the emissions at 385 nm, 429 nm, 521 nm, 586 nm and 620 nm. The exciton recombination related to the near band edge transition (NBE) of ZnO generated the emission peak at about 385nm [202]. The 429 nm emission may be allocated to electron transition from V_{Zn} to VB. The strong green emission peak is related to on-stoichiometric intrinsic defects [203] is ascribed to the O_2 vacancies (V_o) and antisite oxygen (O_{zn}) according to *Jinzhong Wang et al* [204]. The feeble yellow emission peaks witnessed at 586 nm

and 620 nm which is attributed to the non-stoichiometry, producing intrinsic defects in the material that may originate from Zn vacancy and oxygen interstitials in the ZnO [143–145].
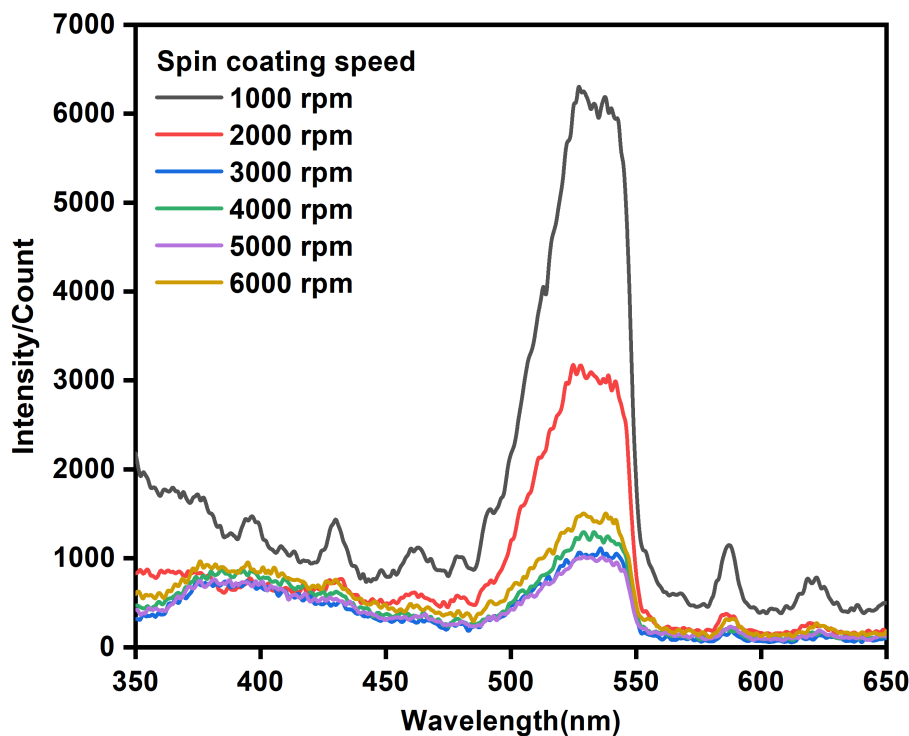
Figure 5.29: Fluorescence spectra of 1 at% Co doped ZnO thin film at synthesized at 1000-6000 rpm

5.4 FABRICATION OF Mn-DOPED ZnO THIN FILMS AND ITS CHARACTERIZATION

5.4.1 Experimental Details

In the first step to prepare 0.5M, 1 at% Mn-doped ZnO solution, zinc acetate dihydrate (ZAD) and manganese acetate tetrahydrate (MATH) are dissolved in 2-methoxy ethanol (2ME) using a stirrer at 70 °C for 30 minutes. Manganese acetate tetrahydrate is used for Mn doping in ZnO. The solution becomes turbid after dissolution because of some un-dissolved residual mass. The next step is to add MEA drops to the solution with the help of a dropper in such a way as to keep the molar ratio of Zn^{2+} and MEA equal to 1:1. The solution becomes translucent and clear. To get a clear and uniform solution, the solution is stirred for another 2 hours at 70 °C. The obtained solution is aged for 48 hours at ambient temperature in air-tight glass bottles. The aged solution is used to deposit the Mn-doped ZOTFs on glass substrates with the help of spin deposition
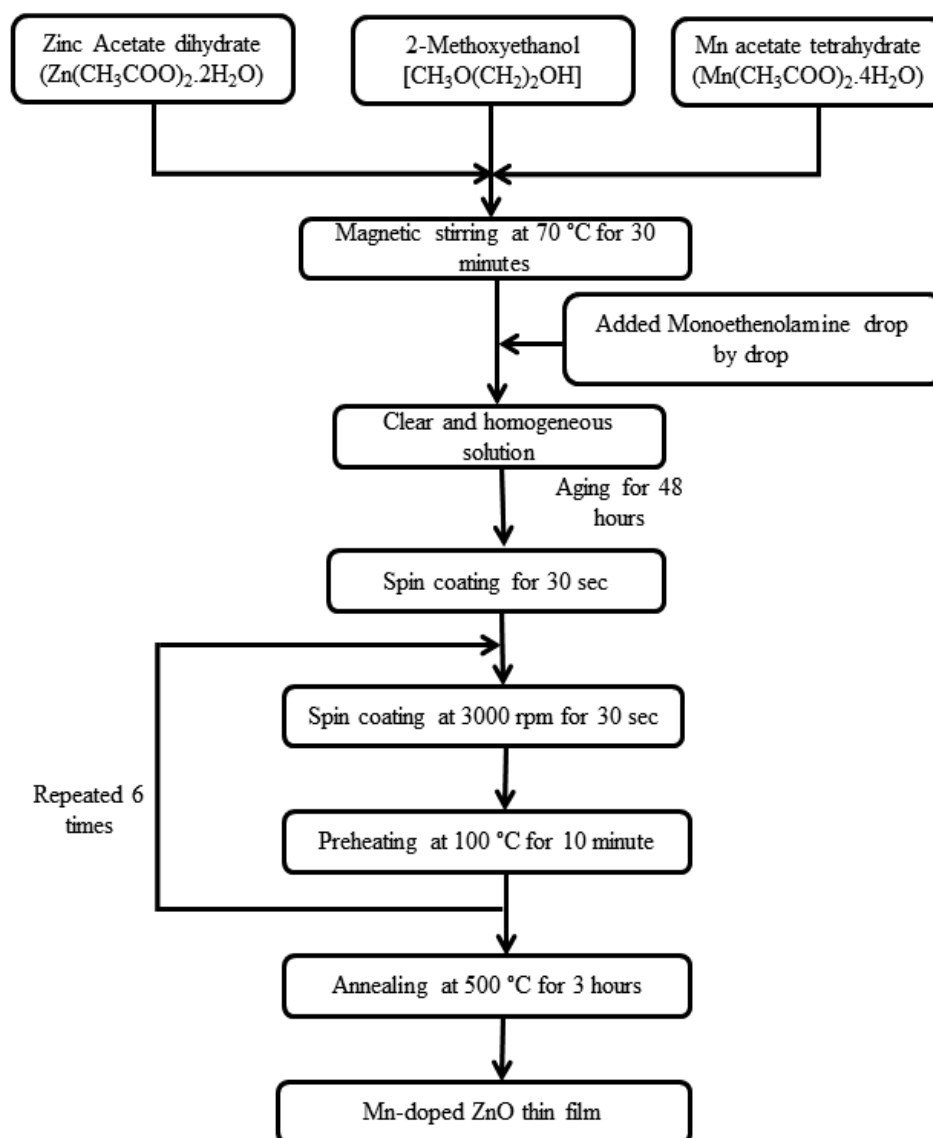
Figure 5.30: Flow chart for fabrication of 1 at% Mn-doped ZnO thin films

method. The cleaning process of glass substrates is already discussed in chapter 3. Glass substrates are cleaned ultrasonically in acetone and DI water and then dried for 30 minutes at 150 °C. The thin films are synthesized by dropping the solution on rotating substrates at the speeds of 1000 rpm to 6000 rpm and then drying at 100 °C to vaporize the organic solvents from the films. The process of depositing and drying is repeated six times in order to achieve the desired thickness of films. In the last step, the thin films are given heat treatment in a tube furnace at 350 °C for three hrs. The block diagram of the process for the deposition of Mn-doped ZnO thin films are represented in Figure 5.30.

5.4.2   Results and Discussion

The absorption and transmission spectrum of Mn-doped ZOTFs is examined by a double-beam UV visible spectrophotometer in 300-1100 nm range of wavelength. The Raman spectrum is studied by Enspectr Enhanced Spectrometry at a wavelength of 532 nm. The photoluminescence spectrum was examined by Fluorescence Spectrometer in the wavelength range of 350-650 nm.

5.4.2.1   UV Visible Spectra

The absorbance spectra of the 1 at% Mn-doped ZOTFs synthesized at rotating speed from 1000 rpm to 6000 rpm were investigated in 300 nm to 1100 nm range of wavelength as shown in Figure 5.31. The film homogeneity as well as the deposition of crack and void free films are dependent on the rotation speed.

It is mentioned that rotation speed affects the quality, uniformity and surface morphology of the thin films which in turn affects the absorption of the thin films. Figure 5.31 shows that the maximum absorbance is noticed at 1000 rpm whereas minimum absorbance is observed at 6000 rpm speed. It is seen from Figure 5.32 and Table 5.7 that the absorption decreases almost linearly from 1000 to 6000 rpm with rotating speed. At the low rotating speed there is a discontinuity in the films due to the lack of enough centrifugal force while at higher speed the discontinuity is possibly due to the excessive centrifugal force which spreads out liquid instantly and causes non-uniform films. As the centrifugal force increases with the rotating speed, so the film thickness decreases with the rotating speed. This is the cause of decreasing absorption with rising rotating speed from 1000 - 6000 rpm. The highest absorbance in visible and NIR region is observed to be for the thin films deposited at the rotation speed of 5000 rpm and 6000 rpm.
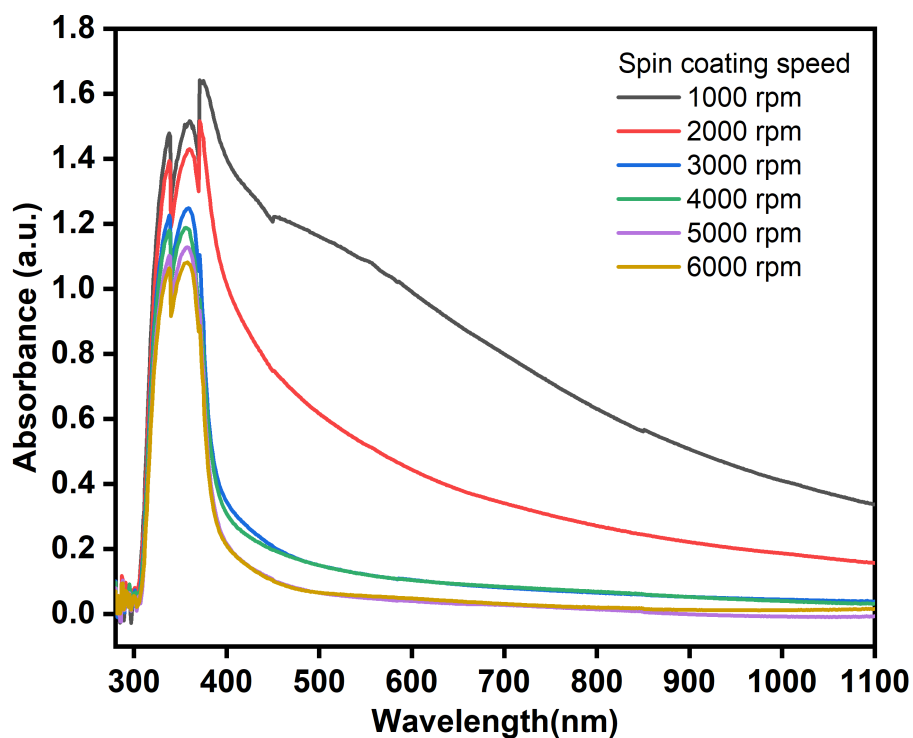
Figure 5.31: Absorption spectra of 1 at% Mn-doped ZnO thin film synthesized at the speed of 1000 rpm to 6000 rpm
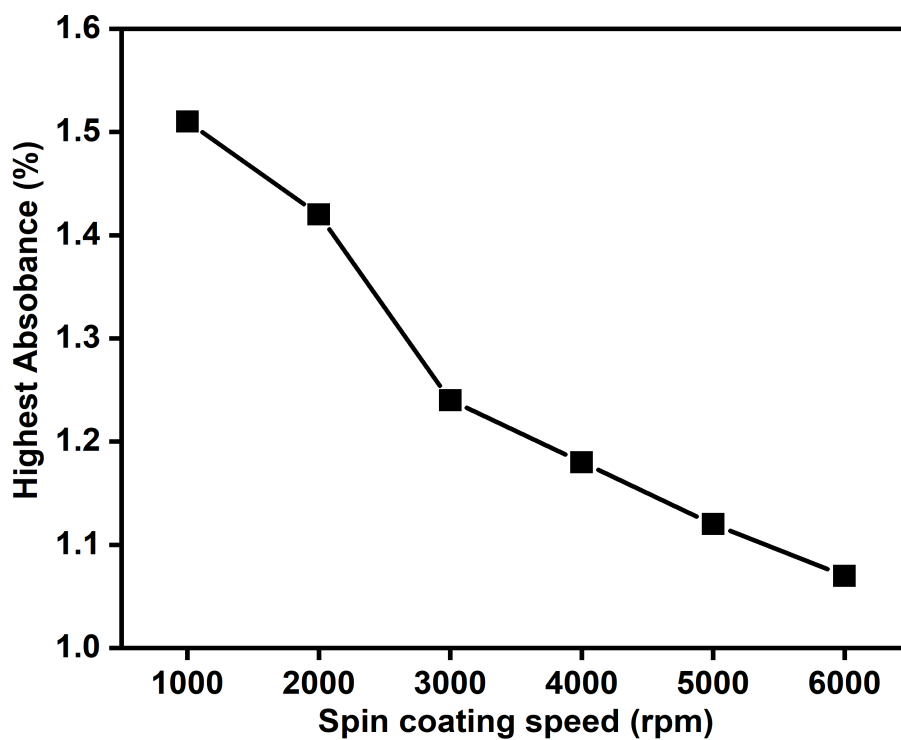
Figure 5.32: Variation of absorbance with spin coating speed from 1000 rpm to 6000 rpm
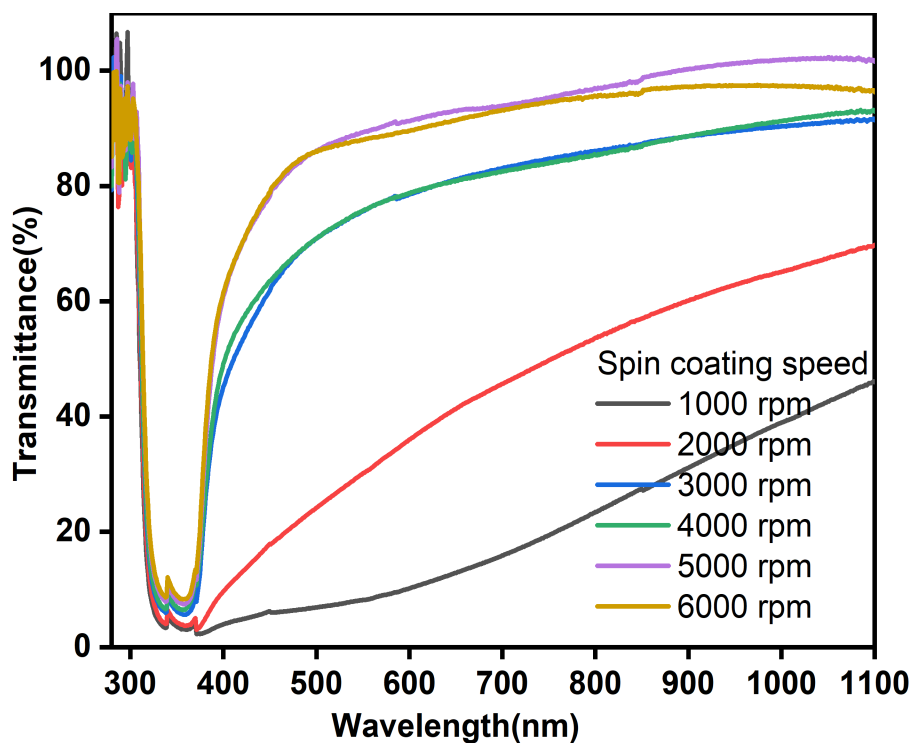
Figure 5.33: Transmittance spectra of 1 at% Mn-doped ZnO thin film synthesized at speed of 1000 rpm to 6000 rpm
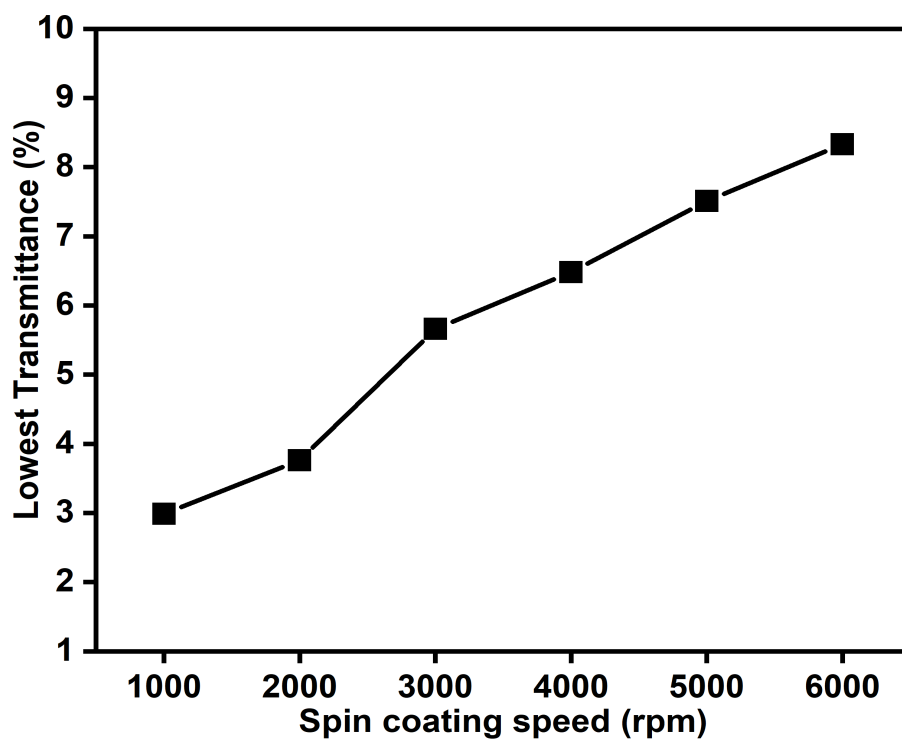
Figure 5.34: Variation of transmittance (%) with spin coating speed from 1000-6000 rpm

Table 5.7: Variation of highest absorbance of Mn-doped ZnO thin films with spin coating speed

| Sr. No.	Spin Coating Speed (rpm)	Highest Absorbance value (a.u.)
1.	1000	1.51
2.	2000	1.42
3.	3000	1.24
4.	4000	1.18
5.	5000	1.12
6.	6000	1.07

Table 5.8: Variation of lowest transmittance of Mn-doped ZnO thin films

Sr. No.	Spin Coating Speed (rpm)	Lowest Transmittance value (%)
1.	1000	2.99
2.	2000	3.76
3.	3000	5.66
4.	4000	6.48
5.	5000	7.51
6.	6000	8.33

Figure 5.33 and 5.34 show the transmittance spectrum and variation of lowest transmittance with rotation speed. It is observed from figure 5.33 and 5.34 that the transmittance of 1 at% Mn doped ZnO thin film increases as the spin speed rises from 1000 to 6000 rpm. The thin films synthesized at 5000 and 6000 rpm speeds have a transmission coefficient greater than 80% in the range of 450 nm to 1100 nm, indicating their potential to be used as transparent conducting oxides for optoelectronic devices [205–207]. In contrast, the transmission value is significantly lower for thin films synthesized at 1000 and 2000 rpm speeds, likely due to the thicker films created by the lower centrifugal forces generated by these slower spin coating speeds. The value of the lowest transmittance increases almost linearly with an increase in the spin coating speed as concluded from Figure 5.34 and Table 5.8.

5.4.2.2 Raman Spectra

Figure 5.35 displays the Raman spectrum of Mn-doped ZOTFs prepared by the sol-gel spin coating process at the spin coating speed of 1000 rpm to 6000 rpm. Raman spectroscopy is a sensitive and effective tool for investigating changes in local structure,
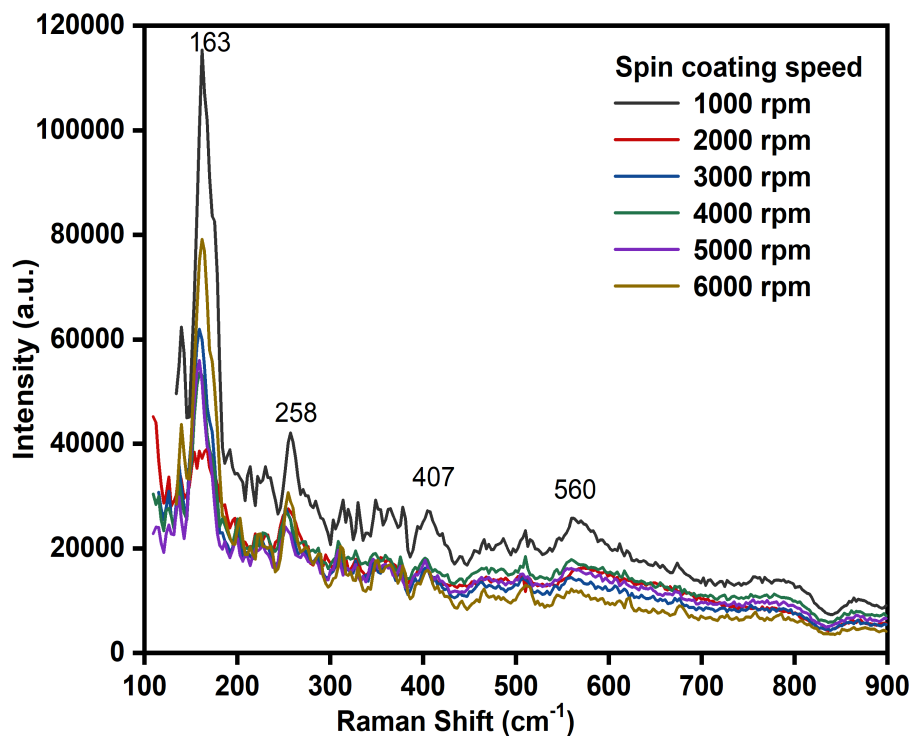
Figure 5.35: Raman spectra of of 1 at% Mn doped ZnO thin film at synthesized at 1000-6000 rpm

defect state and disorder in ZnO. Besides, this technique is used for the study of the crystalline quality of nanostructure. The wurtzite form, which belongs to the C_{6V}^4 (P6$_3$ mc) space group, crystallizes in ZnO. The phonon modes are predicted to correspond to the 2E$_2$, 2E$_1$, 2A$_1$ and 2B$_1$ symmetries by group theory. Normal temperature Raman spectrum of 1 at% Mn-doped ZOTFs synthesized at 1000 rpm to 6000 rpm spin coating speed shown in Figure 5.35 reveals the peaks at frequencies of 163 cm^{-1}, 258 cm^{-1}, 407 cm^{-1}, 464 cm^{-1} and 559 cm^{-1}. The peaks at 161 and 464 cm^{-1} in the low-frequency range are ascribed to the E$_2$ (low) and E$_2$ (high) modes, respectively [208–210]. The low-frequency E$_2$ mode, involves mainly Zn motion and E$_2$ (high) mode represents characteristics of ZnO crystallinity. The peaks near 258 and 407 cm^{-1} may indeed be referred to 2TA and E$_1$ (TO) modes respectively [163, 211]. The development of a peak at a frequency of roughly 559 cm^{-1} indicates A1 (LO) mode, which is associated with lattice defects like oxygen vacancies, zinc interstitials, or a combination of the two [212].

5.4.2.3 Fluorescence Spectra

Fluorescence spectroscopy is an efficient in-depth method for determining a material's specific band edge transition levels. A well-defined fluorescence spectrum of the syn-
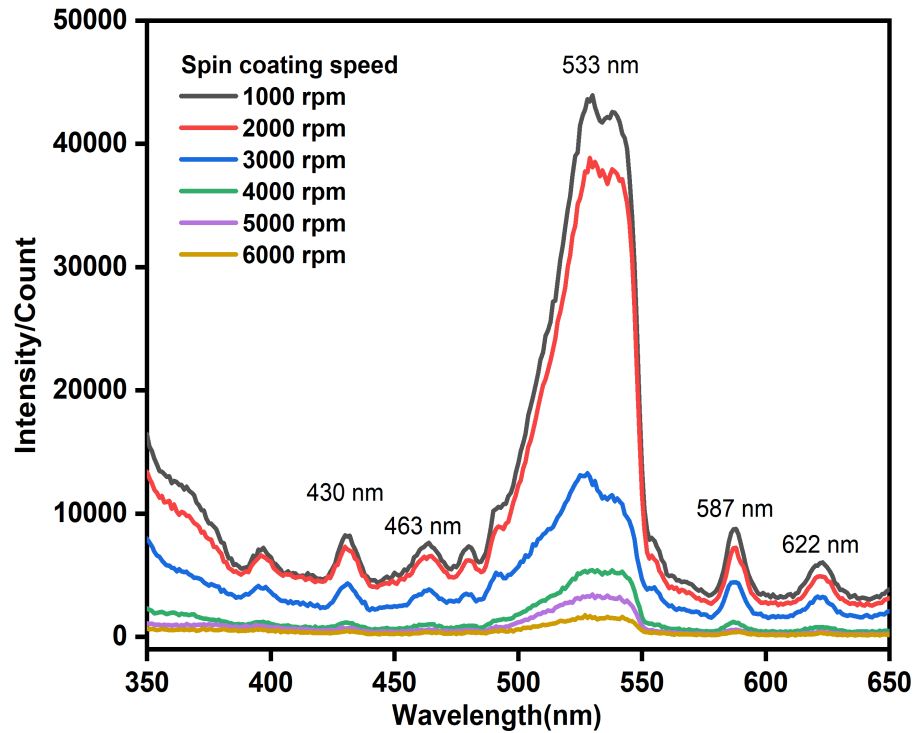
Figure 5.36: Fluorescence spectra of 1 at% Mn-doped ZnO thin film synthesized at 1000-6000 rpm

thesized ZnO thin films ranging from 1000 to 6000 rpm is depicted from Figure 5.36. The fluorescence spectrum exhibited an emission peak at about 395nm, instigated due to the excitonic recombination analogous to the NBE transition of ZnO [138, 213]. The NBE emission is attributed to the radiative annihilation of a hole in the VB with an electron in the CB. This transition is corresponding to the band gap and can be used to calculate it. The emission peaks at 430 nm and 463 nm are allocated to transition from V_{Zn} and Zn_i to VB respectively [35, 214]. The green emission at 533 nm is ascribed to the O_2 vacancies (V_o) and antisite oxygen (O_{zn}) [215]. The 587 nm and 622 nm illumination peaks in ZnO are caused by oxygen interstitial (O_i) or donor defect states, or even the transition from complicated V_oZn_i defects to zinc vacancy defects [216–218].

CHAPTER 6

FABRICATION OF Ni-Al AND Mn-Ni CO-DOPED ZnO THIN FILMS AND THEIR CHARACTERIZATION

6.1 FABRICATION OF Ni-Al CO-DOPED ZnO THIN FILMS AND ITS CHARACTERIZATION

6.1.1 Introduction

Impurities can dramatically change the properties of a semiconductor like ZnO when added to it [219]. It is necessary to dope ZnO with various elements in order to manipulate and optimize its various properties. It has been reported that ZnO has been doped with elements of groups IA, IIIA, VA and VIII such as Li, Al, N and Ni, Co, etc [220, 221]. Doping of Al in the lattice of ZnO has been reported to enhance the electrical property as well as the transparency in the visible range making it a suitable candidate for TCO. Furthermore, ZnO can be improved in terms of its magnetic behaviour by doping it with magnetic ions such as Ni. This process results in the formation of dilute magnetic semiconductors (DMS), which are vital for spintronic applications. The development of zinc oxide-based diluted magnetic semiconductors (DMS) is of considerable importance due to the high Curie temperature requirement of spintronic devices [222]. The incorporation of multiple atoms into ZnO can induce and amplify various properties of the material. As an illustration, the doping of Al in ZnO enhances the electrical property whereas the doping of transition metal such as Ni can induce high-temperature ferromagnetism in it. So with the help of co-doping of Al and Ni both in ZnO can enrich the material with suitable electrical and ferromagnetic properties which
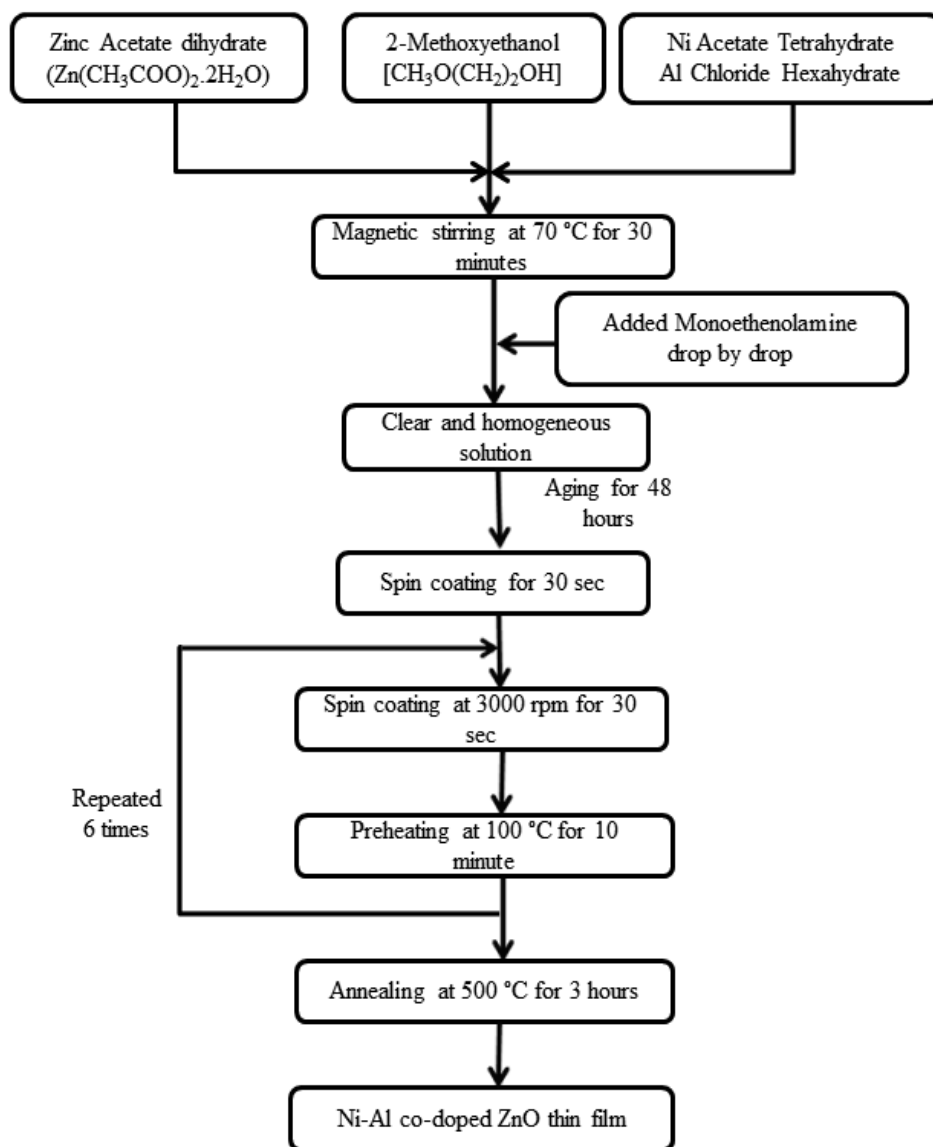
Figure 6.1: Flow Chart for fabricating 1 at% Ni and 1 at% Al co-doped ZnO thin films

in turn opens the way for the generation of new devices. The doping of ZnO with transition metals and Al has recently been studied for both practical and scientific purposes. Increasing Ni content resulted in enhanced ferromagnetic behaviour for the Ni and Al co-doped thin film [223–225]. In this section, Ni-Al co-doped ZOTFs have been fabricated using sol-gel on glass substrates by spin deposition process at spin revolution speed of 1000 rpm to 6000 rpm. The optical, vibrational and fluorescence properties of a ZnO thin film deposited on a glass substrate, which was co-doped with Ni-Al, were studied using UV-visible, Raman and fluorescence spectroscopy. The effects of the co-doping on these properties were closely examined.

6.1.2   Experimental Details

The 0.5M, Ni-Al co-doped ZnO solution was made by dissolving ZAD, nickel acetate tetrahydrate and aluminum chloride hexahydrate in 2-methoxy ethanol by using magnetic stirrer at 70 °C for 30 minutes. After 30 minutes the solution becomes turbid and some un-dissolved residual mass is left in the solution. Drop by drop, monoethanolamine (MEA) has been added to the resultant solution, keeping the Zn^{2+}/MEA molar ratio at unity. This results in the dissolution of un-dissolved residual mass and solution becomes transparent. The solution is further stirred using magnetic stirrer for 2 hours at 70 °C to make a homogeneous solution. The prepared solution is filled in air tight glass bottles and kept for ageing for 48 hours at room temperature. Spin coating was utilized to deposit thin films on pre-cleaned glass surfaces using an aged solution. Ni-Al co-doped ZOTFs were synthesized at spin revolution speed of 1000 rpm to 6000 rpm, then dried for 10 minutes on a hot plate at 100 °C. To get the appropriate thickness of the films, the depositing and drying procedure was repeated six times. Finally, in a tube furnace, the samples are annealed for 3 hours at 350°C. The flow chart for the deposition of Ni-Al co-doped thin films is shown in Figure 6.1.

6.1.3   Results and Discussion
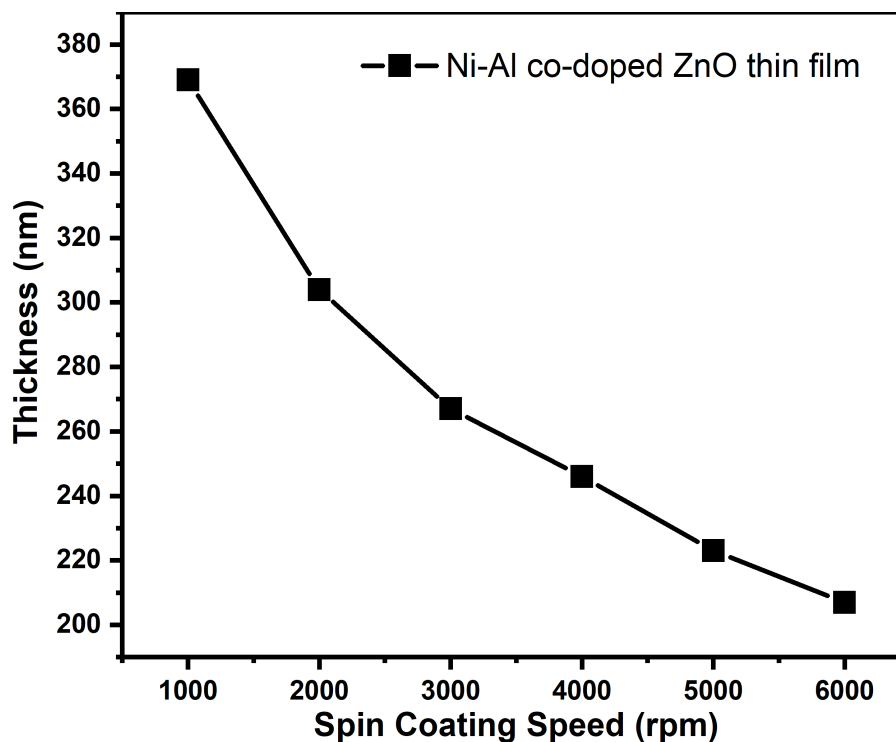
Figure 6.2: Variation of thickness of Ni-Al co-doped ZnO thin film with spin coating speed

Double beam UV visible spectrophotometer is used to analyze the absorption and transmission spectrum in 300 nm to 1100 nm range of wavelength. The Raman spectrum is studied by Enspectr Enhanced Spectrometry using a laser of wavelength 532 nm. The fluorescence spectrum was examined by Fluorescence Spectrometer in 350-700 nm range of wavelength. Figure 6.2 illustrates the variation of the thin film thickness of Ni-Al co-doped ZnO. A cross-sectional view of SEM images was used to measure the thickness of the films. As the rotation speed of the spin coater is increased, the thickness of the resulting film decreases. This is caused by the increased centrifugal force generated by the higher spin speed, which causes the liquid to spread more quickly, resulting in a thinner film.

6.1.3.1 UV Visible Spectra

The absorbance and transmission spectra of the 1 at% Ni and 1 at% Al co-doped ZOTFs synthesized at rotating speed from 1000-6000 rpm were investigated in 300 nm to 1100 nm range of wavelength as shown in Figure 6.3 and Figure 6.5 respectively.
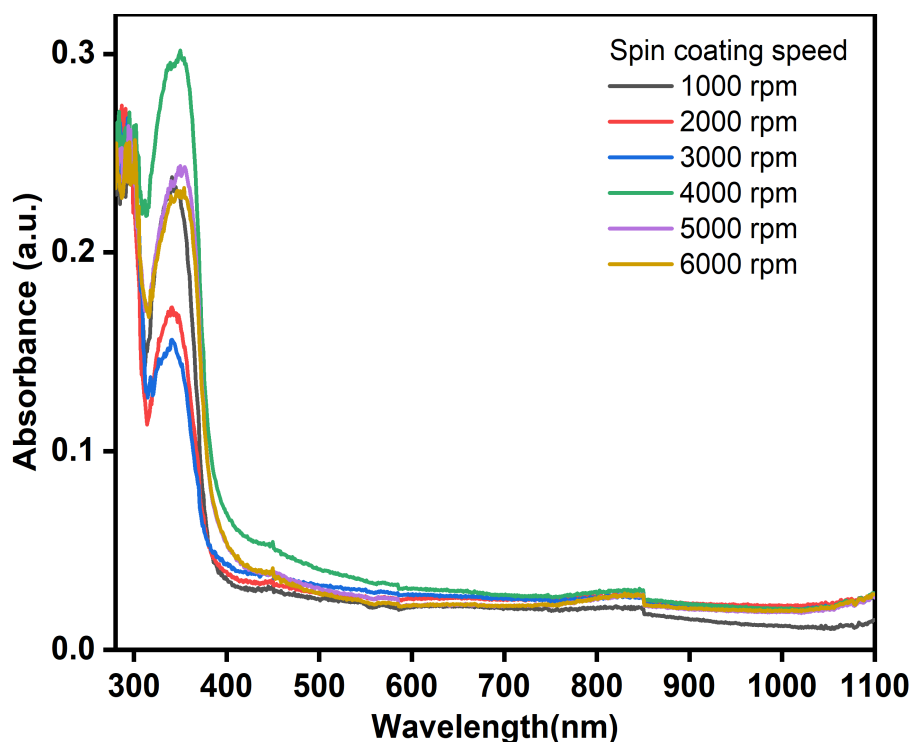
Figure 6.3: Absorption spectra of of 1 at% Ni and 1 at% Al co-doped ZnO thin film at 1000-6000 rpm

The value of absorbance is highest at 340 nm for all thin films. The absorbance starts decreasing sharply at 340 nm and stabilizes almost after 580 nm. The value of absorbance is low in visible and NIR region. Figure 6.4 and Table 6.1 shows the variation
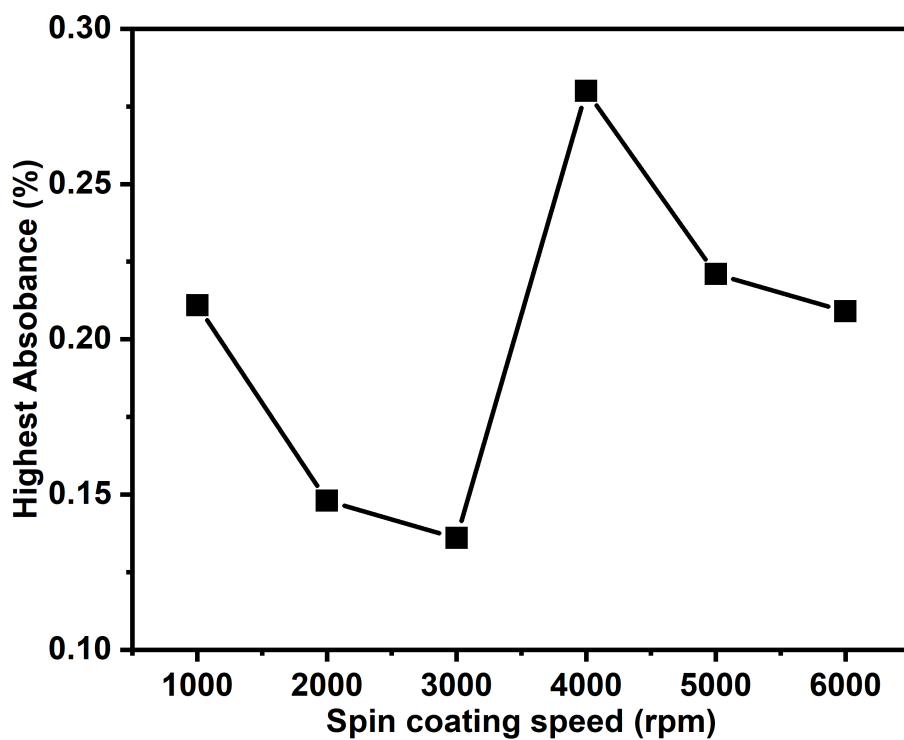
Figure 6.4: Variation of absorbance wrt spin coating speed from 1000-6000 rpm
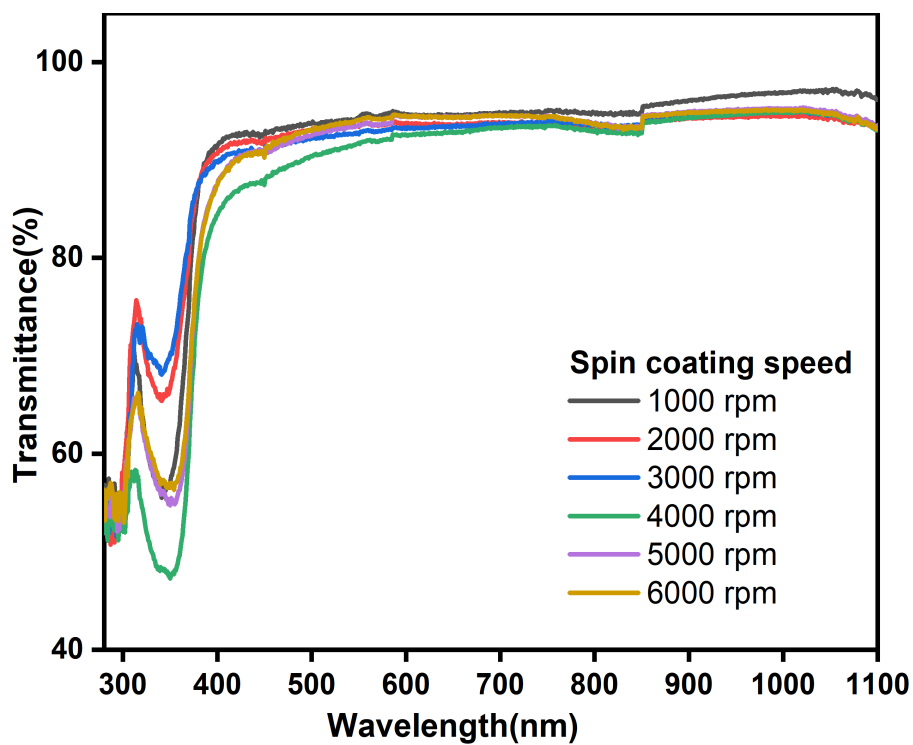
Figure 6.5: Transmittance spectra of 1 at% Ni and 1 at% Al co-doped ZnO thin film at 1000-6000 rpm
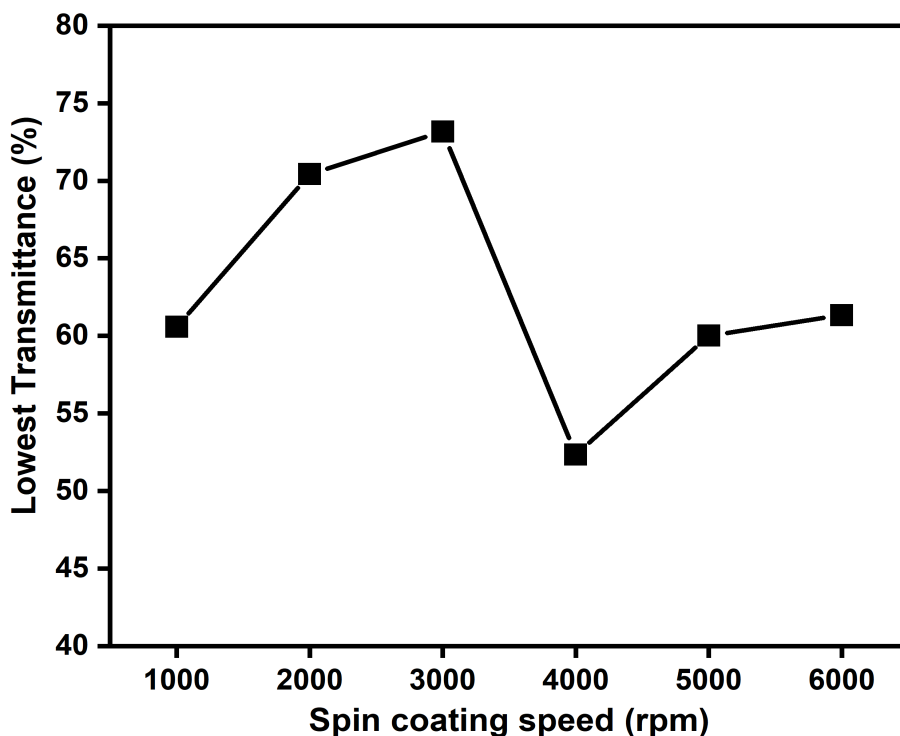
Figure 6.6: Variation of transmittance (%) with spin coating speed from 1000-6000 rpm

Table 6.1: Variation of peak absorbance of Ni-Al co-doped ZnO thin films with spin coating speed

Sr. No.	Spin Coating Speed (rpm)	Peak Absorbance value (a.u.)
1.	1000	0.211
2.	2000	0.148
3.	3000	0.136
4.	4000	0.280
5.	5000	0.221
6.	6000	0.209

of highest absorbance with spin coating speed. The maximum and minimum absorption are observed at 4000 rpm speed and 3000 rpm speed respectively. It is seen that the absorption upsurges almost linearly from 2000 rpm to 4000 rpm and then decreases from 4000 rpm to 6000 rpm. At the low rotating speed, there is a discontinuity in the films due to the lack of enough centrifugal force while at higher speed the discontinuity is possibly due to the excessive centrifugal force which spreads out liquid instantly and causes non-uniform films. So it can be stated that the optimized rotating speed for the deposition of uniform films by spin coating technique is 3000-4000 rpm.

Figure 6.5 displays the transmission spectrum of Ni-Al co-doped ZOTFs deposited at the spinning speed of 1000 to 6000 rpm. In the visible and near-infrared regions, the transmission coefficient of all thin films is higher than 85%, indicating that the thin

Table 6.2: Variation of lowest transmittance of Ni-Al co-doped ZnO thin films with spin coating speed

Sr. No.	Spin Coating Speed (rpm)	Lowest Transmittance value (%)
1.	1000	60.58
2.	2000	70.42
3.	3000	73.17
4.	4000	52.35
5.	5000	60.01
6.	6000	61.34

films may be employed as TCO for optoelectronic devices [226–228]. It is observed from Figure 6.6 and Table 6.2, that the transmittance of 1 at% Ni and 1 at% Al co-doped ZOTFs falls from 1000 to 4000 rpm and then rises from 4000 to 6000 rpm.

6.1.3.2   Refractive Index and Dielectric Constant

Figure 6.7 shows how the refractive index and extinction coefficient varies with energy. The refractive index of thin films shows an increasing trend with increasing energy. The refractive index increases rapidly from 3 eV, reaching its highest value at 3.57 eV. The extinction coefficient slowly decreases from 1.12 eV to 3 eV and then it increases sharply and becomes maximum at 3.5 eV [229–231]. The value of the extinction coefficient rises as the spin revolution speed rises from 1000 to 6000 rpm.
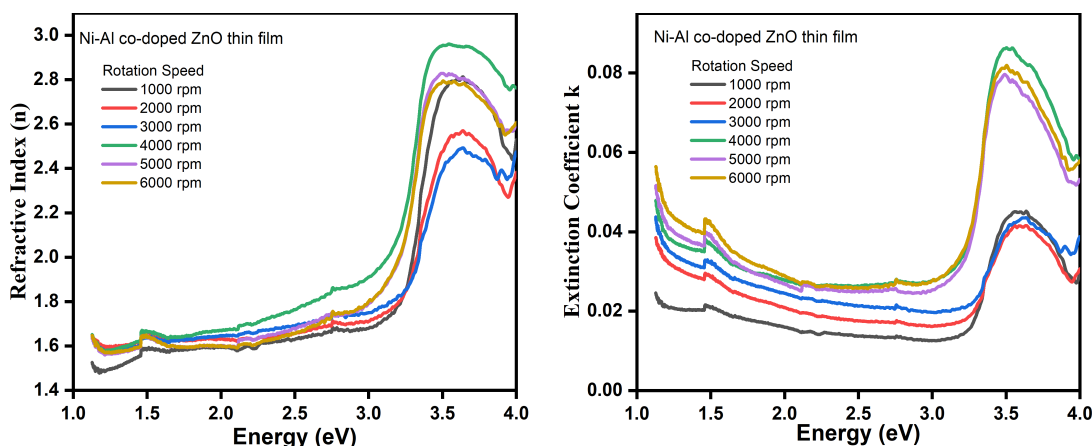
Figure 6.7: Variation of refractive index and extinction coefficient of Ni-Al co-doped ZnO thin films with energy

Spectral response of real part (ε_r) and imaginary (ε_i) parts of dielectric constant for Ni-Al co-doped ZOTFs synthesized at different substrate rotation speed 1000-6000 rpm with energy is illustrated in Figure 6.8 6.8. The values of the real part (ε_r) of the dielectric constant increases slowly from 1.12 eV to 3 eV and after that it increases rapidly.
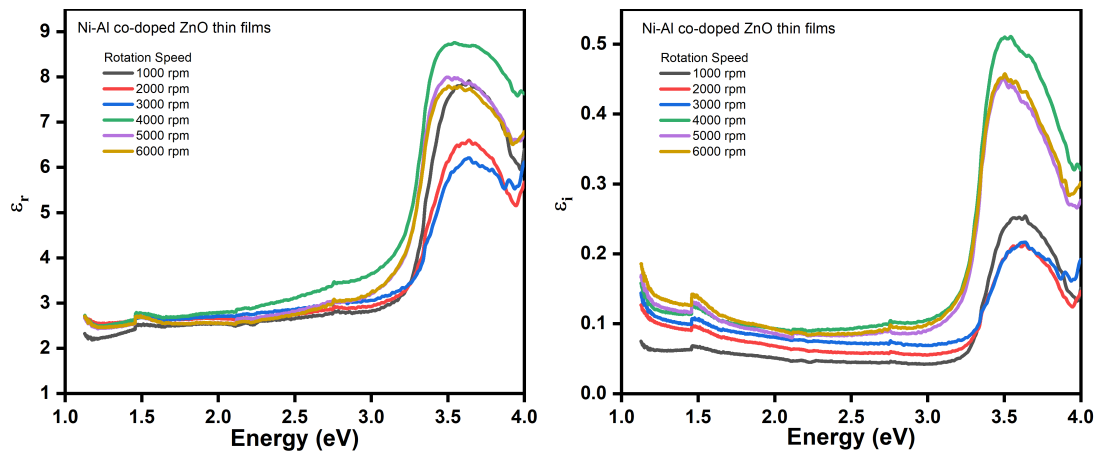
Figure 6.8: Variation of real part (ε_r) and imaginary (ε_i) parts of dielectric constant of Ni-Al co-doped ZnO thin films with energy

The real part (ε_r) of the dielectric constant has a peak value approximately at 3.6 eV. The value of imaginary (ε_i) parts of the dielectric constant decreases very slowly in the 1.12 eV to 3.1 eV range of energy, afterwards rises sharply until attains a peak value approximately at 3.55 eV and then falls up to 4 eV [153, 232, 233]. It is also observed from Figure 6.8 that the imaginary (ε_i) parts of the dielectric constant increases with an increase in spin coating speed from 1000 - 6000 rpm in the visible region of the spectrum.

6.1.3.3   Raman Spectra
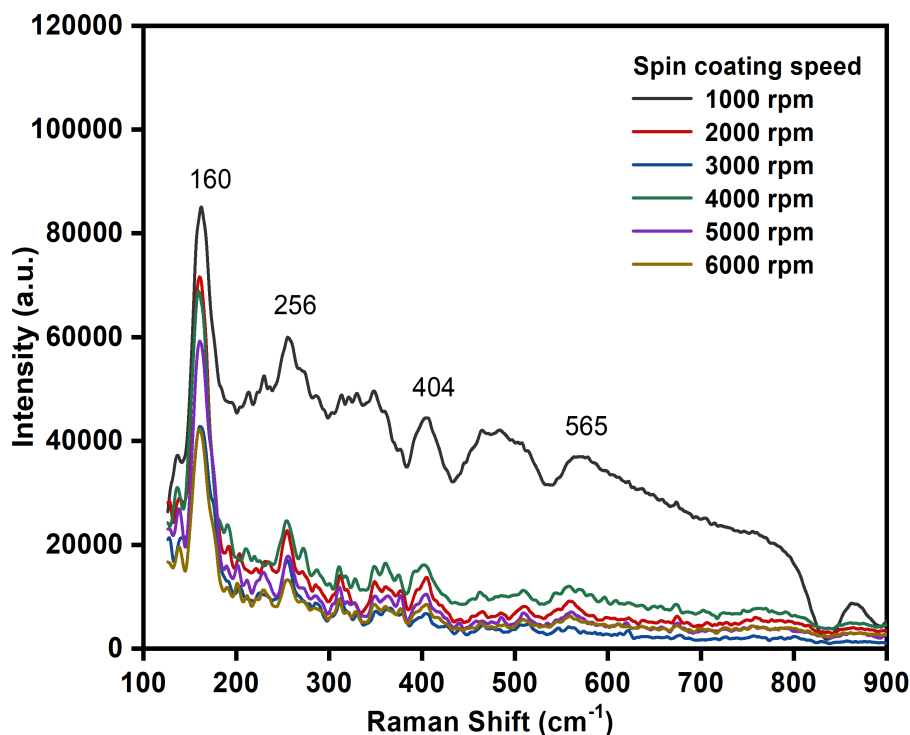
Figure 6.9: Raman spectra of 1 at% Ni and 1 at% Al co-doped ZnO thin film at 1000-6000 rpm

Figure 6.9 shows the Raman spectra of Ni-Al co-doped ZnO thin film deposited at 1000 rpm to 6000 rpm rotation speed by the sol-gel spin coating process. Wurtzite is a kind of ZnO structure that belongs to the C_{6V}^4 (P6$_3$ mc) space group.

Raman spectroscopy is a powerful technique for examining the local structure, defect state, and disorder in ZnO. It is also used to evaluate the crystalline quality of nanostructures. Room temperature Raman spectra of Ni-Al co-doped ZOTFs synthesized at 1000-6000 rpm have revealed Raman peaks at frequencies of 160 cm^{-1}, 256 cm^{-1}, 404 cm^{-1}, 462 cm^{-1} and 565 cm^{-1}. Overtones of TA phonons near the M point are responsible for the peak at 161 cm^{-1} [135]. E$_2$ (high) mode may be assigned to peak observed at frequency 462 cm^{-1} and represents the characteristic of ZnO crystallinity. The peaks at 256, 404 and 565 cm^{-1} may be ascribed to 2TA, E$_1$ (TO) and A$_1$ (LO) modes [136, 137]. The peak at 559 cm^{-1} (A$_1$ (LO) modes) might be attributed to lattice defects, such as oxygen vacancies, zinc interstitials, or a combination of the two.

6.1.3.4 Fluorescence Spectra

The photoluminescence spectrum of the synthesized Ni-Al co-doped ZOTFs ranging from 1000 to 6000 rpm is depicted in Figure 6.10. Spectrofluorometer (FluoroSENS
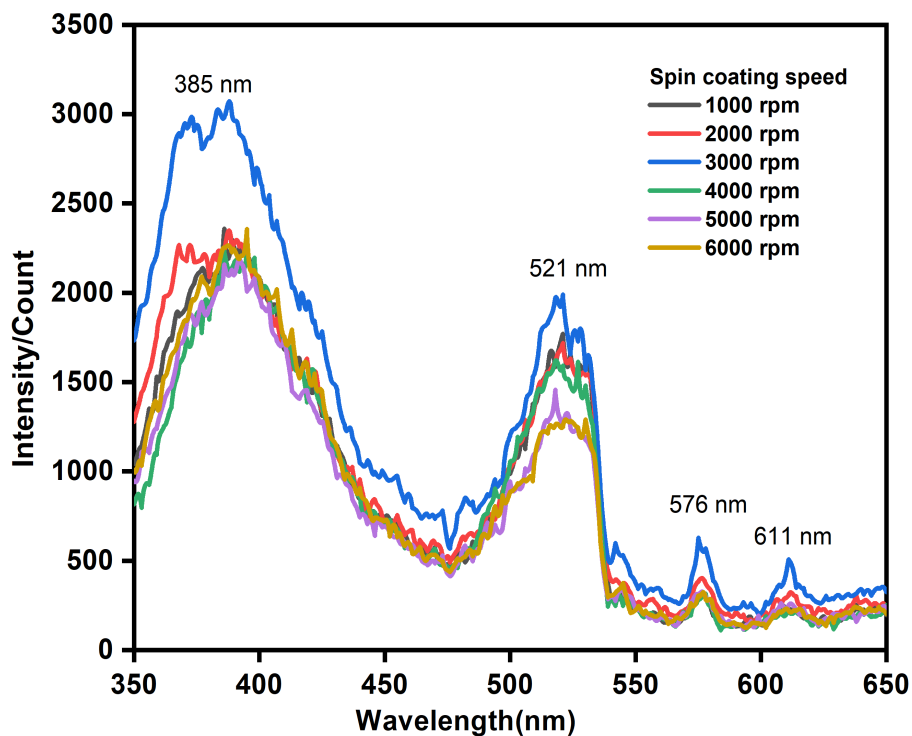
Figure 6.10: Fluorescence spectra of 1 at% Ni and 1 at% Al co-doped ZnO thin film at 1000-6000 rpm

Camlin Photonics) has been used to investigate the photoluminescence spectrum of Ni-Al co-doped ZOTFs deposited by spin deposition technique at spinning speed of 1000 rpm to 6000 rpm. The spectrum reveals a UV emission peak at 385 nm, a green emission peak at around 521 nm and feeble yellow and orange peaks at about 576 nm and 611 nm respectively. The UV emission at 385 nm is credited to the excitonic emission corresponding to the NBE transition from the conduction band to the valance band [234–236]. The visible emission peak at about 521 nm corresponds to the green emission, which is ascribed to the oxygen vacancies (V_o) and radiative emission from the conduction band to antisite oxygen (O_{zn}) [237, 238]. The orange emission peak at about 576 nm is accredited to the non-stoichiometry and complex defects (V_oZn_i) of oxygen vacancies and Zn interstitials [239, 240]. Ni-Al co-doped ZOTFs also exhibit yellow emission at about 611 nm which may be assigned to oxygen vacancies [240, 241].

6.2   FABRICATION OF Mn-Ni CO-DOPED ZnO THIN FILMS AND ITS CHARACTERIZATION

6.2.1   Introduction

ZnO oxide is a multifunctional material for the application in the semiconductor industry since multidimensional properties can be induced and tailored by the doping of various atoms. The doping of multiple atoms can induce multiple properties in ZnO. Transition metal element doping in ZnO induces the normal temperature ferromagnetism in films which have the application in spintronic devices. In this work, Mn-Ni co-doped ZOTFs were synthesized using the spin sol-gel route and the effect of annealing temperature was studied on the structural, vibrational, optical, and fluorescent possessions of the films. The Mn and Ni element concentrations in all samples were fixed at 1%.

6.2.2   Experimental Details

The 0.6M, 1 at% Mn and 1 at% Ni co-doped ZnO solution was prepared by dissolving ZAD, manganese acetate tetrahydrate and nickel acetate tetrahydrate in 2-methoxy ethanol by using a magnetic stirrer at 65 °C for 2 hours. The solution became turbid, therefore monoethanolamine (MEA) was added drop by drop to stabilize it by setting the Zn^{2+}/MEA molar ratio to unity. The solution is then stirred for another two hours to produce a clear yellowish homogenous solution. The glass substrate (2.5 cm × 2.5 cm) was rinsed and washed with deionized water(DI), acetone, and then ultrasonically cleaned with acetone, methanol and deionized water(DI) to remove any oil, dirt, or grease before fabricating the thin layers. The glass slides were dried for 30 minutes in a 150°C oven. The prepared sol is aged in airtight bottles at room temperature for 48 hours. Spin coating was used to deposit aged solutions on pre-cleaned glass surfaces. Mn-Ni co-doped ZOTFs were synthesized at 3000 rpm speed, and then drying for 10 minutes on hot plate at 100 °C. This depositing and drying procedure was done numerous times to get the appropriate film thickness. The samples were then annealed at temperatures 200 °C, 300 °C, 400 °C and 500 °C for 4 hours. The flow chart for the fabrication of Mn-Ni co-doped ZOTFs is revealed in Figure 6.11. The thickness of thin films measured by SEM cross section is 336 nm for all samples. There is no change in thickness of films by annealing temperature.
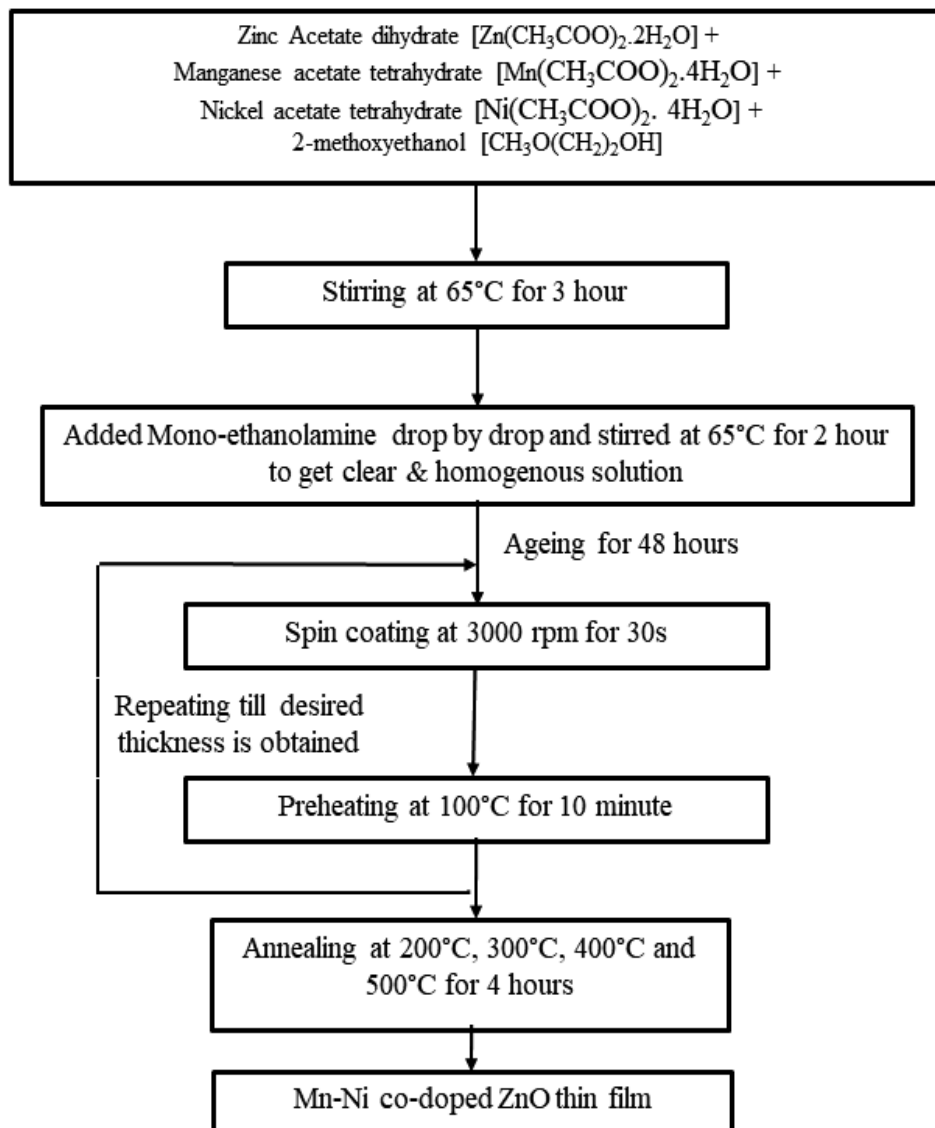
Figure 6.11: Flow chart for the fabrication of Mn-Ni co-doped ZnO thin films

6.2.3   Results and Discussion

6.2.3.1   X-ray Diffraction

The X-ray Diffraction of the Mn and Ni co-doped ZOTFs annealed at 200 °C, 300 °C, 400 °C and 500 °C were shown in Figure 6.12. The XRD revealed that all the films are constituted by hexagonal wurtzite Structure with (002) preferred direction along the c-axis. No Extra diffraction peak from Mn or Ni related second phases were observed. This is due to the fact that Mn^{2+} replaced Zn^{2+} in the ZnO host without affecting the wurtzite structure. It is observed that intensity of (002) peak increases as the annealing temperature increases. With a rise in annealing temperature, the peak's intensity sharply increases. As the annealing temperature rises, the strength of the (002) peak increases, indicating that the crystallinity of the films improves.
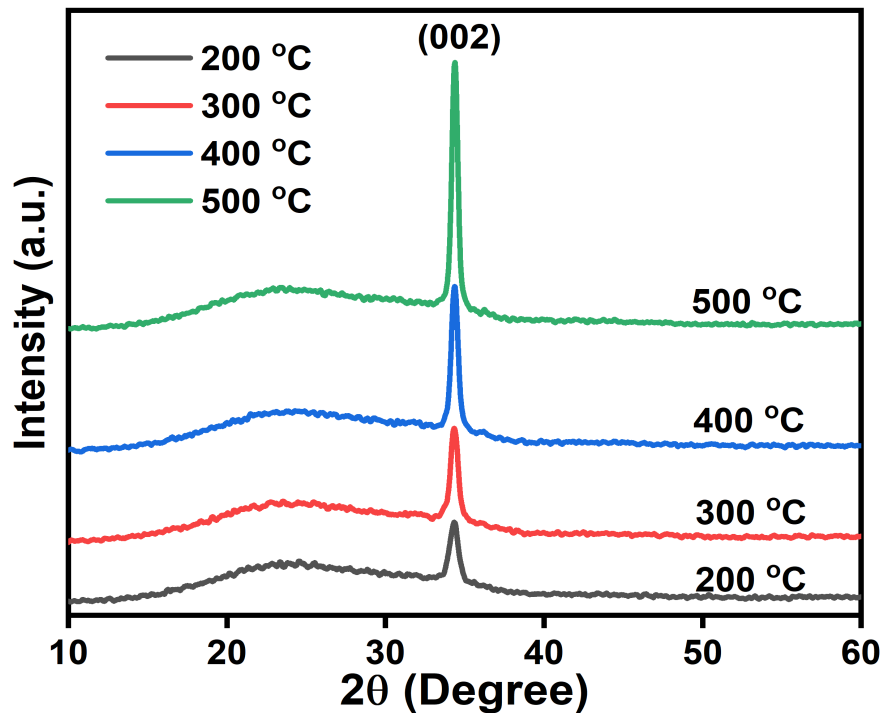
Figure 6.12: XRD of Mn-Ni co-doped ZnO thin films annealed at different temperature

The size of crystallite 'D' is computed using Scherrer's formula

$$D = \frac{0.9\lambda}{(\beta \, cos\theta)}$$

(6.1)

where D is the crystallite size, 2θ is the Bragg's diffraction angle, β is FWHM. It is seen from Figure 6.13 and Table 6.3 that the size of crystallite of Mn-Ni co-doped ZOTFs increases linearly with variation of annealing temperature from 200 °C - 500 °C. This

indicates that the crystallinity of ZnO thin films enhanced with rise in annealing temperature which is consistent with increase in the intensity of (002) peak [242]. The dislocation density (δ) and lattice strain (η), due to mismatching between glass substrate and Mn-Ni co-doped ZOTFs, is given by $\delta = 1/D^2$ and $\eta = \beta/(4 \tan\theta)$ respectively [243]. The value of dislocation density decreased from 5.62×10^{-3} nm^{-2} to 2.53×10^{-3} nm^{-2} with rising in annealing temperature from 200°C to 500°C. The increase in crystallite size is responsible for the decrease in dislocation density. This demonstrates that when the annealing temperature is raised, the quality of crystalline thin films improves. The inter-planer spacing d_{hkl} for (002) plane was calculated employing XRD data using the expression

$$\frac{1}{d_{hkl}^2} = \frac{4}{3}\left(\frac{h^2 + hk + k^2}{a^2}\right) + \frac{l^2}{c^2} \tag{6.2}$$

Where the lattice parameters a and c are computed using the expression [244]

$$a = b = \frac{\lambda}{\sqrt{3}\sin\theta} \tag{6.3}$$

$$c = \frac{\lambda}{\sin\theta} \tag{6.4}$$

The variation of the residual stress (σ) for Mn-Ni co-doped ZOTFs having hexagonal structure were obtained using the following expression

$$\sigma = \frac{2C_{13}^2 - C_{33}(C_{11} - C_{12})}{2C_{13}} \times \frac{C - C_o}{C_o} \tag{6.5}$$

where C_{11}, C_{12}, C_{13}, C_{33} are the elastic stiffness constant of ZnO thin films in various directions with values 208.8, 119.7, 104.2 and 213.8 GPa respectively [245] and C and C_o are the calculated and standard values of the lattice constant. The various measured parameters of Mn-Ni co-doped ZOTFs annealed at successively increasing temperatures from 200°C to 500°C are shown in Table 6.3.

Table 6.3: List of several measured parameters of Mn-Ni co-doped ZnO thin films annealed at various temperatures

Annealing temperature (°C)	2θ of (002) peak (°)	FWHM of (002) peak (°)	Crystallite size (nm)	Lattice constants (Å)		Dislocation density (δ) ($\times 10^{-3}$ nm^{-2})	Lattice micro strain (η) ($\times 10^{-3}$)	Compressive residual stress (GPa)
				a=b	c			
200	34.315	0.6237	13.329	3.0151	5.222	5.6282	8.815	-0.6822
300	34.336	0.4862	17.101	3.0133	5.219	3.4193	6.866	-0.5406
400	34.357	0.4514	18.418	3.0115	5.216	2.9477	6.372	-0.4049
500	34.368	0.4186	19.864	3.0105	5.214	2.5343	5.906	-0.3289
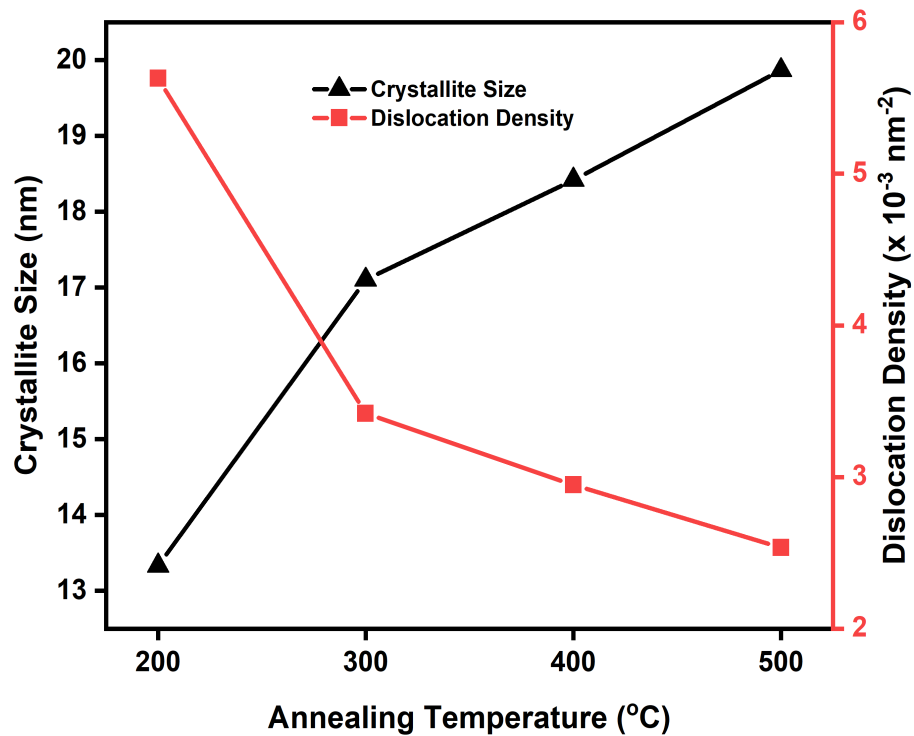
Figure 6.13: Variation of crystallite size and dislocation density (δ) with annealing temperature

Figure 6.14: Variation of micro strain and compressive residual stress with annealing temperature

Perusal of data presented in Table 6.3, decrease in lattice parameter *c* has been observed with increasing annealing temperature. This might be due to residual stress produced by defects and mismatch between glass substrate and thin films. The density of dislocation of thin films reduces from 5.6282×10^{-3} nm^{-2} to 2.5343×10^{-3} nm^{-2} with rise in the annealing temperature. The annealing process results in the formation of larger grains by merging the defects and lattice imperfections thereby decreases the dislocation density and stress in the thin films [246]. The change of crystallite size and dislocation density with annealing temperature is seen in Figure 6.13. Also, lattice micro-strain shows similar trends as that of dislocation density. From Table 6.3, it can be observed that the calculated values of residual stress are negative, representing the compressive stress in prepared thin films. The thin films annealed at various temperature exhibit compressive stress because of the substitution of Zn^{2+} ($\sim$0.74Å) ions by doping elements Mn^{2+} ($\sim$0.66Å) and Ni^{2+} ($\sim$0.69Å), with smaller radius ions. The compressive stress of thin films reduces from 0.68216 GPa to 0.32891 GPa as the annealing temperature was raised from 200°C to 500°C. This reduction in the compressive stress may be because of the transfer of dopant/impurity atom from an unstable position to a stable position, thereby relaxing the compressive stress [247]. Figure 6.14 shows the variation of micro-strain (η) and compressive residual stress (σ) with annealing temperature.

6.2.3.2 Surface Morphology

SEM micrographs of Mn-Ni co-doped ZOTFs annealed at temperatures 200°C, 300°C, 400°C and 500°C for 4 hours are depicted in Figure 6.15. All the annealed films appear to be polycrystalline, crackless and have uniformly distributed grains throughout the films. The morphology of the surface of the thin films shows that grains become denser and larger with the rise in the annealing temperature. Films surface annealed at 200°C seems flatter, whereas the surface roughness increases as the annealing temperature rises owing to grain growth. Some micro-pores appeared in the films that are annealed at 400°C and 500°C the temperature which may be ascribed to the release of stress by growing the grain size and creating micro-pores [248, 249].
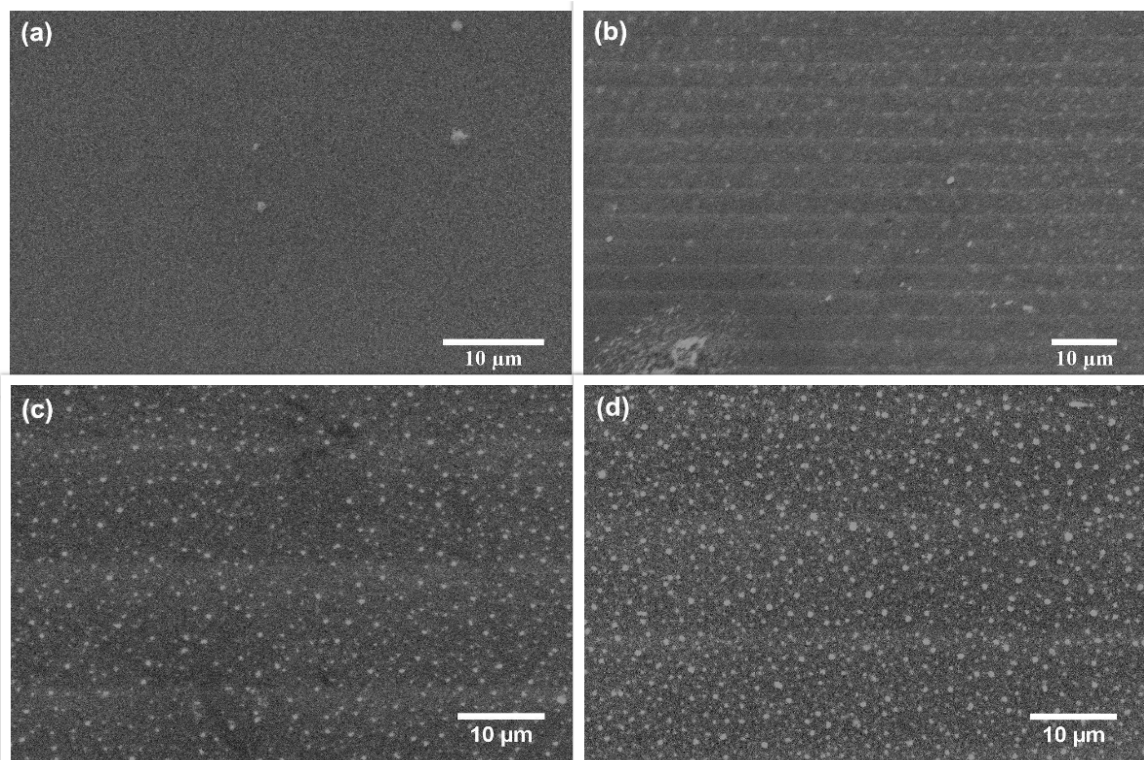
Figure 6.15: SEM micrographs of Mn-Ni co-doped ZnO thin films annealed at temperature (a) 200°C (b) 300°C (c) 400°C (d) 500°C

The morphology of surface of Mn-Ni co-doped ZOTFs was analyzed by AFM. 2-dimensional and 3-dimensional AFM micrographs of films that are annealed at 200°C, 300°C, 400°C and 500°C for 4 hours are shown in Figure 6.16. Perusal of data presented in Figure 6.16 it is understood that the surface of all films displays hill like structure uniformly distributed over the scanned area. With the exception of the thin film that is annealed at 400°C, the number of hills per unit area increases as the annealing temperature rises, as observed in AFM images. Hills' maximum peak height rises from
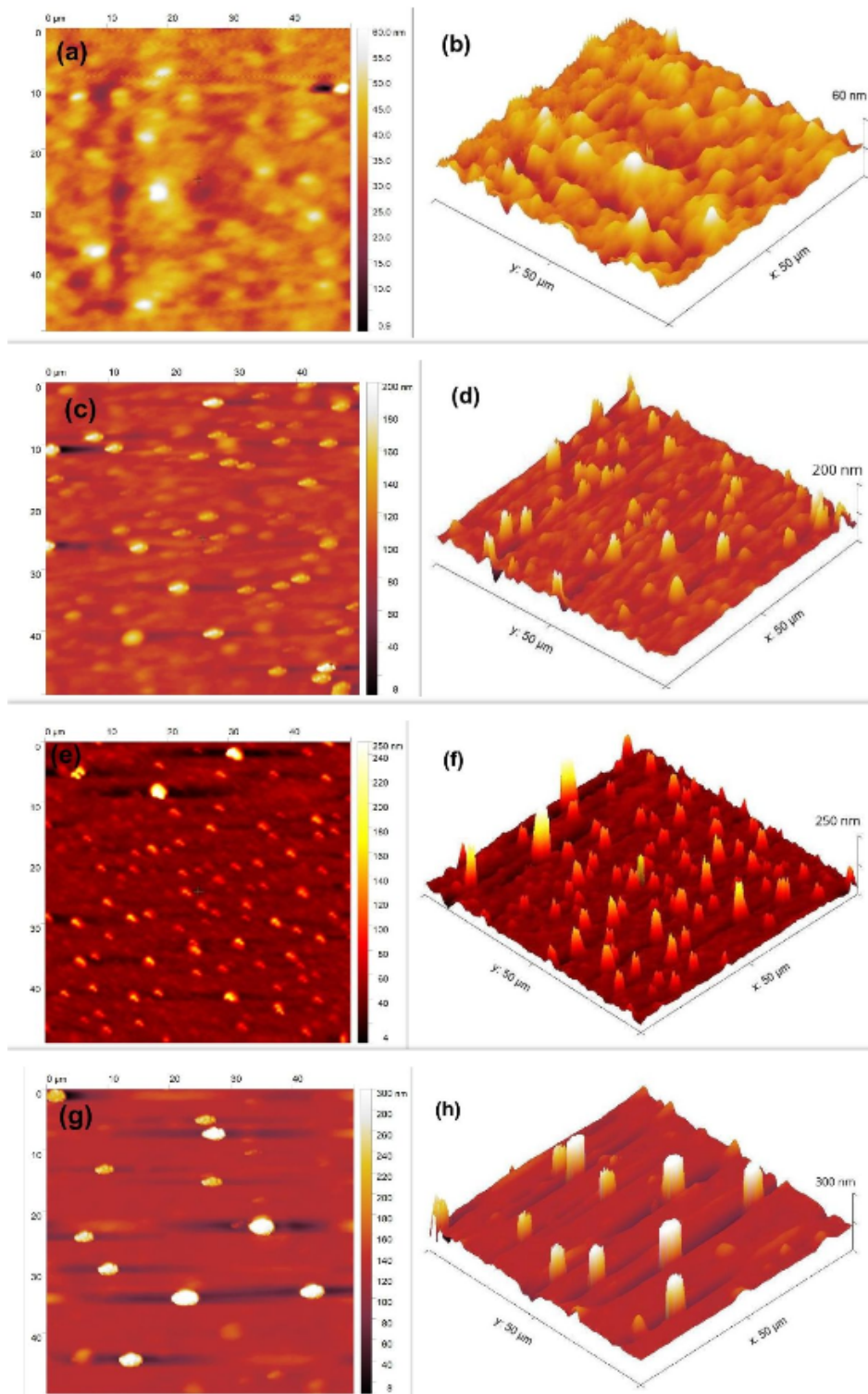
Figure 6.16: AFM images of Mn-Ni co-doped ZnO thin films annealed at, 2D images: (a) 200°C (c) 300°C (e) 400°C (g) 500°C; 3D images: (b) 200°C (d) 300°C (f) 400°C (h) 500°C.

60 nm to 300 nm and RMS roughness increases from 5.39 nm to 26.22 nm, with the rise in temperature i.e, from 200°C to 500°C. The relationship graph between anneal-ing temperature and RMS roughness is presented in Figure 6.17. Similar findings have
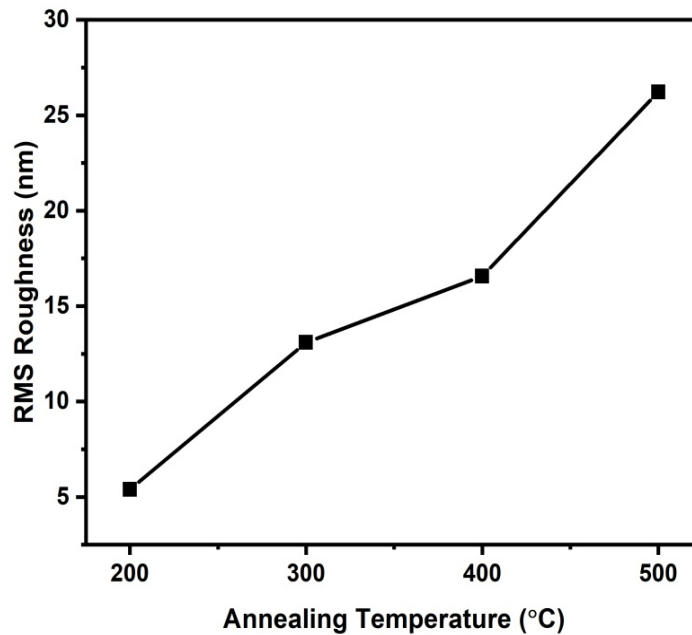
Figure 6.17: Relationship graph between annealing temperature and RMS surface roughness

been widely documented in the literature [250]. The annealing temperature causes the creation of a hill-like structure as a function of the annealing temperature, resulting in grain growth as the annealing temperature rises. This assertion is consistent with XRD and SEM results. AFM image of thin film annealed at 500°C has multiple straight and parallel micro-channels with an average depth of 100 nm and an average width of 1.9 m. There are structural hills of height 180-300 nm, average base area 7.0 m^2 and average hill volume 1.94 m^3 within these micro-channels. The formation of these micro-channels and hills are complementary. Atoms had adequate diffusion activation energy to migrate to a favourable position in the crystal lattice at 500°C temperatures, thus lower surface energy grains grew in size [251]. This caused the formation of hills by the coalescence of the mass of channels.

6.2.3.3   Raman Analysis

Raman spectroscopy is an excellent tool known to be used for the study of crystalline quality, crystal defects and lattice disorders in doped semiconductor crystal [252]. Group theory suggests that ZnO have 9 optical and 3 acoustic phonon modes. The optical phonons at Brillouin zone-center (Γ point) can be given by following irreducible representation: $\Gamma_{opt} = E_1 + 2E_2 + A_1 + 2B_1$ [253].

Figure 6.18 depicts Raman spectra of Mn-Ni co-doped ZOTFs annealed at successively
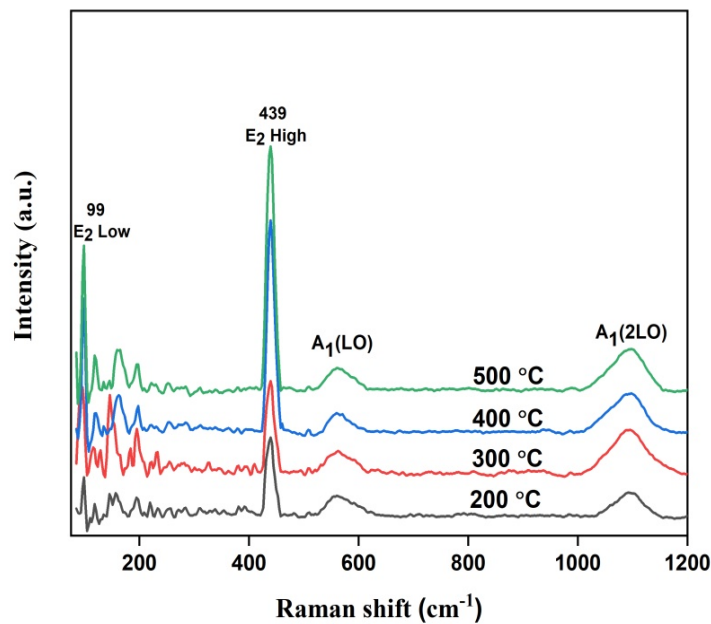
Figure 6.18: Room temperature Raman spectra of Mn-Ni co-doped ZnO thin films annealed at 200°C, 300°C, 400°C and 500°C

increasing temperature from 200°C to 500°C measured in spectral range 80 cm^{-1} to 1200 cm^{-1} at room temperature. Major Raman peaks were observed at 99 cm^{-1}, 119 cm^{-1}, 160 cm^{-1}, 195 cm^{-1}, 439 cm^{-1}, 560 cm^{-1} and 1098 cm^{-1}, for all thin films. The intense peaks at $\sim$ 99 cm^{-1} and $\sim$ 439 cm^{-1} correspond to E$_2$ nonpolar optical phonon mode and assigned to E_2^{Low} and E_2^{High}. The presence of E_2^{Low} and E_2^{High} optical phonon modes confirms hexagonal wurtzite structure of ZnO [254, 255]. The improvement in crystalline quality and grain size is indicated by an increase in the intensity of the E_2^{High} peak as the annealing temperature increases, which is also supported by the XRD and SEM data. The peak at 119 cm^{-1} might have arisen due to Raman scattering from glass substrate while overtones of TA phonons near the M point were attributed peaks at 160 cm^{-1} [134, 256]. *J. Serrano et al.* calculated phonon dispersion of ZnO and expressed that E_2^{High} mode decay into 2 acoustic modes at 190 cm^{-1} and 250 cm^{-1} [257]. A$_1$(LO) mode or B$_1$(high) mode might be responsible for the broad peak detected at 560 cm^{-1}. This Raman peak was caused by oxygen vacancies, zinc interstitials, or a complicated combination of these two [258]. But *A. El Manouni* explained that these Raman active phonon modes are induced by increase in the electric field around the grain that polarizes the field of excitonic states [259, 260]. At the H and K Brillouin zone points, the Raman peaks at 1098 cm^{-1} may be attributed to A$_1$(2LO). In Raman scattering, there

were no additional peaks due to Mn, Ni, or any other contaminants.

6.2.3.4   Optical Properties

Photoluminescence spectra of Mn-Ni co-doped ZOTFs annealed at various temperatures of 200°C, 300°C, 400°C and 500°C, obtained at ambient temperature with a 330 nm wavelength of excitation is shown in Figure 6.19. The photoluminescence spectra
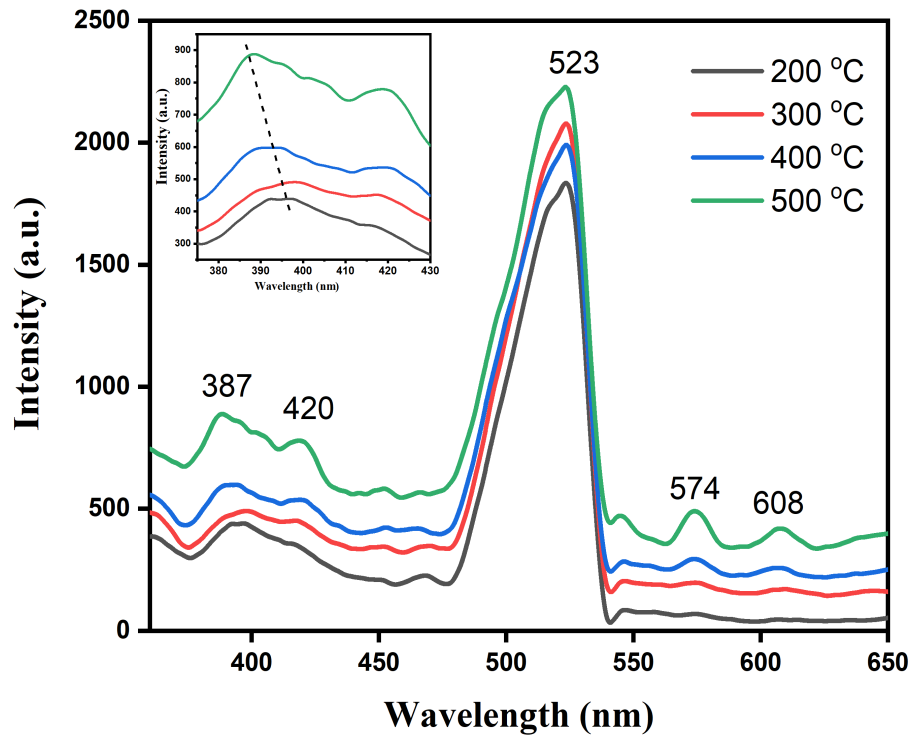
Figure 6.19: The Pl spectra of Mn-Ni co-doped ZnO thin films annealed at various temperatures; inset shows the enlarged view of UV peaks from 388 nm to 396 nm.

for all thin films were found to be almost identical except the change in the intensity of thin films. A UV emission about 387 nm, violet emission around 420 nm and a prominent green emission band from 475 nm to 540 nm has been observed as seen from Figure 6.19. In addition, two more emission peaks one around 574 nm and other near 607 nm were noticed. The UV illumination around 387 nm represents the NBE emission correlated to excitonic radiative recombination, which is consistent with the energy gap of thin films. The intensity of UV emission increases as annealing temperature of the thin films increased from 200°C to 500°C. This clearly shows that raising the annealing temperature improves crystallinity. As the annealing temperature was raised, the UV peaks blue-shifted from 396 to 388 nm. The blue-shift of UV peaks may be attributed to relaxation of compressive stress upon increasing the annealing temperature. In the visible region (400 nm to 620 nm), violet, a wide green, yellow, and orange emis-

sion peaks may be seen, followed by a UV peak. The origin of these visible emissions is controversial because of complicated defects in ZOTFs. It is well reported that ZOTFs have different types of intrinsic defects and impurities which includes, vacancy of zinc (V_{Zn}), vacancy of oxygen (V_O), interstitial of zinc (Zn_i), interstitial of oxygen (O_i), antisite oxygen (O_{Zn}) and donor-acceptor pairs (DAP), out of which V_{Zn}, O_{Zn} and O_i are acceptors, while Zn_i and V_O are donors. Radiative defects Zn_i and V_{Zn} associated to interfacial traps and dislocations at grain boundaries may indeed be responsible for the violet emission peaks detected around 418 nm [261]. The green emission peak at around 523 nm can be attributed to the transition from the conduction band to anti-site oxygen (O_{Zn}) defect, or interstitial zinc (Zn_i) and O_2 vacancies (V_O) to the valence band. Furthermore, the green emission peak at 574 nm was attributed to oxygen interstitial (O_i) or the transition from donor defect levels produced by Mn-Ni doping to the valence band, whereas the yellow emission peak at 608 nm was attributed to the transition from complex V_oZn_i defects to zinc vacancies defects [256]. It could be further noted from Figure 6.19 that there is no appreciable change in the intensity of photoluminescence peaks due to increasing annealing temperature, which elucidates the slow rate of development of defects with temperature. This is because of low annealing temperature (up to 500°C) being unable to provide required energy. At higher temperature (>500°C) more defects like V_{Zn}, V_O, Zn_i, O_i, O_{Zn}, might be created resulting in increased PL emission intensity of peaks (due to the transition from increased defects). Optical properties of the annealed ZOTFs were analyzed from transmittance and absorption spectra recorded using UV-visible spectrophotometer. Figure 6.20 shows the transmittance spectra of ZOTFs annealed at various temperatures. The absorption spectra of thin films, which are analogous to the transmittance spectra, are shown in the inset. Perusal of data presented in Figure 6.20 revealed more than 80% transmittance in the visible region, which is one important parameter for the application of thin films in TCOs. The films displayed a pronounced absorption edge in the UV area at wavelength 378 nm, which corresponds to the fundamental energy band gap of ZnO, according to transmittance spectra. Except for thin films annealed at 500°C, the absorption edge shifted towards longer wavelengths as the annealing temperature increased. This result may be correlated with the formation of micro-channels and hills as shown by AFM micrographs [262, 263]. Increasing the annealing temperature may cause the absorption edge to shift towards longer wavelengths, as a result of an increase in grain size, a decrease in the band gap, and a decrease in residual stress [173, 264]. As the annealing temperature increases from 200°C to 500°C, the transmittance in the visible spectrum
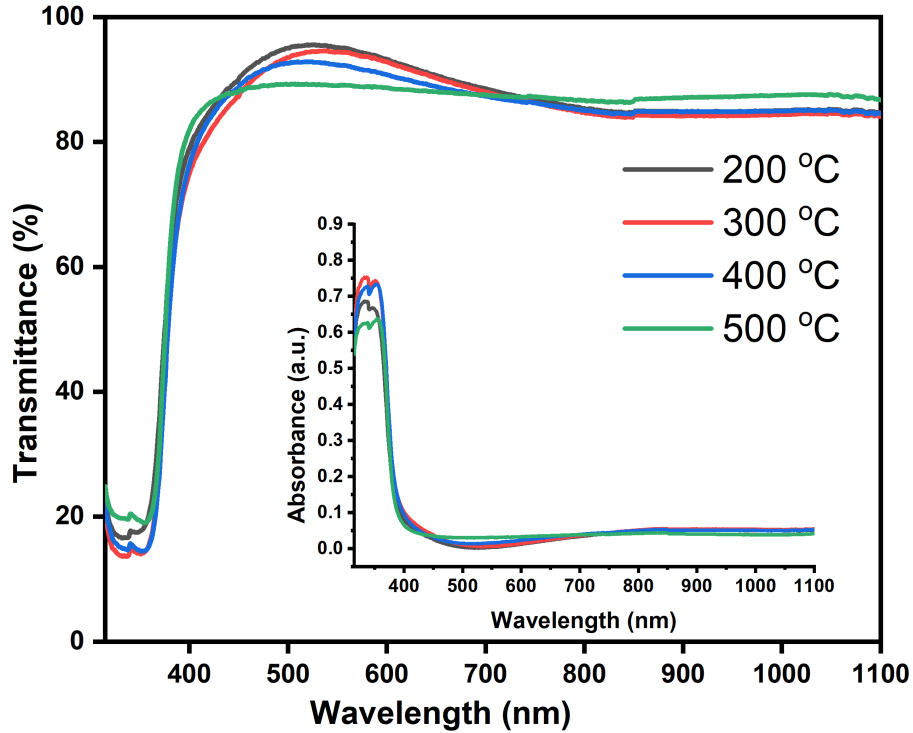
Figure 6.20: Transmittance spectra of Mn-Ni co-doped ZnO thin films annealed at 200°C, 300°C, 400°C and 500°C (Inset shows absorption spectra of thin films)

decreases. The roughness of the surface of thin films increases with an increase in temperature as revealed by SEM and AFM images. The reduction in transmittance as the annealing temperature rises might be attributed to scattering from thin film surfaces [265, 266].

The Tauc's relation was used to compute the optical direct band gap of Mn-Ni co-doped ZnO thin films annealed at different temperatures given by [112]:

$$\alpha h v = B \left(h v - E_g \right)^n \tag{6.6}$$

where α is the absorption coefficient, B is a characteristic parameter, h is Planck's constant, v is frequency of light and E_g is the optical band gap. The value of n is 1/2 and 3/2 for direct and forbidden transition in semiconductors respectively. The value of n is taken 1/2 which was found most suitable for ZnO thin films [267]. The absorption coefficient (α) was computed using the equation:

$$\alpha = 2.303 \frac{\log_{10}(1/T)}{d} \tag{6.7}$$

where T is transmittance and d is the thickness of thin film.

Figure 6.21 shows plot of $(\alpha h v)^2$ versus energy hv in the absorption edge region.
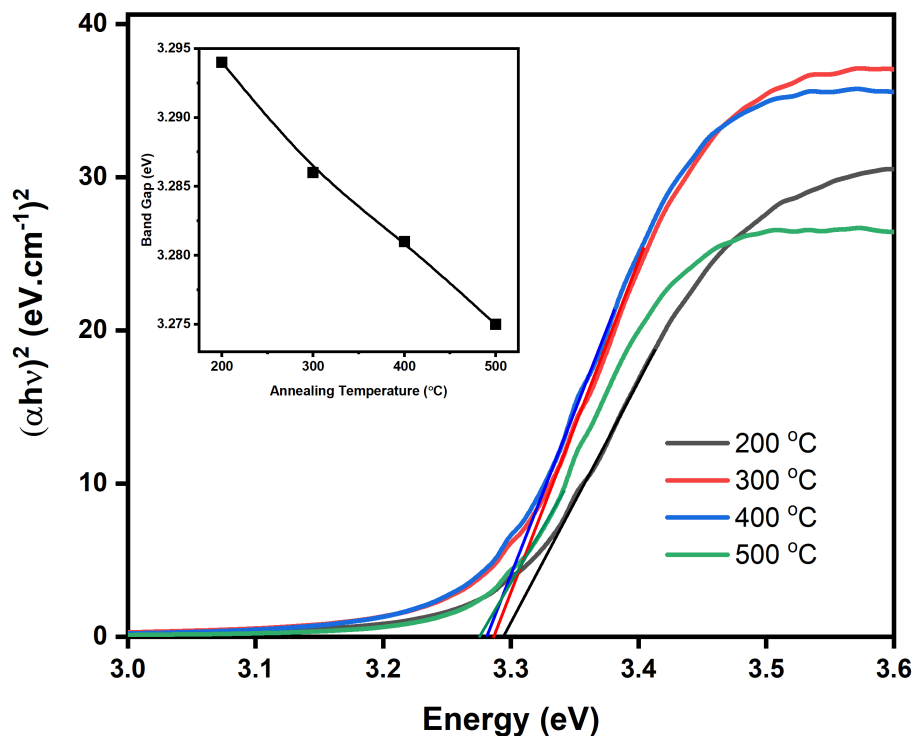
Figure 6.21: $(\alpha h\nu)^2$ versus energy $h\nu$ curve for Mn-Ni Co-doped ZnO thin films annealed at different temperatures; inset shows the variation of optical band gap with annealing temperature)

Table 6.4: Variation of lowest transmittance of Ni doped ZnO thin films with spin coating speed

Annealing temperature (°C)	RMS Roughness (nm)	Average Transmittance %	Energy band gap (eV) (%)
200	05.39	91.5	3.275
300	13.10	90.5	3.270
400	16.57	89.5	3.263
500	26.22	88.0	3.255

The optical energy gaps were found by extrapolating the linear absorption edge part of Tauc's plot to intercept the energy axis [268] and achieved values are shown in Table 6.4. With an rise in annealing temperature from 200°C to 500°C, the optical band gap of the films fell from 3.275 eV to 3.255 eV. The inset shows how the energy band gap change as the annealing temperature rises. The decline in the energy band gap with increased annealing temperature may be due to the grain size increase. The results of the SEM and AFM analyses corroborate these conclusions. Similar results are well reported in literature [248, 269]. The average value of the band gap calculated from the Tauc's plot was approximately ˜3.265 eV, which is less than the bulk ZnO material's value of 3.37 eV. The values of RMS roughness, average transmittance and energy band gap of Mn-Ni co-doped ZOTFs which are annealed at various temperatures are listed in

Table 6.4.

6.2.3.5   Refractive Index and Dielectric Constant

Figure 6.22 shows the refractive index and extinction coefficient spectrum variation of Mn-Ni co-doped ZOTFs annealed at 200 to 500 °C. The highest value of the refractive index for all thin films is 2.94 located at 373nm, whereas the minimum value of the refractive index occurs at 525nm. The maximum contrast in refractive index is observed
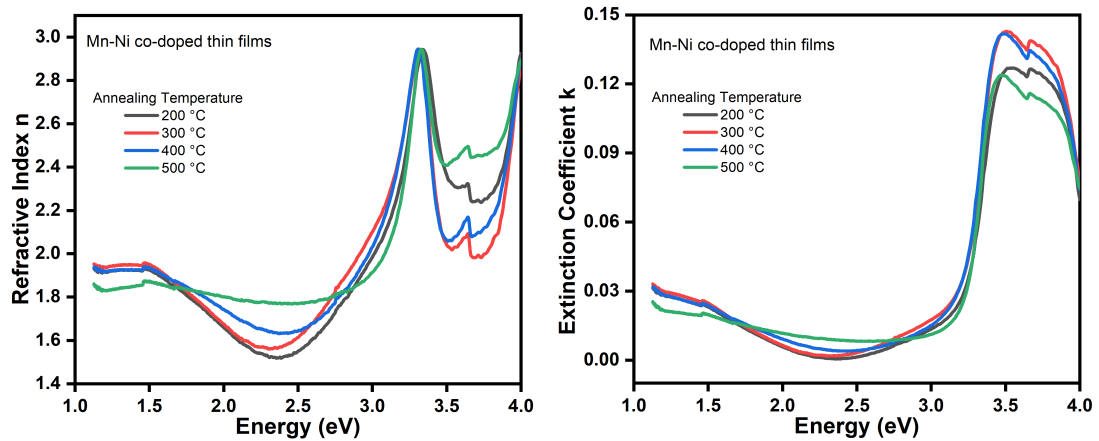
Figure 6.22: Variation of refractive index and extinction coefficient of Mn-Ni co-doped ZnO thin films with energy

at 525nm. In the visible spectrum, increasing the annealing temperature from 200 to 500 °C raises the refractive index value.

Variation of real part (ε_r) and imaginary (ε_i) parts of DC for Mn-Ni co-doped ZOTFs annealed at 200 to 500 °C temperature with energy is depicted in Figure 6.23. The value of the real part (ε_r) of DC is observed to be highest at 3.32 eV and lowest at about
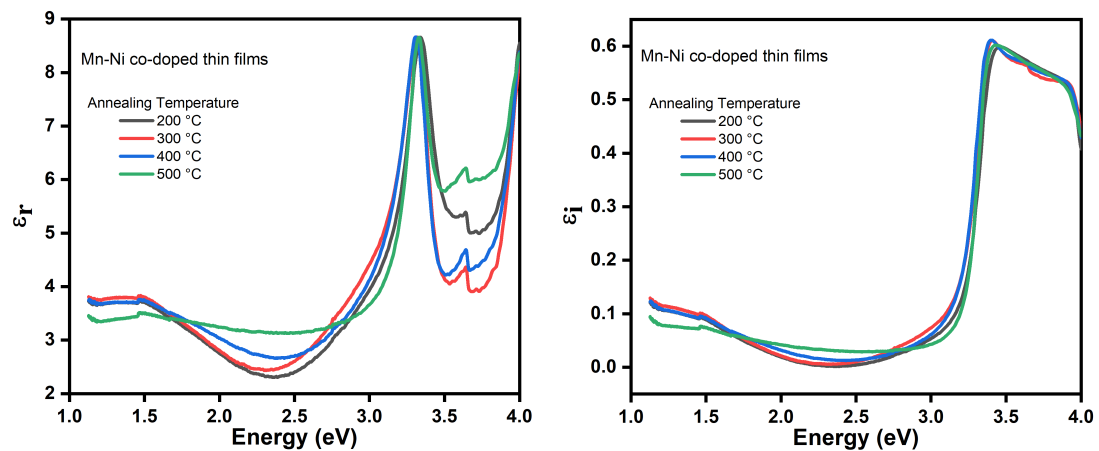
Figure 6.23: Variation of real part (ε_r) and imaginary (ε_i) parts of dielectric constant with energy

2.38 eV. The highest value of the real part (ε_r) of the dielectric constant is observed to be the same for all samples but the lowest value of the real part (ε_r) of DC increases with annealing temperature rise from 200 to 500 °C. The value of imaginary (ε_i) parts of the dielectric constant increases from energy 1.12 eV to about 2.40 eV after which it increases to the peak value at about 3.42 eV. The Figure 6.22 also revealed that ε_i upsurges in the visible region with an annealing temperature increase indicating the increase in the absorbance with increasing annealing temperature.

6.2.3.6 Resistivity

The Vander Pauw technique was used to measure the resistivity of Mn-Ni co-doped ZOTFs grown at a spin rotation speed of 3000 rpm and annealed at temperatures ranging from 200 to 500 degrees Celsius. As the annealing temperature is raised, the re-
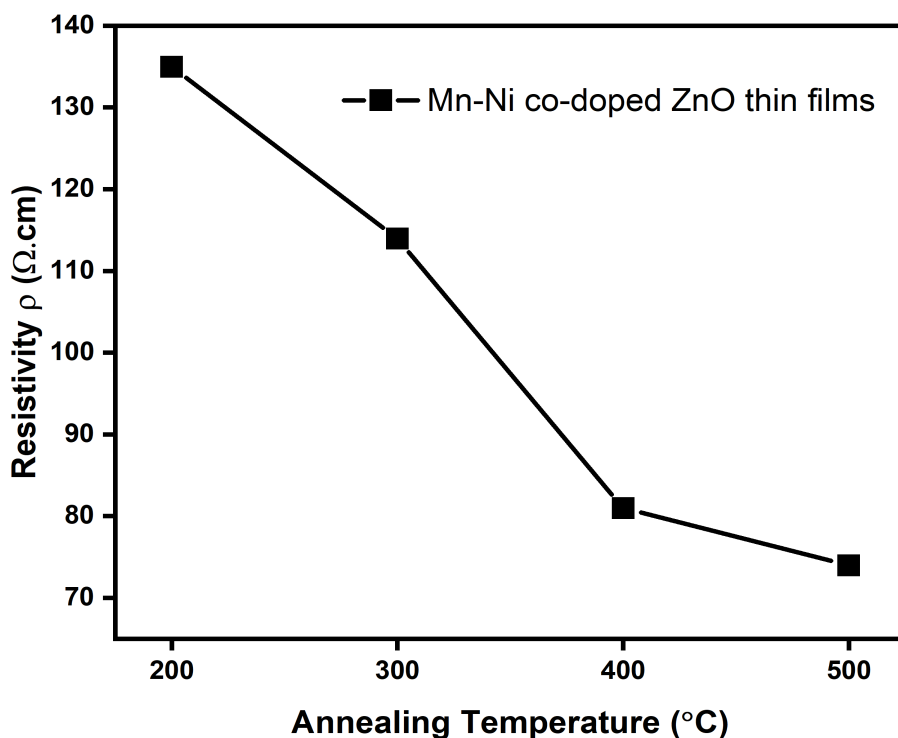
Figure 6.24: Variation of resistivity of Mn-Ni co-doped ZnO films with annealing temperature

sistivity of thin films drops from 134 cm to 73 cm. The drop in resistivity might be attributable to the increased crystallinity of thin films annealed at higher temperatures [270]. Figure 6.24 shows the change of resistivity of ZOTFs deposited at various spin revolution speeds.

CHAPTER 7

CONCLUSIONS AND SCOPE FOR FUTURE WORK

7.1 CONCLUSIONS

Undoped ZnO thin films were successfully fabricated on glass substrates through a solution-based sol-gel process with a spin deposition technique. The rotating speed of the technique was varied from 1000 rpm to 6000 rpm. The deposited films were studied by various characterization techniques such as UV-visible, optical, fluorescent and Raman spectroscopy. The effect of spin deposition speed on the optical and vibrational properties of undoped zinc oxide thin films (ZOTFs) was studied. In addition, doping elements Ni, Al, Co, and Mn were also used to prepare ZnO thin films, and these doped films were subsequently evaluated and characterized. A variety of spectroscopic techniques such as UV-visible, optical, fluorescent and Raman spectroscopy were used to investigate the influence of spin deposition speed on the properties of doped zinc oxide thin films (ZOTFs). Co-doped Zinc Oxide Thin Films (ZOTFs) were also successfully synthesized for the pair of doping elements Al-Ni and Mn-Ni. The effect of spin deposition speed was investigated for Al-Ni co-doped films, while the influence of annealing temperature was examined for Mn-Ni co-doped ZOTFs. The structural, surface morphology, UV-visible, optical, fluorescent and vibrational properties of the co-doped ZOTFs were investigated in order to gain insight into the effects of the dopants on the properties of the films. The results of this study provide a better understanding of the influence of doping elements on the properties of ZOTFs, which may be useful for the development of new applications for these materials. The thickness of Ni-doped, Ni-Al co-doped and Mn-Ni co-doped zinc oxide thin films (ZOTFs) were examined by employing a cross-section view of Scanning Electron Microscopy (SEM)

images. It was found that the thickness of the thin films decreased as the spin deposition speed increased. This indicates that the spin deposition speed has a significant effect on the thickness of these ZOTFs. The optical transmittance of doped thin films has been estimated to be higher than 80% in the visible spectrum, according to U-V visible spectra. Al and Ni doping further improve the optical transparency in the visible region. Furthermore, research has revealed that an increase in spin coating speed increases the transparency of the thin films. Owing to these characteristics, doped ZnO thin films have the potential to be used as a transparent conducting oxide (TCO) or transparent electrode in solar cells. An analysis of the thin films has revealed a direct optical band gap of approximately 3.27 eV.

The refractive index (n), extinction coefficient (k) and real part (ε_r) & imaginary (ε_i) parts of dielectric constant were determined for Ni-doped, Ni-Al co-doped and Mn-Ni co-doped ZOTFs. The effect of spin coating speed on the refractive index and extinction coefficient of Ni-doped and Ni-Al co-doped ZOTFs was studied, whereas the influence of annealing temperature on the refractive index, extinction coefficient, and dielectric coefficient of Mn-Ni co-doped ZOTF was investigated. All thin films exhibited refractive indices within the range of 1.2 to 3 and extinction coefficients less than 0.35. The refractive index and extinction coefficient varied significantly with the energy. In the energy range from 1.12 eV to 4 eV, the values of the real and imaginary parts of the dielectric constant (DC) were calculated. The highest values of the real and imaginary parts of DC were observed in the vicinity of the band edge, and the values of the real and imaginary parts of the dielectric coefficient generally increased with increasing energy until reaching their highest values near the band gap.

The resistivity of Nickel-doped, Nickel-Aluminium co-doped and Manganese-Nickel co-doped Zinc Oxide Thin Film (ZOTF) was determined using the Vander Pauw four-probe technique. In Ni-doped and Ni-Al co-doped ZOTFs, substrate rotation speed influenced resistivity, while Mn-Ni co-doped thin films were examined for the effect of annealing temperature. The results showed that, for Nickel-doped and Nickel-Aluminium co-doped ZOTFs, resistivity increases as substrate rotation speed increases. The resistivity rise was slow up to 3000 rpm, but after this point, it increases rapidly. Therefore, to achieve maximum transmittance and lowest resistivity for application in transparent conducting oxides (TCOs), 3000 rpm spin coating speed was found to be optimal. The resistivity of Mn-Ni co-doped samples decreases with an increase in annealing temperature from 200ºC to 500ºC. This decrease in resistivity may be attributed to the increased crystallinity of ZOTFs with higher annealing temperatures.

The photoluminescence spectrum of ZnO thin films typically shows an emission peak at around 385 nm, which is associated with the exciton recombination associated with the near band edge (NBE) transition. Additionally, a green emission peak is observed at around 520 nm, which is attributed to oxygen vacancies and antisite oxygen. Furthermore, a broad illumination peak is found to be present between 565 to 620 nm, which arises from the non-stoichiometry of the material, Zn vacancy and antisite defects in the ZnO. Raman spectroscopy further reveals peaks at 161 and 464 cm^{-1} which are related to E_2 (low) and E_2 (high) modes respectively. The low-frequency E_2 mode involves mainly Zn motion, while the E_2 (high) mode indicates characteristics of ZnO crystallinity. The peaks at 255, 400 and 557 cm^{-1} are attributed to 2TA, E_1 (TO) and A_1 (LO) modes respectively. The A_1 (LO) mode peak at 559 cm^{-1} is thought to be caused by lattice defects such as oxygen vacancies, zinc interstitials, or a combination of the two.

The X-ray Diffraction (XRD) patterns of Mn and Ni co-doped Zinc Oxide Thin Films (ZOTFs) annealed at 200, 300, 400 and 500 °C temperatures revealed that they possess a hexagonal wurtzite structure with (002) preferred orientation along the c-axis and without any extra diffraction peaks from Mn or Ni related second phases. This indicates that Mn^{2+} has replaced Zn^{2+} of the ZnO host without altering the wurtzite structure. Additionally, the intensity of the (002) peak was observed to increase with the rise in the annealing temperature, signifying an improvement in grain size and crystallinity. Scanning Electron Microscopy (SEM) images of Mn and Ni co-doped Zinc Oxide Thin Films (ZOTFs) annealed at temperatures of 200, 300, 400, and 500 °C showed that all the films were crack-free and had a uniformly distributed grain structure. Furthermore, it was observed that the crystallinity and grain size improved with increasing annealing temperature.

7.2   FUTURE SCOPE OF WORK

1. Doped ZnO thin films could be grown by using the precursor other than zinc acetate dihydrate and 2-methoxy ethanol to study the effect of precursors.

2. Other fabrication techniques like sputtering, spray pyrolysis etc. could be utilized to analyze the effect of deposition techniques.

3. Growth of p-type ZnO semiconductor remains problematic due limited solubility of p-type dopants and their compensation by plentiful n-type impurities. The

lack of p-type ZnO limits its electronic and optoelectronic applications, which typically need n-type and p-type material junctions.

4. Further work could be carried out to produce a stable and reproducible p-type ZnO semiconductor.

References

[1] P Prepelita, C Baban, and F Iacomi. "The study of the influence of Al and Sn doping on the optical and electrical properties of ZnO thin films". In: *Journal of Optoelectronics and Advanced Materials* 9.7 (2007), p. 2166.

[2] Zhong Lin Wang. "Zinc oxide nanostructures: growth, properties and applications". In: *Journal of physics: condensed matter* 16.25 (2004), R829.

[3] RJ Winfield et al. "Excimer laser processing of ZnO thin films prepared by the sol–gel process". In: *Applied Surface Science* 254.4 (2007), pp. 855–858.

[4] L Znaidi et al. "Oriented ZnO thin films synthesis by sol–gel process for laser application". In: *Thin solid films* 428.1-2 (2003), pp. 257–262.

[5] MI Khan et al. "Synthesis and characterization of Co and Ga co-doped ZnO thin films as an electrode for dye sensitized solar cells". In: *Ceramics International* 46.17 (2020), pp. 26590–26597.

[6] Seema Rani et al. "Synthesis of nanocrystalline ZnO powder via sol–gel route for dye-sensitized solar cells". In: *Solar Energy Materials and Solar Cells* 92.12 (2008), pp. 1639–1645.

[7] Hyun Wook Kang et al. "Simple ZnO nanowires patterned growth by micro-contact printing for high performance field emission device". In: *The Journal of Physical Chemistry C* 115.23 (2011), pp. 11435–11441.

[8] CJ Lee et al. "Field emission from well-aligned zinc oxide nanowires grown at low temperature". In: *Applied Physics Letters* 81.19 (2002), pp. 3648–3650.

[9] Sanghyun Ju et al. "N-type field-effect transistors using multiple Mg-doped ZnO nanorods". In: *IEEE Transactions on nanotechnology* 6.3 (2007), pp. 390–395.

[10] Rafiq Ahmad et al. "Ammonium ion detection in solution using vertically grown ZnO nanorod based field-effect transistor". In: *RSC advances* 6.60 (2016), pp. 54836–54840.

[11] Heiko Frenzel et al. "Recent progress on ZnO-based metal-semiconductor field-effect transistors and their application in transparent integrated circuits". In: *Advanced Materials* 22.47 (2010), pp. 5332–5349.

[12] G Vijayaprasath et al. "Characterization of dilute magnetic semiconducting transition metal doped ZnO thin films by sol–gel spin coating method". In: *Applied surface science* 313 (2014), pp. 870–876.

[13] He Wei et al. "Role of Co clusters in wurtzite Co: ZnO dilute magnetic semiconductor thin films". In: *Journal of Applied Physics* 105.4 (2009), p. 043903.

[14] Arun Kumar et al. "Investigation of the room temperature ferro-magnetism in transition metal-doped ZnO thin films". In: *Applied Physics A* 126.12 (2020), pp. 1–10.

[15] Arindam Mallick and Durga Basak. "Revisiting the electrical and optical transmission properties of co-doped ZnO thin films as n-type TCOs". In: *Progress in Materials Science* 96 (2018), pp. 86–110.

[16] Songül Fiat Varol et al. "Synthesis of sol–gel derived nano-crystalline ZnO thin films as TCO window layer: effect of sol aging and boron". In: *RSC advances* 4.100 (2014), pp. 56645–56653.

[17] Amaresh Das et al. "High conductivity along with high visible light transparency in Al implanted sol-gel ZnO thin film with an elevated figure of merit value as a transparent conducting layer". In: *Journal of Alloys and Compounds* 835 (2020), p. 155221.

[18] Gae Hun Jo, Sun-Ho Kim, and Jung-Hyuk Koh. "Enhanced electrical and optical properties based on stress reduced graded structure of Al-doped ZnO thin films". In: *Ceramics International* 44.1 (2018), pp. 735–741.

[19] Ramzi Nasser and Habib Elhouichet. "Production of acceptor complexes in sol-gel ZnO thin films by Sb doping". In: *Journal of Luminescence* 196 (2018), pp. 11–19.

[20] Zhizhen Ye, Haiping He, and Li Jiang. "Co-doping: an effective strategy for achieving stable p-type ZnO thin films". In: *Nano Energy* 52 (2018), pp. 527–540.

[21] Vivtoria A Coleman and Chennupati Jagadish. "Zinc oxide bulk, thin films and nanostructures". In: *UK, Elsevier* (2006), pp. 1–5.

[22] David C Look et al. "Electrical properties of bulk ZnO". In: *Solid state communications* 105.6 (1998), pp. 399–401.

[23]   Masakazu Anpo and Yutaka Kubokawa. "Photoluminescence of zinc oxide pow-der as a probe of electron-hole surface processes". In: *The Journal of Physical Chemistry* 88.23 (1984), pp. 5556–5560.

[24]   Dana C Olson et al. "Effect of ZnO processing on the photovoltage of ZnO/poly (3-hexylthiophene) solar cells". In: *The Journal of Physical Chemistry C* 112.26 (2008), pp. 9544–9547.

[25]   Magnus Willander et al. "Zinc oxide nanorod based photonic devices: recent progress in growth, light emitting diodes and lasers". In: *Nanotechnology* 20.33 (2009), p. 332001.

[26]   Y Yoshino et al. "Optimization of zinc oxide thin film for surface acoustic wave filters by radio frequency sputtering". In: *Vacuum* 59.2-3 (2000), pp. 538–545.

[27]   Sourajeet Roy and Sukumar Basu. "Improved zinc oxide film for gas sensor applications". In: *Bulletin of Materials Science* 25.6 (2002), pp. 513–515.

[28]   Tapan K Gupta. "Application of zinc oxide varistors". In: *Journal of the American Ceramic Society* 73.7 (1990), pp. 1817–1840.

[29]   T Fukumura et al. "Exploration of oxide-based diluted magnetic semiconductors toward transparent spintronics". In: *Applied Surface Science* 223.1-3 (2004), pp. 62–67.

[30]   Nargis Bano et al. "ZnO-organic hybrid white light emitting diodes grown on flexible plastic using low temperature aqueous chemical method". In: *Journal of Applied Physics* 108.4 (2010), p. 043103.

[31]   Young Hwan Hwang, Seok-Jun Seo, and Byeong-Soo Bae. "Fabrication and characterization of sol-gel-derived zinc oxide thin-film transistor". In: *Journal of Materials Research* 25.4 (2010), pp. 695–700.

[32]   J Meyer et al. "Indium-free transparent organic light emitting diodes with Al doped ZnO electrodes grown by atomic layer and pulsed laser deposition". In: *Applied Physics Letters* 93.7 (2008), p. 306.

[33]   Jin-A Jeong et al. "Flexible Al-doped ZnO films grown on PET substrates using linear facing target sputtering for flexible OLEDs". In: *Journal of Physics D: Applied Physics* 43.46 (2010), p. 465403.

[34]   Vijendra Singh Bhati, Mirabbos Hojamberdiev, and Mahesh Kumar. "Enhanced sensing performance of ZnO nanostructures-based gas sensors: A review". In: *Energy Reports* 6 (2020), pp. 46–62.

[35]   Lukas Schmidt-Mende and Judith L MacManus-Driscoll. "ZnO–nanostructures, defects, and devices". In: *Materials today* 10.5 (2007), pp. 40–48.

[36] Knut Erik Knutsen et al. "Zinc vacancy and oxygen interstitial in ZnO revealed by sequential annealing and electron irradiation". In: *Physical Review B* 86.12 (2012), p. 121203.

[37] Anderson Janotti and Chris G Van de Walle. "Fundamentals of zinc oxide as a semiconductor". In: *Reports on progress in physics* 72.12 (2009), p. 126501.

[38] Klaus Ellmer and André Bikowski. "Intrinsic and extrinsic doping of ZnO and ZnO alloys". In: *Journal of Physics D: Applied Physics* 49.41 (2016), p. 413002.

[39] Chris G Van de Walle. "Defect analysis and engineering in ZnO". In: *Physica B: Condensed Matter* 308 (2001), pp. 899–903.

[40] Hirotoshi Sato, Tadatsugu Minami, and Shinzo Takata. "Highly transparent and conductive group IV impurity-doped ZnO thin films prepared by radio frequency magnetron sputtering". In: *Journal of Vacuum Science & Technology A: Vacuum, Surfaces, and Films* 11.6 (1993), pp. 2975–2979.

[41] Jianhua Hu and Roy G Gordon. "Textured fluorine-doped ZnO films by atmospheric pressure chemical vapor deposition and their use in amorphous silicon solar cells". In: *Solar cells* 30.1-4 (1991), pp. 437–450.

[42] Lionel Vayssieres. "Growth of arrayed nanorods and nanowires of ZnO from aqueous solutions". In: *Advanced Materials* 15.5 (2003), pp. 464–466.

[43] Sheng Xu and Zhong Lin Wang. "One-dimensional ZnO nanostructures: solution growth and functional properties". In: *Nano Research* 4.11 (2011), pp. 1013–1098.

[44] Kuveshni Govender et al. "Understanding the factors that govern the deposition and morphology of thin films of ZnO from aqueous solution". In: *Journal of Materials Chemistry* 14.16 (2004), pp. 2575–2591.

[45] Haikuo Sun et al. "Position and density control in hydrothermal growth of ZnO nanorod arrays through pre-formed micro/nanodots". In: *Nanotechnology* 19.39 (2008), p. 395602.

[46] Conor P Burke-Govey and Natalie OV Plank. "Review of hydrothermal ZnO nanowires: Toward FET applications". In: *Journal of Vacuum Science & Technology B, Nanotechnology and Microelectronics: Materials, Processing, Measurement, and Phenomena* 31.6 (2013), 06F101.

[47] Ümit Özgür et al. "A comprehensive review of ZnO materials and devices". In: *Journal of applied physics* 98.4 (2005), p. 11.

[48] Václav Štengl et al. "ZnO/Bi2O3 nanowire composites as a new family of photocatalysts". In: *Powder Technology* 270 (2015), pp. 83–91.

[49]   Keh-moh Lin and Paijay Tsai. "Growth mechanism and characterization of ZnO: Al multi-layered thin films by sol–gel technique". In: *Thin Solid Films* 515.24 (2007), pp. 8601–8604.

[50]   Hua Wang et al. "Low temperature synthesis of sol–gel derived Al-doped ZnO thin films with rapid thermal annealing process". In: *Journal of Materials Science: Materials in Electronics* 21.6 (2010), pp. 589–594.

[51]   Chien-Yie Tsay, Kai-Shiung Fan, and Chien-Ming Lei. "Synthesis and characterization of sol–gel derived gallium-doped zinc oxide thin films". In: *Journal of alloys and compounds* 512.1 (2012), pp. 216–222.

[52]   H Mahdhi et al. "The effects of dopant concentration and deposition temperature on the structural, optical and electrical properties of Ga-doped ZnO thin films". In: *Superlattices and Microstructures* 72 (2014), pp. 60–71.

[53]   Nazanin Rashidi et al. "Highly conducting and optically transparent Si-doped ZnO thin films prepared by spray pyrolysis". In: *Journal of Materials Chemistry C* 1.42 (2013), pp. 6960–6969.

[54]   Zhong Yan et al. "Impacts of preparation conditions on photoelectric properties of the ZnO: Ge transparent conductive thin films fabricated by pulsed laser deposition". In: *Journal of Alloys and Compounds* 812 (2020), p. 152093.

[55]   Mejda Ajili, Michel Castagné, and Najoua Kamoun Turki. "Study on the doping effect of Sn-doped ZnO thin films". In: *Superlattices and Microstructures* 53 (2013), pp. 213–222.

[56]   A Polian, M Grimsditch, and I Grzegory. "Elastic constants of gallium nitride". In: *Journal of Applied Physics* 79.6 (1996), pp. 3343–3344.

[57]   A Hernández Battez et al. "CuO, ZrO2 and ZnO nanoparticles as antiwear additive in oil lubricants". In: *Wear* 265.3-4 (2008), pp. 422–428.

[58]   Frank C Porter. *Zinc handbook: properties, processing, and use in design*. Crc Press, 1991.

[59]   Victoria A Coleman et al. "Mechanical properties of ZnO epitaxial layers grown on a-and c-axis sapphire". In: *Applied Physics Letters* 86.20 (2005), p. 203105.

[60]   Andrea Dal Corso et al. "Ab initio study of piezoelectricity and spontaneous polarization in ZnO". In: *Physical Review B* 50.15 (1994), p. 10715.

[61]   John Frederick Nye et al. *Physical properties of crystals: their representation by tensors and matrices*. Oxford university press, 1985.

[62]   Fabio Bernardini, Vincenzo Fiorentini, and David Vanderbilt. "Spontaneous polarization and piezoelectric constants of III-V nitrides". In: *Physical Review B* 56.16 (1997), R10024.

[63] M Catti, Y Noel, and Roberto Dovesi. "Full piezoelectric tensors of wurtzite and zinc blende ZnO and ZnS by first-principles calculations". In: *Journal of physics and Chemistry of Solids* 64.11 (2003), pp. 2183–2190.

[64] Yves Noel et al. "Performance of various Hamiltonians in the study of the piezoelectric properties of crystalline compounds: The case of BeO and ZnO". In: *Physical Review B* 66.21 (2002), p. 214107.

[65] JG Lu et al. "Low-resistivity, stable p-type ZnO thin films realized using a Li–N dual-acceptor doping method". In: *Applied Physics Letters* 88.22 (2006), p. 222114.

[66] Rajib Sahu et al. "Stable p-type conductivity in B and N co-doped ZnO epitaxial thin film". In: *physica status solidi (b)* 253.3 (2016), pp. 504–508.

[67] Kong Chun-Yang et al. "Effect of post-annealing on microstructural and electrical properties of N+ ion-implanted into ZnO: In films". In: *Chinese Physics Letters* 25.3 (2008), p. 1128.

[68] Gaurav Malik et al. "Effect of annealing parameters on optoelectronic properties of highly ordered ZnO thin films". In: *Materials Science in Semiconductor Processing* 100 (2019), pp. 200–213.

[69] Afrina Sharmin et al. "Depositions and characterization of sol–gel processed Al-doped ZnO (AZO) as transparent conducting oxide (TCO) for solar cell application". In: *Journal of Theoretical and Applied Physics* 13.2 (2019), pp. 123–132.

[70] Chien-Yie Tsay and Wen-Che Lee. "Effect of dopants on the structural, optical and electrical properties of sol–gel derived ZnO semiconductor thin films". In: *Current Applied Physics* 13.1 (2013), pp. 60–65.

[71] AR Babar et al. "Gallium doping in transparent conductive ZnO thin films prepared by chemical spray pyrolysis". In: *Journal of Physics D: Applied Physics* 41.13 (2008), p. 135404.

[72] Ki-Chul Kim, Eung-kwon Kim, and Young-Sung Kim. "Growth and physical properties of sol–gel derived Co doped ZnO thin film". In: *Superlattices and Microstructures* 42.1-6 (2007), pp. 246–250.

[73] R Siddheswaran et al. "Fabrication and characterization of a diluted magnetic semiconducting TM co-doped Al: ZnO (TM= Co, Ni) thin films by sol–gel spin coating method". In: *Spectrochimica Acta Part A: Molecular and Biomolecular Spectroscopy* 106 (2013), pp. 118–123.

[74]   G Vijayaprasath et al. "Characterization of dilute magnetic semiconducting tran-
       sition metal doped ZnO thin films by sol–gel spin coating method". In: *Applied
       surface science* 313 (2014), pp. 870–876.

[75]   Hua-Chi Cheng, Chia-Fu Chen, and Chien-Yie Tsay. "Transparent ZnO thin
       film transistor fabricated by sol-gel and chemical bath deposition combination
       method". In: *Applied physics letters* 90.1 (2007), p. 012113.

[76]   Xiangliu Chen, Qingshuang Xie, and Jitao Li. "Significantly improved photo-
       luminescence properties of ZnO thin films by lithium doping". In: *Ceramics
       International* 46.2 (2020), pp. 2309–2316.

[77]   BJ Jin et al. "Relationship between photoluminescence and electrical proper-
       ties of ZnO thin films grown by pulsed laser deposition". In: *Applied Surface
       Science* 169 (2001), pp. 521–524.

[78]   Shinobu Fujihara, Yusuke Ogawa, and Asayo Kasai. "Tunable visible photolu-
       minescence from ZnO thin films through Mg-doping and annealing". In: *Chem-
       istry of materials* 16.15 (2004), pp. 2965–2968.

[79]   Mangesh Lanjewar and Jignasa V Gohel. "Enhanced performance of Ag-doped
       ZnO and pure ZnO thin films DSSCs prepared by sol-gel spin coating". In:
       Inorganic and Nano-Metal Chemistry 47.7 (2017), pp. 1090–1096.

[80]   Khushboo Sharma, Vinay Sharma, and SS Sharma. "Dye-sensitized solar cells:
       fundamentals and current status". In: *Nanoscale research letters* 13.1 (2018),
       pp. 1–46.

[81]   MI Khan et al. "Synthesis and characterization of Co and Ga co-doped ZnO thin
       films as an electrode for dye sensitized solar cells". In: *Ceramics International*
       46.17 (2020), pp. 26590–26597.

[82]   Muhammad Bilal Tahir et al. "ZnO THIN FILMS: recent development, future
       perspectives and applications for dye sensitized solar cell". In: *Surface Review
       and Letters* 25.07 (2018), p. 1930001.

[83]   Jia Huang, Zhigang Yin, and Qingdong Zheng. "Applications of ZnO in or-
       ganic and hybrid solar cells". In: *Energy & Environmental Science* 4.10 (2011),
       pp. 3861–3877.

[84]   Anuradha Purohit et al. "Impact of low temperature annealing on structural,
       optical, electrical and morphological properties of ZnO thin films grown by
       RF sputtering for photovoltaic applications". In: *Optical Materials* 49 (2015),
       pp. 51–58.

[85] Marco Laurenti et al. "Zinc oxide thin films for memristive devices: a review". In: *Critical Reviews in Solid State and Materials Sciences* 42.2 (2017), pp. 153–172.

[86] C Bayram et al. "Fabrication and characterization of novel hybrid green light emitting diodes based on substituting n-type ZnO for n-type GaN in an inverted p-n junction". In: *Journal of Vacuum Science & Technology B: Microelectronics and Nanometer Structures Processing, Measurement, and Phenomena* 27.3 (2009), pp. 1784–1788.

[87] IT Drapak. *Visible luminescence of a ZnO-Cu2O heterojunction.* 1968.

[88] Ricky W Chuang et al. "ZnO-on-GaN heterojunction light-emitting diode grown by vapor cooling condensation technique". In: *Applied Physics Letters* 91.23 (2007), p. 231113.

[89] Ya I Alivov et al. "Fabrication and characterization of n-ZnO/p-AlGaN heterojunction light-emitting diodes on 6H-SiC substrates". In: *Applied Physics Letters* 83.23 (2003), pp. 4719–4721.

[90] Daotong You et al. "Interface control for pure ultraviolet electroluminescence from nano-ZnO-based heterojunction devices". In: *Science Bulletin* 63.1 (2018), pp. 38–45.

[91] Do-Kyun Kwon, Yoann Porte, and Jae-Min Myoung. "Fabrication of ZnO nanorods p–n homojunction light-emitting diodes using Ag film as self-doping source for p-type ZnO nanorods". In: *The Journal of Physical Chemistry C* 122.22 (2018), pp. 11993–12001.

[92] Hideaki Agura et al. "Low resistivity transparent conducting Al-doped ZnO films prepared by pulsed laser deposition". In: *Thin solid films* 445.2 (2003), pp. 263–267.

[93] Sang-Moo Park, Tomoaki Ikegami, and Kenji Ebihara. "Effects of substrate temperature on the properties of Ga-doped ZnO by pulsed laser deposition". In: *Thin Solid Films* 513.1-2 (2006), pp. 90–94.

[94] Amaresh Das et al. "High conductivity along with high visible light transparency in Al implanted sol-gel ZnO thin film with an elevated figure of merit value as a transparent conducting layer". In: *Journal of Alloys and Compounds* 835 (2020), p. 155221.

[95] Gun Woo Hyung et al. "Storage stability improvement of pentacene thin-film transistors using polyimide passivation layer fabricated by vapor deposition polymerization". In: *Solid-state electronics* 54.4 (2010), pp. 439–442.

[96] Jyh-Liang Wang et al. "The effects of oxygen annealing on the electrical characteristics of hydrothermally grown zinc oxide thin-film transistors". In: *Solid-state electronics* 77 (2012), pp. 72–76.

[97] RL Hoffman, Benjamin J Norris, and JF Wager. "ZnO-based transparent thin-film transistors". In: *Applied Physics Letters* 82.5 (2003), pp. 733–735.

[98] R Majithia, S Ritter, and KE Meissner. "Heterogeneous nucleation for synthesis of sub-20 nm ZnO nanopods and their application to optical humidity sensing". In: *Analytica Chimica Acta* 812 (2014), pp. 206–214.

[99] SJ Pearton et al. "Wide bandgap nanowire sensors". In: *Micro (MEMS) and Nanotechnologies for Space, Defense, and Security II* 6959 (2008), pp. 11–21.

[100] Jae-Hun Kim et al. "Toluene-and benzene-selective gas sensors based on Pt- and Pd-functionalized ZnO nanowires in self-heating mode". In: *Sensors and Actuators B: Chemical* 294 (2019), pp. 78–88.

[101] Xiangxiang Chen et al. "NO_2 sensing properties of one-pot-synthesized ZnO nanowires with Pd functionalization". In: *Sensors and Actuators B: Chemical* 280 (2019), pp. 151–161.

[102] D Anbuselvan et al. "Room temperature ferromagnetic behavior of nickel-doped zinc oxide dilute magnetic semiconductor for spintronics applications". In: *Physica E: Low-dimensional Systems and Nanostructures* 129 (2021), p. 114665.

[103] Dandan Wang et al. "Robust room-temperature ferromagnetism with giant anisotropy in Nd-doped ZnO nanowire arrays". In: *Nano letters* 12.8 (2012), pp. 3994–4000.

[104] R Elilarassi and G Chandrasekaran. "Optical, electrical and ferromagnetic studies of ZnO: Fe diluted magnetic semiconductor nanoparticles for spintronic applications". In: *Spectrochimica Acta Part A: Molecular and Biomolecular Spectroscopy* 186 (2017), pp. 120–131.

[105] T Asokan and R Freer. "Grain and grain boundary conduction in zinc oxide varistors before and after DC degradation". In: *Journal of the European Ceramic Society* 11.6 (1993), pp. 545–550.

[106] Jay W Grate, Stephen J Martin, and Richard M White. "Acoustic wave microsensors". In: *analytical Chemistry* 65.21 (1993), 940A–948A.

[107] Klaus Ellmer, Andreas Klein, and Bernd Rech. "Transparent conductive zinc oxide: basics and applications in thin film solar cells". In: (2007).

[108] Ahmad H Adl et al. "Schottky barrier thin film transistors using solution-processed n-ZnO". In: *ACS Applied Materials & Interfaces* 4.3 (2012), pp. 1423–1428.

[109] S Chakrabarti, D Ganguli, and S Chaudhuri. "Substrate dependence of preferred orientation in sol–gel-derived zinc oxide films". In: *Materials letters* 58.30 (2004), pp. 3952–3957.

[110] Yee-Shin Chang and Jyh-Ming Ting. "Growth of ZnO thin films and whiskers". In: *Thin Solid Films* 398 (2001), pp. 29–34.

[111] L Znaidi et al. "Elaboration of ZnO thin films with preferential orientation by a soft chemistry route". In: *Journal of Sol-Gel Science and Technology* 26.1 (2003), pp. 817–821.

[112] Davood Raoufi and Taha Raoufi. "The effect of heat treatment on the physical properties of sol–gel derived ZnO thin films". In: *Applied surface science* 255.11 (2009), pp. 5812–5817.

[113] R Kraya et al. "Ultra-low resistivity aluminum doped ZnO thin films on flexible substrates using sol-gel solution deposition". In: *Thin Solid Films* 664 (2018), pp. 41–45.

[114] Faran Baig et al. "A comparative analysis for effects of solvents on optical properties of Mg doped ZnO thin films for optoelectronic applications". In: *Optik* 208 (2020), p. 164534.

[115] Mingsong Wang et al. "Low-temperature solution growth of high-quality ZnO thin films and solvent-dependent film texture". In: *The Journal of Physical Chemistry C* 112.6 (2008), pp. 1920–1924.

[116] Lamia Znaidi. "Sol—gel deposited ZnO thin films: A review". In: *Materials Science and Engineering: B* 174.1-3 (2010), pp. 18–30.

[117] P Hosseini Vajargah et al. "Sol–gel derived ZnO thin films: effect of amino-additives". In: *Applied Surface Science* 285 (2013), pp. 732–743.

[118] D L Pavia et al. *Spectroscopy*. CBS Publishers and Distributors, 1997.

[119] Colin N Banwell, Elaine M McCash, et al. *Fundamentals of molecular spectroscopy*. McGraw-Hill, 1994.

[120] Christopher Hammond. *The basics of crystallography and diffraction*. Vol. 21. International Union of Crystal, 2015.

[121] Mario Birkholz. *Thin film analysis by X-ray scattering*. John Wiley & Sons, 2006.

[122] M Wohlschlögel et al. "Application of a single-reflection collimating multilayer optic for X-ray diffraction experiments employing parallel-beam geometry". In: *Journal of Applied Crystallography* 41.1 (2008), pp. 124–133.

[123] P Scherrer et al. "Determination of the size and internal structure of colloidal particles using X-rays". In: *Nachr. Ges. Wiss. Göttingen* 2 (1918), pp. 98–100.

[124]   Marcin Wojdyr. "Fityk: a general-purpose peak fitting program". In: *Journal of applied crystallography* 43.5-1 (2010), pp. 1126–1128.

[125]   V Kazmiruk. *Scanning Electron Microscopy*. Intech, 2012.

[126]   Robert Edward Lee. *Scanning electron microscopy and X-ray microanalysis*. 1993.

[127]   Milton Ohring. *The Materials Science of Thin Films*. Academic Press, 1992.

[128]   Ali Fatima Abdul Razak et al. "Effect of annealing on structural and optical properties of ZnO thin films by sol gel technique". In: *Chalcogenide Letters* 8.9 (2011), pp. 511–519.

[129]   David Adegboyega Ajadi, Saint Muyiwa Agboola, Oluwaseun Adedokun, et al. "Effect of spin coating speed on some optical properties of ZnO thin films". In: *Journal of Materials Science and Chemical Engineering* 4.05 (2016), p. 1.

[130]   CL Du et al. "Raman spectroscopy of (Mn, Co)-codoped ZnO films". In: *Journal of Applied Physics* 99.12 (2006), p. 123515.

[131]   Said Benramache et al. "Study on the correlation between crystallite size and optical gap energy of doped ZnO thin film". In: *Journal of Nanostructure in Chemistry* 3.1 (2013), pp. 1–6.

[132]   S Ben Yahia et al. "Raman study of oriented ZnO thin films deposited by sol–gel method". In: *Spectrochimica Acta Part A: Molecular and Biomolecular Spectroscopy* 71.4 (2008), pp. 1234–1238.

[133]   Harish Kumar Yadav et al. "Defect induced activation of Raman silent modes in rf co-sputtered Mn doped ZnO thin films". In: *Journal of Physics D: Applied Physics* 40.19 (2007), p. 6005.

[134]   JM Calleja and Manuel Cardona. "Resonant raman scattering in ZnO". In: *Physical Review B* 16.8 (1977), p. 3753.

[135]   Ramon Cuscó et al. "Temperature dependence of Raman scattering in ZnO". In: *Physical Review B* 75.16 (2007), p. 165202.

[136]   JS Thakur et al. "Raman scattering studies of magnetic Co-doped ZnO thin films". In: *Journal of Applied Physics* 102.9 (2007), p. 093904.

[137]   Apu Mondal et al. "Raman investigation of N-implanted ZnO: Defects, disorder and recovery". In: *Journal of Raman Spectroscopy* 50.12 (2019), pp. 1926–1937.

[138]   Jianzi Li et al. "Preparation and characterization of Al doped ZnO thin films by sol–gel process". In: *Journal of alloys and compounds* 542 (2012), pp. 151–156.

[139] Byeong Kyun Choi et al. "Optical characterization of ZnO thin films deposited by Sol-gel method". In: *Journal of Materials Science: Materials in Electronics* 17.12 (2006), pp. 1011–1015.

[140] Xue-Ran Deng et al. "Preparation of highly transparent conductive Al-doped ZnO thin films and annealing effects on properties". In: *Journal of Materials Science: Materials in Electronics* 23.2 (2012), pp. 413–417.

[141] JJ Ding, HX Chen, and SY Ma. "Structural and photoluminescence properties of Al-doped ZnO films deposited on Si substrate". In: *Physica E: Low-Dimensional Systems and Nanostructures* 42.6 (2010), pp. 1861–1864.

[142] Tao Wang et al. "Low temperature synthesis wide optical band gap Al and (Al, Na) co-doped ZnO thin films". In: *Applied Surface Science* 257.6 (2011), pp. 2341–2345.

[143] K Vanheusden et al. "Mechanisms behind green photoluminescence in ZnO phosphor powders". In: *Journal of Applied Physics* 79.10 (1996), pp. 7983–7990.

[144] A Chelouche et al. "Low cerium doping investigation on structural and photoluminescence properties of sol-gel ZnO thin films". In: *Journal of Luminescence* 181 (2017), pp. 448–454.

[145] XL Wu et al. "Photoluminescence and cathodoluminescence studies of stoichiometric and oxygen-deficient ZnO films". In: *Applied Physics Letters* 78.16 (2001), pp. 2285–2287.

[146] BB Li et al. "Study of structure and magnetic properties of Ni-doped ZnO-based DMSs". In: *Materials science in semiconductor processing* 9.1-3 (2006), pp. 141–145.

[147] Shenghong Yang and Yueli Zhang. "Structural, optical and magnetic properties of Mn-doped ZnO thin films prepared by sol–gel method". In: *Journal of magnetism and magnetic materials* 334 (2013), pp. 52–58.

[148] Hideo Ohno. "Making nonmagnetic semiconductors ferromagnetic". In: *science* 281.5379 (1998), pp. 951–956.

[149] Zohra Nazir Kayani et al. "Dielectric and magnetic properties of dilute magnetic semiconductors Ag-doped ZnO thin films". In: *Applied Physics A* 126.7 (2020), pp. 1–10.

[150] Jacek K Furdyna. "Diluted magnetic semiconductors". In: *Journal of Applied Physics* 64.4 (1988), R29–R64.

[151] J Ramesh et al. "Structural and optical properties of Ni doped ZnO thin films using sol–gel dip coating technique". In: *Optik* 124.15 (2013), pp. 2023–2027.

[152]   ME Ghazi et al. "Studying Mn-and Ni-doped ZnO thin films synthesized by the sol–gel method". In: *Journal of superconductivity and novel magnetism* 25.1 (2012), pp. 101–108.

[153]   AAM Farag et al. "Photoluminescence and optical properties of nanostructure Ni doped ZnO thin films prepared by sol–gel spin coating technique". In: *Journal of Alloys and Compounds* 509.30 (2011), pp. 7900–7908.

[154]   Vinod Kumar et al. "Role of film thickness on the properties of ZnO thin films grown by sol-gel method". In: *Thin solid films* 539 (2013), pp. 161–165.

[155]   M Ayachi et al. "Synthesis and Characterization of Ni-Doped ZnO Thin Films Prepared by Sol–Gel Spin-Coating Method". In: *Semiconductors* 55.5 (2021), pp. 482–490.

[156]   Narinder Kaur et al. "Highly transparent and lower resistivity of yttrium doped ZnO thin films grown on quartz glass by sol–gel method". In: *Physica B: Condensed Matter* 500 (2016), pp. 179–185.

[157]   Seval Aksoy et al. "Effect of Sn dopants on the optical and electrical properties of ZnO films". In: *Optica Applicata* 40.1 (2010), pp. 7–14.

[158]   Aradhana Tiwari and PP Sahay. "The effects of Sn–in co-doping on the structural, optical, photoluminescence and electrical characteristics of the sol-gel processed ZnO thin films". In: *Optical Materials* 110 (2020), p. 110395.

[159]   MR Islam and J Podder. "Optical properties of ZnO nano fiber thin films grown by spray pyrolysis of zinc acetate precursor". In: *Crystal Research and Technology: Journal of Experimental and Industrial Crystallography* 44.3 (2009), pp. 286–292.

[160]   YC Liu, SK Tung, and JH Hsieh. "Influence of annealing on optical properties and surface structure of ZnO thin films". In: *Journal of crystal growth* 287.1 (2006), pp. 105–111.

[161]   Fahrettin Yakuphanoglu et al. "The effects of fluorine on the structural, surface morphology and optical properties of ZnO thin films". In: *Physica B: Condensed Matter* 394.1 (2007), pp. 86–92.

[162]   C Lung et al. "Characterization of the structural and optical properties of ZnO thin films doped with Ga, Al and (Al+ Ga)". In: *Journal of Alloys and Compounds* 725 (2017), pp. 1238–1243.

[163]   SS Shinde, CH Bhosale, and KY Rajpure. "Photoelectrochemical properties of highly mobilized Li-doped ZnO thin films". In: *Journal of Photochemistry and Photobiology B: Biology* 120 (2013), pp. 1–9.

[164] Kaniz Naila Tonny et al. "Electrical, optical and structural properties of transparent conducting Al doped ZnO (AZO) deposited by sol-gel spin coating". In: *AIP Advances* 8.6 (2018), p. 065307.

[165] Shuqun Chen, Michael EA Warwick, and Russell Binions. "Effects of film thickness and thermal treatment on the structural and opto-electronic properties of Ga-doped ZnO films deposited by sol–gel method". In: *Solar Energy Materials and Solar Cells* 137 (2015), pp. 202–209.

[166] Tadatsugu Minami. "Transparent conducting oxide semiconductors for transparent electrodes". In: *Semiconductor science and technology* 20.4 (2005), S35.

[167] Tadatsugu Minami. "Present status of transparent conducting oxide thin-film development for Indium-Tin-Oxide (ITO) substitutes". In: *Thin Solid Films* 516.17 (2008), pp. 5822–5828.

[168] Klaus Ellmer. "Transparent conductive zinc oxide and its derivatives". In: *Handbook of transparent conductors*. Springer, 2011, pp. 193–263.

[169] David C Look. "Recent advances in ZnO materials and devices". In: *Materials science and engineering: B* 80.1-3 (2001), pp. 383–387.

[170] Ahmed A Al-Ghamdi et al. "Semiconducting properties of Al doped ZnO thin films". In: *Spectrochimica Acta Part A: Molecular and Biomolecular Spectroscopy* 131 (2014), pp. 512–517.

[171] Min-Chul Jun, Sang-Uk Park, and Jung-Hyuk Koh. "Comparative analysis of Al-doped ZnO and Ga-doped ZnO thin films". In: *Integrated Ferroelectrics* 140.1 (2012), pp. 166–176.

[172] M Sahal et al. "Structural, electrical and optical properties of ZnO thin films deposited by sol–gel method". In: *Microelectronics Journal* 39.12 (2008), pp. 1425–1428.

[173] Jianguo Lv et al. "Effect of annealing temperature on photocatalytic activity of ZnO thin films prepared by sol–gel method". In: *Superlattices and Microstructures* 50.2 (2011), pp. 98–106.

[174] Kartikey Verma et al. "Investigation of structural, morphological and optical properties of Mg: ZnO thin films prepared by sol-gel spin coating method". In: *Vacuum* 146 (2017), pp. 524–529.

[175] A Chelouche et al. "Influence of Ag doping on structural and optical properties of ZnO thin films synthesized by the sol–gel technique". In: *Applied Physics A* 115.2 (2014), pp. 613–616.

[176] M Dutta, S Mridha, and D Basak. "Effect of sol concentration on the properties of ZnO thin films prepared by sol–gel technique". In: *Applied Surface Science* 254.9 (2008), pp. 2743–2747.

[177] E Andrade, M Miki-Yoshida, et al. "Growth, structure and optical characterization of high quality ZnO thin films obtained by spray pyrolysis". In: *Thin solid films* 350.1-2 (1999), pp. 192–202.

[178] XM Zhang et al. "Co-doped Y-shape ZnO nanostructures: Synthesis, structure and properties". In: *Solid state communications* 149.7-8 (2009), pp. 293–296.

[179] Manjula G Nair et al. "Structural, optical, photo catalytic and antibacterial activity of ZnO and Co doped ZnO nanoparticles". In: *Materials Letters* 65.12 (2011), pp. 1797–1800.

[180] Hong Seong Kang et al. "Structural, electrical, and optical properties of p-type ZnO thin films with Ag dopant". In: *Applied Physics Letters* 88.20 (2006), p. 202108.

[181] T Ghosh et al. "Effect of Cu doping in the structural, electrical, optical, and optoelectronic properties of sol-gel ZnO thin films". In: *Journal of the Electrochemical Society* 156.4 (2009), H285.

[182] K Kumar et al. "Effect of solvents on sol–gel spin-coated nanostructured Al-doped ZnO thin films: a film for key optoelectronic applications". In: *Applied Physics A* 123.12 (2017), pp. 1–11.

[183] Jung-Hyeok Bae and Han-Ki Kim. "Characteristics of Al doped ZnO co-sputtered InZnO anode films prepared by direct current magnetron sputtering for organic light-emitting diodes". In: *Thin Solid Films* 516.21 (2008), pp. 7866–7870.

[184] Jian Sun et al. "The ultraviolet photoconductive detector based on Al-doped ZnO thin film with fast response". In: *Science China Physics, Mechanics and Astronomy* 54.1 (2011), pp. 102–105.

[185] ZA Wang et al. "Growth of ZnO: Al films by RF sputtering at room temperature for solar cell applications". In: *Solid-State Electronics* 53.11 (2009), pp. 1149–1153.

[186] Mei Xin et al. "Effect of Mn doping on the optical, structural and photoluminescence properties of nanostructured ZnO thin film synthesized by sol–gel technique". In: *Superlattices and Microstructures* 74 (2014), pp. 234–241.

[187] Neeru Kumar, Ravinder Kaur, and RM Mehra. "Photoluminescence studies in sol–gel derived ZnO films". In: *Journal of Luminescence* 126.2 (2007), pp. 784–788.

[188] WL Li et al. "Orientation degree dependence of magnetic properties of Co doped ZnO thin films by sol–gel process". In: *Journal of sol-gel science and technology* 54.3 (2010), pp. 335–339.

[189] Robina Ashraf et al. "Structural and magnetic properties of Mn/Fe co-doped ZnO thin films prepared by sol–gel technique". In: *IEEE Transactions on Magnetics* 50.8 (2014), pp. 1–4.

[190] Premalatha Ariyakkani, Lakshmikanthan Suganya, and Balakrishnan Sundaresan. "Investigation of the structural, optical and magnetic properties of Fe doped ZnO thin films coated on glass by sol-gel spin coating method". In: *Journal of Alloys and Compounds* 695 (2017), pp. 3467–3475.

[191] Jianping Xu et al. "Luminescence properties of cobalt-doped ZnO films prepared by sol–gel method". In: *Journal of electronic materials* 42.12 (2013), pp. 3438–3444.

[192] A Kaushik et al. "Influence of Co doping on the structural, optical and magnetic properties of ZnO nanocrystals". In: *Journal of alloys and compounds* 578 (2013), pp. 328–335.

[193] Nupur Bahadur et al. "Influence of cobalt doping on the crystalline structure, optical and mechanical properties of ZnO thin films". In: *Thin Solid Films* 518.18 (2010), pp. 5257–5264.

[194] Aihua Wang et al. "Study on field-emission characteristics of electrodeposited Co-doped ZnO thin films". In: *Physica B: Condensed Matter* 406.5 (2011), pp. 1049–1052.

[195] Husam S Al-Salman and MJ Abdullah. "Effect of Co-doping on the structure and optical properties of ZnO nanostructure prepared by RF-magnetron sputtering". In: *Superlattices and Microstructures* 60 (2013), pp. 349–357.

[196] Jae Hyun Kim et al. "Optical and magnetic properties of laser-deposited Co-doped ZnO thin films". In: *Solid state communications* 131.11 (2004), pp. 677–680.

[197] R Baghdad et al. "Structural and magnetic properties of Co-doped ZnO thin films grown by ultrasonic spray pyrolysis method". In: *Superlattices and Microstructures* 104 (2017), pp. 553–569.

[198] FL Xian et al. "Crystallographic, optical and magnetic properties of Co-doped ZnO thin films synthesized by sol gel route". In: *Crystal Research and Technology* 47.4 (2012), pp. 423–428.

[199] J El Ghoul et al. "Sol–gel synthesis, structural, optical and magnetic properties of Co-doped ZnO nanoparticles". In: *Journal of Materials Science: Materials in Electronics* 26.4 (2015), pp. 2614–2621.

[200] Xiaming Zhu et al. "Photoluminescence and resonant Raman scattering in N-doped ZnO thin films". In: *Optics Communications* 283.13 (2010), pp. 2695–2699.

[201] YM Hu et al. "Identification of Mn-related Raman modes in Mn-doped ZnO thin films". In: *Journal of Raman Spectroscopy* 42.3 (2011), pp. 434–437.

[202] Hongen Nian et al. "Sol–gel derived N-doped ZnO thin films". In: *Materials Letters* 63.26 (2009), pp. 2246–2248.

[203] R Ayouchi et al. "Growth of pure ZnO thin films prepared by chemical spray pyrolysis on silicon". In: *Journal of crystal growth* 247.3-4 (2003), pp. 497–504.

[204] Jinzhong Wang et al. *Luminescence properties of ZnO films annealed in growth ambient and oxygen.* 2004.

[205] Mehmet Yilmaz and Şakir Aydoğan. "The effect of Mn incorporation on the structural, morphological, optical, and electrical features of nanocrystalline ZnO thin films prepared by chemical spray pyrolysis technique". In: *Metallurgical and Materials Transactions A* 46.6 (2015), pp. 2726–2735.

[206] Kamal Rudra and YK Prajapati. "Effect of Mn doping on defect-related photoluminescence and nanostructure of dense 3-D nano-root network of ZnO". In: *Ceramics International* 46.8 (2020), pp. 10135–10141.

[207] Fouaz Lekoui et al. "Investigation of the effects of thermal annealing on the structural, morphological and optical properties of nanostructured Mn doped ZnO thin films". In: *Optical Materials* 118 (2021), p. 111236.

[208] Arun Aravind et al. "Structural, optical and magnetic properties of Mn doped ZnO thin films prepared by pulsed laser deposition". In: *Materials Science and Engineering: B* 177.13 (2012), pp. 1017–1022.

[209] JB Wang et al. "Raman scattering and high temperature ferromagnetism of Mn-doped ZnO nanoparticles". In: *Applied Physics Letters* 88.25 (2006), p. 252502.

[210] Shiv Kumar et al. "Sol–gel-derived ZnO: Mn nanocrystals: study of structural, Raman, and optical properties". In: *The Journal of Physical Chemistry C* 116.31 (2012), pp. 16700–16708.

[211] R Vinodkumar et al. "Structural, spectroscopic and electrical studies of nanostructured porous ZnO thin films prepared by pulsed laser deposition". In: *Spectrochimica Acta Part A: Molecular and Biomolecular Spectroscopy* 118 (2014), pp. 724–732.

[212] Fatemeh Bakhtiargonbadi et al. "Fabrication of novel electrospun Al and Cu doped ZnO thin films and evaluation of photoelectrical and sunlight-driven photoelectrochemical properties". In: *Materials Chemistry and Physics* 252 (2020), p. 123270.

[213] FK Shan et al. "Blueshift of near band edge emission in Mg doped ZnO thin films and aging". In: *Journal of Applied Physics* 95.9 (2004), pp. 4772–4776.

[214] AiLing Yang et al. "Photoluminescence and defect evolution of nano-ZnO thin films at low temperature annealing". In: *Science China Technological Sciences* 56.1 (2013), pp. 25–31.

[215] Hong Seong Kang et al. "Annealing effect on the property of ultraviolet and green emissions of ZnO thin films". In: *Journal of Applied Physics* 95.3 (2004), pp. 1246–1250.

[216] PM Ratheesh Kumar et al. "On the properties of indium doped ZnO thin films". In: *Semiconductor science and technology* 20.2 (2004), p. 120.

[217] Jianguo Lü et al. "Preparation and characterization of Na-doped ZnO thin films by sol–gel method". In: *Physica B: Condensed Matter* 405.15 (2010), pp. 3167–3171.

[218] Doyoung Kim et al. "The properties of plasma-enhanced atomic layer deposition (ALD) ZnO thin films and comparison with thermal ALD". In: *Applied Surface Science* 257.8 (2011), pp. 3776–3779.

[219] Dianwu Wu et al. "Preparation and properties of Ni-doped ZnO rod arrays from aqueous solution". In: *Journal of colloid and interface science* 330.2 (2009), pp. 380–385.

[220] RJ Hong et al. "Studies on ZnO: Al thin films deposited by in-line reactive mid-frequency magnetron sputtering". In: *Applied Surface Science* 207.1-4 (2003), pp. 341–350.

[221] YR Ryu et al. "Synthesis of p-type ZnO films". In: *Journal of crystal growth* 216.1-4 (2000), pp. 330–334.

[222] Tomasz Dietl et al. "Zener model description of ferromagnetism in zinc-blende magnetic semiconductors". In: *science* 287.5455 (2000), pp. 1019–1022.

[223]   Mingpeng Yu et al. "Structural and physical properties of Ni and Al co-doped ZnO films grown on glass by direct current magnetron co-sputtering". In: *Physica B: Condensed Matter* 404.12-13 (2009), pp. 1829–1834.

[224]   Mingpeng Yu et al. "Magnetic, magnetoresistance and electrical transport properties of Ni and Al co-doped ZnO films grown on glass substrates by direct current magnetron co-sputtering". In: *Materials Chemistry and Physics* 120.2-3 (2010), pp. 571–575.

[225]   R Siddheswaran et al. "Fabrication and characterization of a diluted magnetic semiconducting TM co-doped Al: ZnO (TM= Co, Ni) thin films by sol–gel spin coating method". In: *Spectrochimica Acta Part A: Molecular and Biomolecular Spectroscopy* 106 (2013), pp. 118–123.

[226]   Theopolina Amakali et al. "Structural and optical properties of ZnO thin films prepared by molecular precursor and sol–gel methods". In: *Crystals* 10.2 (2020), p. 132.

[227]   Mohd Arif et al. "Effect of annealing temperature on structural and optical properties of sol–gel-derived ZnO thin films". In: *Journal of Electronic Materials* 47.7 (2018), pp. 3678–3684.

[228]   AR Khantoul et al. "Structural and optical properties of ZnO and Co doped ZnO thin films prepared by sol-gel". In: *Acta Phys. Pol. A* 133 (2018), pp. 114–117.

[229]   Linhua Xu et al. "Structural and optical properties of ZnO thin films prepared by sol–gel method with different thickness". In: *Applied Surface Science* 257.9 (2011), pp. 4031–4037.

[230]   H Aydın et al. "Refractive index dispersion properties of Cr-doped ZnO thin films by sol–gel spin coating method". In: *Optik* 127.4 (2016), pp. 1879–1883.

[231]   Jianguo Lv et al. "Optical constants of Na-doped ZnO thin films by sol–gel method". In: *Optics Communications* 284.12 (2011), pp. 2905–2908.

[232]   Abdel-Sattar Gadallah and MM El-Nahass. "Structural, optical constants and photoluminescence of ZnO thin films grown by sol-gel spin coating". In: *Advances in Condensed Matter Physics* 2013 (2013), p. 234546.

[233]   H Aydin et al. "Synthesis and characterization of nanostructured undoped and Sn-doped ZnO thin films via sol–gel approach". In: *Applied Surface Science* 350 (2015), pp. 109–114.

[234]   F Boudjouan et al. "Effects of stabilizer ratio on photoluminescence properties of sol-gel ZnO nano-structured thin films". In: *Journal of Luminescence* 158 (2015), pp. 32–37.

[235] Deyi Wang, Jian Zhou, and Guizhen Liu. "The microstructure and photoluminescence of Cu-doped ZnO nano-crystal thin films prepared by sol–gel method". In: *Journal of Alloys and Compounds* 487.1-2 (2009), pp. 545–549.

[236] Seung Hwangbo, Yun-Ji Lee, and Kyu-Seog Hwang. "Photoluminescence of ZnO layer on commercial glass substrate prepared by sol–gel process". In: *Ceramics International* 34.5 (2008), pp. 1237–1239.

[237] Bixia Lin, Zhuxi Fu, and Yunbo Jia. "Green luminescent center in undoped zinc oxide films deposited on silicon substrates". In: *Applied physics letters* 79.7 (2001), pp. 943–945.

[238] M Silambarasan, S Saravanan, and T Soga. "Effect of Fe-doping on the structural, morphological and optical properties of ZnO nanoparticles synthesized by solution combustion process". In: *Physica E: Low-dimensional Systems and Nanostructures* 71 (2015), pp. 109–116.

[239] Mohd Farooqi, Mubashshir Hasan, and Rajneesh Kumar Srivastava. "Effect of annealing temperature on structural, photoluminescence and photoconductivity properties of ZnO thin film deposited on glass substrate by sol–gel spin coating method". In: *Proceedings of the National Academy of Sciences, India Section A: Physical Sciences* 90.5 (2020), pp. 845–859.

[240] AB Djurišić et al. "Green, yellow, and orange defect emission from ZnO nanostructures: Influence of excitation wavelength". In: *Applied Physics Letters* 88.10 (2006), p. 103107.

[241] Vinod Kumar et al. "Origin of the red emission in zinc oxide nanophosphors". In: *Materials Letters* 101 (2013), pp. 57–60.

[242] G Srinivasan et al. "Influence of post-deposition annealing on the structural and optical properties of ZnO thin films prepared by sol–gel and spin-coating method". In: *Superlattices and Microstructures* 43.2 (2008), pp. 112–119.

[243] Md Nasrul Haque Mia et al. "Influence of Mg content on tailoring optical bandgap of Mg-doped ZnO thin film prepared by sol-gel method". In: *Results in physics* 7 (2017), pp. 2683–2691.

[244] Anit K Ambedkar et al. "Structural, optical and thermoelectric properties of Al-doped ZnO thin films prepared by spray pyrolysis". In: *Surfaces and Interfaces* 19 (2020), p. 100504.

[245] Amanpal Singh et al. "Effect of post annealing temperature on structural and optical properties of ZnCdO thin films deposited by sol–gel method". In: *Applied Surface Science* 258.5 (2011), pp. 1881–1887.

[246] Nur Hasyimah Hashim et al. "Properties of undoped ZnO and Mg doped ZnO thin films by sol-gel method for optoelectronic applications". In: _Journal of the Australian Ceramic Society_ 53.2 (2017), pp. 421–431.

[247] Gae Hun Jo, Sun-Ho Kim, and Jung-Hyuk Koh. "Enhanced electrical and optical properties based on stress reduced graded structure of Al-doped ZnO thin films". In: _Ceramics International_ 44.1 (2018), pp. 735–741.

[248] Mingsong Wang et al. "Influence of annealing temperature on the structural and optical properties of sol–gel prepared ZnO thin films". In: _physica status solidi (a)_ 203.10 (2006), pp. 2418–2425.

[249] Lin Cui et al. "Effect of film thickness and annealing temperature on the structural and optical properties of ZnO thin films deposited on sapphire (0001) substrates by sol–gel". In: _Ceramics International_ 39.3 (2013), pp. 3261–3268.

[250] Yidong Zhang et al. "Effect of annealing temperature on the structural and optical properties of ZnO thin films prepared by sol–gel method". In: _Ionics_ 16.9 (2010), pp. 815–820.

[251] Joydip Sengupta et al. "Influence of annealing temperature on the structural, topographical and optical properties of sol–gel derived ZnO thin films". In: _Materials Letters_ 65.17-18 (2011), pp. 2572–2574.

[252] Kousik Samanta, Pijush Bhattacharya, and Ram S Katiyar. "Raman scattering studies of p-type Sb-doped ZnO thin films". In: _Journal of Applied Physics_ 108.11 (2010), p. 113501.

[253] Ümit Özgür et al. "A comprehensive review of ZnO materials and devices". In: _Journal of applied physics_ 98.4 (2005), p. 11.

[254] Xiaomeng Sui et al. "Structural and photoluminescent properties of ZnO hexagonal nanoprisms synthesized by microemulsion with polyvinyl pyrrolidone served as surfactant and passivant". In: _Chemical Physics Letters_ 424.4-6 (2006), pp. 340–344.

[255] TS Jeong et al. "Raman scattering and photoluminescence of As ion-implanted ZnO single crystal". In: _Journal of applied physics_ 96.1 (2004), pp. 175–179.

[256] Dongyu Fang, Pei Yao, and Huijun Li. "Influence of annealing temperature on the structural and optical properties of Mg–Al co-doped ZnO thin films prepared via sol–gel method". In: _Ceramics International_ 40.4 (2014), pp. 5873–5880.

[257] J Serrano et al. "Dispersive phonon linewidths: The E 2 phonons of ZnO". In: _Physical review letters_ 90.5 (2003), p. 055510.

[258] ZQ Chen et al. "Microvoid formation in hydrogen-implanted ZnO probed by a slow positron beam". In: _Physical Review B_ 71.11 (2005), p. 115213.

[259] A El Manouni et al. "Effect of aluminium doping on zinc oxide thin films grown by spray pyrolysis". In: *Superlattices and Microstructures* 39.1-4 (2006), pp. 185–192.

[260] Sanjeev Kumar and R Thangavel. "Structural and optical properties of Na doped ZnO nanocrystalline thin films synthesized using sol–gel spin coating technique". In: *Journal of sol-gel science and technology* 67.1 (2013), pp. 50–55.

[261] Songqing Zhao et al. "Violet luminescence emitted from Ag-nanocluster doped ZnO thin films grown on fused quartz substrates by pulsed laser deposition". In: *Physica B: Condensed Matter* 373.1 (2006), pp. 154–156.

[262] Y Natsume and H Sakata. "Zinc oxide films prepared by sol-gel spin-coating". In: *Thin solid films* 372.1-2 (2000), pp. 30–36.

[263] Young-Sung Kim, Weon-Pil Tai, and Su-Jeong Shu. "Effect of preheating temperature on structural and optical properties of ZnO thin films by sol–gel process". In: *Thin solid films* 491.1-2 (2005), pp. 153–160.

[264] A Khorsand Zak et al. "Effects of annealing temperature on some structural and optical properties of ZnO nanoparticles prepared by a modified sol–gel combustion method". In: *Ceramics International* 37.1 (2011), pp. 393–398.

[265] Jen-Po Lin and Jenn-Ming Wu. "The effect of annealing processes on electronic properties of sol-gel derived Al-doped ZnO films". In: *Applied Physics Letters* 92.13 (2008), p. 134103.

[266] SS Tneh et al. "The structural and optical characterizations of ZnO synthesized using the "bottom-up" growth method". In: *Physica B: Condensed Matter* 405.8 (2010), pp. 2045–2048.

[267] Su-Shia Lin, Jow-Lay Huang, and P Šajgalik. "The properties of heavily Al-doped ZnO films before and after annealing in the different atmosphere". In: *Surface and Coatings Technology* 185.2-3 (2004), pp. 254–263.

[268] J Tauc, Radu Grigorovici, and Anina Vancu. "Optical properties and electronic structure of amorphous germanium". In: *physica status solidi (b)* 15.2 (1966), pp. 627–637.

[269] Dinghua Bao et al. "Band-gap energies of sol-gel-derived SrTiO 3 thin films". In: *Applied Physics Letters* 79.23 (2001), pp. 3767–3769.

[270] Chien-Hsun Chu, Hung-Wei Wu, and Jow-Lay Huang. "Effect of annealing temperature and atmosphere on aluminum-doped ZnO/Au/aluminum-doped ZnO thin film properties". In: *Thin Solid Films* 605 (2016), pp. 121–128.

BIO-DATA OF RESEARCH SCHOLAR

Personal Details

Name : Shital Prasad

Father's Name : Late Sh. Tika Ram

Date of Birth : 15-06-1976

Nationality : Indian

Marital Status : Married

Language Known : Hindi, English

Email address : shitalprasad@yahoo.com

Address for correspondence :

Shital Prasad

N-215, Piyush Heights

Sector-89, Greater Faridabad

Faridabad-121002

Haryana, India

Phone No.: (+91)-9871733760

Academic Qualifications :

Ph. D.: Ph. D. thesis submitted to Department of Physics, JC Bose university of Science and Technology, YMCA, Faridabad.

M. Tech.: Solid State Materials from Indian Institute of Technology, New Delhi in 2000, with CGPA= 8.22 on 10 point scale.

M. Sc.: Physics with specialization in Electronics from Ch. Charan Singh University, Meerut, UP, in 1998 with 70.2% marks

B. Sc.: Physics, Mathematics and Chemistry from from Ch. Charan Singh University, Meerut, UP, in 1996 with 68.4% marks

Publications :

1. Shital Prasad, Sonia Bansal, and S. P. Pandey. "Effect of substrate rotation speed on structural, morphological, vibrational and optical properties of sol-gel derived Mn-Ni co-doped ZnO thin films." *Materials Today: Proceedings* 49 (2022) 3008–3014.
   DOI: https://doi.org/10.1016/j.matpr.2020.10.172

2. Shital Prasad, Sonia Bansal, and S. P. Pandey. "Structural, raman, photo-luminescent and optical investigation of sol–gel derived Co, Al and Ni doped ZnO thin films." *Materials Today: Proceedings* 49 (2022) 3022–3027.
   DOI: ttps://doi.org/10.1016/j.matpr.2020.10.235

3. Presented a paper **"Review on ZnO based CO and CO2 Gas sensors"** at National Conference on **"Role of Science and Technology Towards 'Make in India (RSTTMI-2016)** on March 05-07, 2016 at YMCAUST, Faridabad".

4. Presented a paper **"Light emitting diodes: A potential application of ZnO"** at National Conference on **"Role of Science and Technology Towards 'Make in India (RSTTMI-2016)** on March 05-07, 2016 at YMCAUST, Faridabad".

5. Presented a paper **"Potential applications of ZnO nanostructure materials: A Review"** at **"Symposium on Nanotechnology: Interdisciplinary Aspects** (12th December 2012)" at YMCA University of Science and Technology, Faridabad.

6. Presented a paper **"A review on hydrogen gas sensors based on ZnO nanostructures"** at **"National Conference on Emerging trends in physics and materials science (etpms-2015)** march 9-10, 2015, at Department of Physics, Chaudhary Devi Lal University, Sirsa-125055, Haryana.

LIST OF PUBLICATIONS

In Journals

1. Shital Prasad, Sonia Bansal, and S. P. Pandey. "Effect of substrate rotation speed on structural, morphological, vibrational and optical properties of sol-gel derived Mn-Ni co-doped ZnO thin films." Materials Today: Proceedings 49 (2022) 3008–3014.
   DOI: https://doi.org/10.1016/j.matpr.2020.10.172

2. Shital Prasad, Sonia Bansal, and S. P. Pandey. "Structural, raman, photo-luminescent and optical investigation of sol–gel derived Co, Al and Ni doped ZnO thin films." Materials Today: Proceedings 49 (2022) 3022–3027.
   DOI: https://doi.org/10.1016/j.matpr.2020.10.235

3. Shital Prasad, Sonia Bansal, Amir Mansoori, Manju Bala and Preeti Sharma. "Effect of Annealing Temperature on Excitonic Binding Energy and Other Optical Properties of Mn-Ni Co-Doped Transparent ZnO Thin Films" Transactions of the Indian Ceramic Society 82 (2023) 31-39.
   DOI: https://doi.org/10.1080/0371750X.2022.2160376

In Conferences

1. Presented a paper **"Review on ZnO based CO and CO2 Gas sensors"** at National Conference on **"Role of Science and Technology Towards 'Make in India (RSTTMI-2016)** on March 05-07, 2016 at YMCAUST, Faridabad".

2. Presented a paper **"Light emitting diodes: A potential application of ZnO"** at National Conference on **"Role of Science and Technology Towards 'Make in India (RSTTMI-2016)** on March 05-07, 2016 at YMCAUST, Faridabad".

3. Presented a paper **"A review on hydrogen gas sensors based on ZnO nanostructures"** at **"National Conference on Emerging trends in physics and materials science (etpms-2015)** march 9-10, 2015, at Department of Physics, Chaudhary Devi Lal University, Sirsa-125055, Haryana.

4. Presented a paper **"Potential applications of ZnO nanostructure materials: A Review"** at **"Symposium on Nanotechnology: Interdisciplinary Aspects** (12th December 2012)" at YMCA University of Science and Technology, Faridabad.